CONTRIBUTION OF VARISTEM® STEMMING PLUGS TOWARDS THE REDUCTION OF BLAST INDUCED GROUND VIBRATIONS IN A QUARRY

by

Nkosinathi Rian Mndawe (69582068)

submitted in accordance with the requirements for the degree of

MASTER OF ENGINEERING

in the subject

MINING ENGINEERING

at the

UNIVERSITY OF SOUTH AFRICA

Supervisor: Prof Francois Mulenga

2025

Declaration

I hereby declare that this dissertation submitted for the degree Master of Engineering (M Eng): Mining Engineering, at the University of South Africa, is my original work and has not previously been submitted to any other institution for any degree or examination.

I further declare that all sources cited or quoted are indicated and acknowledged through a comprehensive list of references

NKOSINATHI MNDAWE

27/01/2025

Signature

Date

University of South Africa

Johannesburg, South Africa

Dedication

This dissertation is dedicated to my family, whose unwavering support, love, and encouragement have been my strength throughout this journey. To my parents, for instilling in me the value of education and hard work, and to my siblings, for always believing in my dreams.

Finally, this work is dedicated to all those who strive for knowledge and pursue their passions. Your determination is an inspiration to me and to many.

Acknowledgements

This dissertation would not have been possible without the support and encouragement of the following individuals.

First and foremost, I would like to express my deepest gratitude to my supervisor, Prof Francois Mulenga, for his invaluable guidance, patience, and unwavering support throughout this journey. Your insightful feedback and expertise have been crucial in shaping this work, and I am immensely grateful for your mentorship.

I would also like to extend my heartfelt thanks to my colleagues, Dr Tiyani Chauke and Prof Elvis Fosso Kankeu, for their thoughtful comments, constructive criticism, and encouragement. Your input has enriched this research and helped me push my work further.

To my family, especially Maria Sithole (Mom), Abednigo Mndawe (Dad), and Enhle Mndawe (my daughter), thank you for your endless love, support, and understanding. Your belief in me gave me the strength to persevere.

Lastly, I would like to acknowledge UNISA for their financial support, which made this research possible.

To everyone who has been part of this journey, thank you.

Abstract

Although blasting is the most fundamental and economically sound way of conducting mining, it has been proven to have a significant impact on the surrounding environment. This includes but is not limited to structural damage, disruption of nearby communities, and operational limitations due to regulatory compliance. This research work investigates the contribution of Varistem® stemming plugs toward the reduction of blast-induced ground vibrations. Stemming plugs, designed to enhance the confinement of explosive gases help to direct the explosive energy towards breaking the rock instead of being wasted as fly rock, air blast, and ground vibrations.

Field experiments were conducted in a quarry using both conventional stemming materials and stemming plugs under controlled blasting conditions. Vibration data, including peak particle velocity, frequency, and scaled distance, were collected using geophones placed at two different distances from the blast site. Statistical methods are employed to analyse the data, ranking the empirical predictor models according to their performance and comparing the effectiveness of stemming plugs in reducing ground vibrations relative to conventional stemming techniques. Statistical metrics such as MAE, R^2 and RMSE were used to rank the predictor models' performance, with the Langefors – Kihlstrom model being the most suitable model for the site. The following key limitations were faced during the study period, the first being time constraints regarding data collection. The second was restricted access to the geological and geomechanical data.

The results indicated that Varistem® stemming plugs contribute to reducing blast-induced ground vibrations. Incorporating these plugs saw a 37% reduction in ground vibration levels.

Keywords: Peak particle velocity, scaled distance, Varistem®, stemming plugs, USBM model, Langefors-Kihlstrom model, Ambraseys-Hendron model, BIS model

Table of contents

List of Figures

List of tables

List of symbols

Symbol	Description (units)
H_0	Null hypothesis (-)
H_1	Alternative hypothesis (-)
K	geological parameter factor (-)
n	Total number of data (-)
P	Threshold probability value for statistical testing generally set at 0.05 for a 95% confidence level (-)
Q	Maximum explosive charge per delay (kg)
R	Distance between blast area and monitoring area (m)
R^2	Coefficient of determination (-)
SD_1	USBM scaled distance ($m/kg^{1/2}$)
SD_2	Scaled distance according to Ambraseys-Hendron ($m/kg^{1/3}$)
SD_3	Scaled distance according to Langefors-Kihlstrom ($m^{1/3}/kg^{1/2}$)
SD_4	Scaled distance according to the Bureau of Indian Standards ($m^{2/3}/kg$)
y_i	Measured value (-)
$\hat{y}_i$	Predicted value (-)
$\bar{y}$	Mean of measured values (-)
β	Attenuation coefficient factor (-)
μ	Mean (-)
σ	Standard deviation (-)

List of acronyms

AN	Ammonium Nitrate
BIS	Bureau of Indian Standards
DDNP	Diazodinitrophenol
ET	Electromagnetic Transmitter
MAE	Mean Average Error
PETN	Pentaerythritol tetranitrate
PIN	Personal Identification Number
PPV	Peak Particle Velocity
PVC	Polyvinyl Chloride
RDX	Research Department Explosive
RF	Radiofrequency
RMSE	Root Mean Squared Error
SD	Scaled Distance
USBM	United States Bureau of Mines
UID	Unique Identification

Chapter 1 Introduction

1.1 Background

Blasting is the most essential and effective method for breaking rock from its in-situ state into more manageable fragments for easy extraction. This process uses explosives and is fundamental to the mining and construction industries. It facilitates the efficient and economical removal of rock and mineral deposits.

Simultaneously, blasting has proven to have some discernible adverse environmental effects such as dust generation, fly rock, noise, air blast, and ground vibrations. Among these, ground vibration emerges as a particularly noteworthy concern due to its significant implications on the structural integrity of buildings, constructions, and roads located near mining sites (Kumar et al., 2016; Noren-Cosgriff et al., 2020; Ismail et al., 2024).

Only a fraction of the approximately 20 – 30% of the energy released through explosive blasting is directly employed for rock breakage. The remaining energy is dissipated in the form of ground vibrations, air blasts, flying rocks, and noise (Hu et al., 2018; Hagan, 1977; Khandelwal et al., 2010; Yan et al., 2020). Mpofu et al. (2021) suggested that explosive energy can be lost through premature ejection of stemming material, due to poor stemming, which causes the rapid venting of explosive gases to the atmosphere. They went on to highlight that poor blasthole stemming can exacerbate ground vibrations thereby affecting the surrounding environment. Although Yan et al. (2020) recognises the influence of stemming over blast-induced ground vibrations, they also admitted that this subject is rarely investigated.

Literature acknowledges the impact that blast-induced ground vibrations have on the surrounding environment but instead of looking at ways to reduce the level of generated vibrations, it focuses more on how to

predict/estimate them (Hasanipanah et al., 2015; Yan et al., 2020; Khan et al., 2025). However, this study seeks to investigate the possibility of reducing the amount of ground vibrations generated during a blast by focusing more on stemming.

1.2 Problem statement

Blasting is considered as the most economical way of extracting mineral resources from the ground. However, blasting has been proven over the years to have negative impacts on the surrounding environment with ground vibrations being the most prevalent. Zhou et al. (2020) described ground vibrations as one of the most destructive results of blasting. This is because of its effects on surrounding buildings, structures, and communities.

Since ground vibration poses a serious environmental problem, Yan et al. (2020) believe that it is necessary to control its magnitude and influence within a certain range of distance. The most prevalent way to control blast-induced ground vibrations is to use empirical predictor models to determine the amount of explosive charge per delay that would result in the PPV not exceeding the recommended level (Hasanipanah et al., 2015; Yan et al., 2020; Khan et al., 2025). This approach limits the amount of explosives that will be detonated per time, thereby affecting fragmentation and muckpile profile (Agrawal, 2017). Furthermore, this approach does not reduce the amount of explosive wasted through premature ejection of the stemming material during blasting.

Indeed, most of the explosive energy is wasted primarily as ground vibrations and fly rock. As such, some of the wasted energy can be redirected towards breaking the rock thereby reducing ground vibrations amongst others. Several stemming contrivances were introduced to try and redirect some of the wasted energy towards rock breaking. These include the Varistem® stemming plug, a high-strength polystyrene plug that is purported to help trap explosive gases within the blasthole for a short while

during blasting (ERG Industrial, 2023). Varistem® plugs are manufactured through a process called dip moulding which helps make the plugs flexible with a high tear strength.

The use of stemming plugs over the years has mostly been directed towards improved rock fragmentation. However, less attention has been paid by the manufacturer towards its effects on ground vibrations. This study seeks to investigate the potential ability of Varistem® stemming plugs to reduce the level of blast-induced ground vibrations. This would help mining companies exploring the adoption of this technology make informed decisions.

1.3 Research objectives

The purpose of this study is to investigate the possibility of using Varistem® plugs in contributing towards reducing blast-induced ground vibrations. To investigate this, the following questions were asked:

- Which is the most suitable empirical model to describe the onsite ground vibration data produced with and without stemming plugs?
- Do Varistem® stemming plugs reduce the level of ground vibrations generated under blasting conditions?

To help answer these questions, the following objectives were developed:

- Determine the most suitable empirical model that describes the onsite ground vibration data produced with and without stemming plugs.
- Compare the level of ground vibrations generated under blasting conditions done with and without Varistem® stemming plugs.

Investigating the potential for Varistem® stemming plugs to reduce blast-induced ground vibrations would help contribute towards the body of knowledge. The mining industry would also benefit from this work in their quest to limit ground vibrations. Finally, the study could provide blasting

engineers with alternative options of reducing the environmental damage inflicted by ground vibrations.

1.4 Outline of the dissertation

This dissertation is structured in six chapters with the current chapter (i.e., Chapter 1) introducing the research problem and the associated research questions.

Chapter 2 provides a literature review on the various blast design parameters that affect ground vibrations. It also presents the most widely used empirical models of ground vibrations and the stemming contrivances for vibration control.

Chapter 3 details the procedure followed in collecting relevant on-site drilling and blasting data and the equipment used for the purpose of this research. The chapter also touched on how the collected data was processed and analysed to meet the study objectives.

In Chapter 4, predictor models are used to probe and empirically model both the data collected with and without Varistem® plugs. This data is further analysed to better understand the contribution of the selected plugs.

In Chapter 5, the empirical predictor models are ranked according to how best they interpret the on-site blasting results. Statistical methods are used to appraise the potential for Varistem® stemming plugs in the control of blast-induced ground vibrations.

Chapter 6 concludes the study by looking at whether the study objectives were met. The chapter goes on to making several recommendations for future studies.

Chapter 2 Literature review

2.1 Introduction

Although rock blasting is regarded as the most effective way of extracting minerals from the earth's crust, it equally has devastating effects on the surrounding environment. These effects present challenges for both the mining companies and the surrounding communities. Several research studies have been conducted to reduce the negative environmental impacts caused by blasting. This chapter reviews specifically the relevant literature on blast-induced ground vibrations and their reduction.

2.2 Blast-induced ground vibrations

Blast-induced vibrations are generated during the detonation of explosives in mining, construction, and quarrying operations. The detonation of explosives during blasting generates a high-pressure and high-temperature gas as well as a shock wave. The shock wave in turn creates a stress wave within the rest of the rock mass which causes the rock to start cracking. Cracks then propagate because of the high-pressure gas (Hu et al., 2018; Ye et al., 2023; Yuana et al., 2019). The process described above occurs in a very short period of time and leads to the breakage of the rock mass. However, the subsequent rock breakage accounts for approximately 20 – 30% of the available blasting energy. Saharan et al. (2017) found that only 7 – 22% of the total explosive energy is utilised towards breakage while the remainder is wasted in the form of noise, air blast, ground vibrations, etc.

2.2.1 Fundamental concepts

Ground vibrations are simply the movement of ground particles due to a sudden disturbance. This disturbance may be caused by the rapid release

of high energy and pressure resulting from the exothermic chemical reaction that takes place during detonation. The rapid release of energy and pressure creates a high-pressure wave that causes ground particles to move. This high-pressure wave is called a shock wave (Nguyen et al., 2019). It propagates radially through the rock mass in the form of seismic waves. These waves create stresses within the rock mass and subsequently cause the rock to crack. As the rock begins to crack, the high-pressure gas that forms as the result of the explosive chemical reaction expands through the newly formed cracks. This then opens up the newly formed cracks and cause the rock to eventually break.

Seismic waves diminish in strength as they travel away from their source. This phenomenon is evident when comparing the damage inflicted on the rock at the source of the explosion to that at a certain distance from it. Indeed, the rock is pulverised at the source of the blast, i.e., around the blasthole. But one moves away from the blasthole, the size of the broken rock gradually increases. And although seismic waves weaken with distance, their rate of dissipation is not rapid enough to prevent significant structural damage in nearby areas.

Seismic waves are commonly classified in three classic waveforms: primary waves, secondary waves, and surface waves (Aldas and Ecevitoglu, 2008). Primary waves (also known as P-waves) are the fastest seismic waves and therefore the first to be detected by seismographs after a blast. These compressional waves travel through solids, liquids, and gases, causing rock particles to move in the direction of wave propagation. Secondary waves (S-waves), on the other hand, are shear waves that move the rock particles perpendicular to their direction of travel. They are slower than the P-waves but can cause more intense shaking. Surface waves travel along the ground surface. They include Rayleigh waves, which cause a rolling motion, and Love waves, which cause horizontal shearing. These two waves typically cause the most damage. Figure 2.1 shows how blast waves travel from the blasting source all the way to neighbouring structures. Note that structures are exposed to both ground vibrations and air blast overpressure.

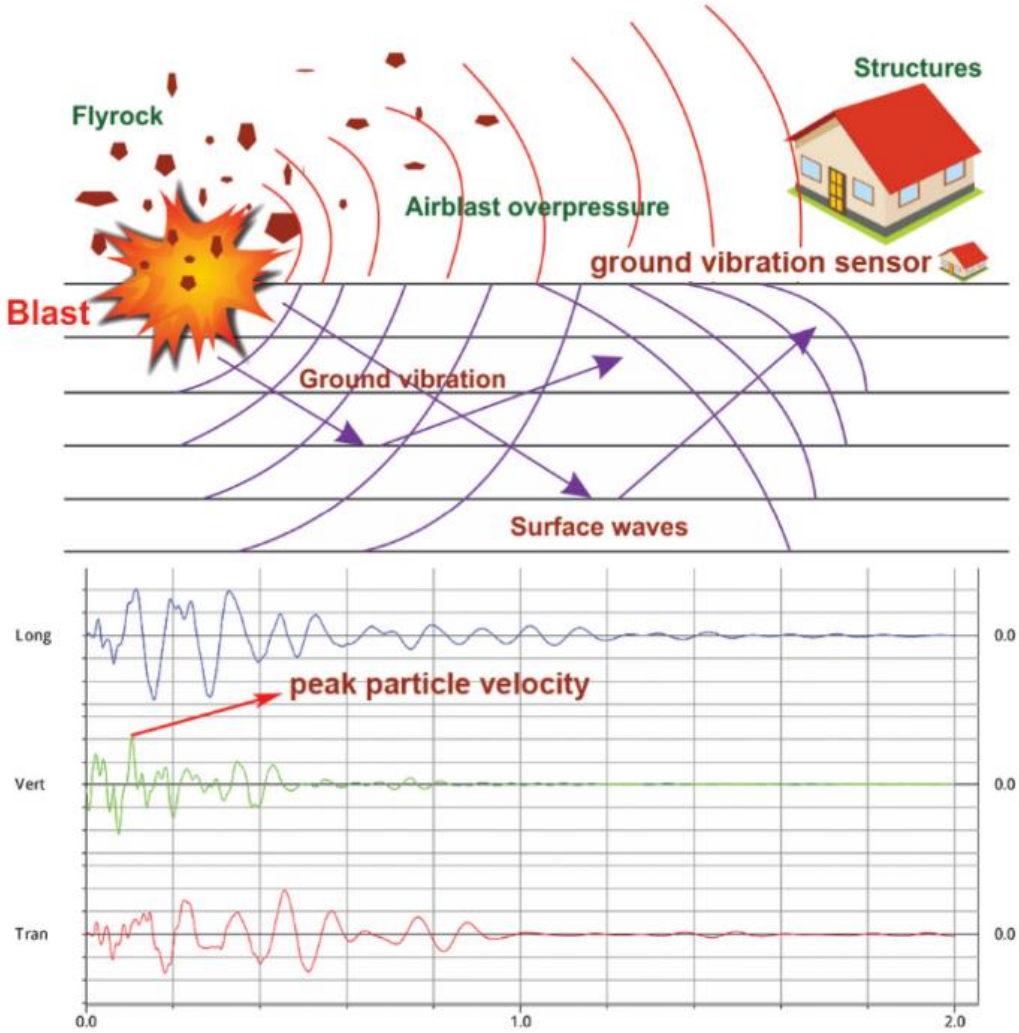

Figure 2.1: Illustration of ground vibrations and how they travel to nearby structures (Nguyen et al., 2019)

One can see from Figure 2.1 that as the blast is set off, both the air and ground experience a sudden overpressure (see peak particle velocity charts). This overpressure causes air blast, and ground vibrations, and at times fly rock. The latter refers to rock fragments thrown off from the blasted area to neighbouring area because of the overpressure. The overpressure also builds up in the air and causes air particles to travel as waves to the surrounding areas. These air waves also have the potential to damage structures. Most importantly, the overpressure also generates ground vibrations which travel through the ground. Some of these ground vibrations is absorbed while the remaining fraction is reflected as it hits the various

geological layers. This is illustrated in Figure 2.1 by the arrows. Reflected ground waves also have the potential to damage any nearby structures.

2.2.2 Factors influencing blast-induced ground vibrations

Ground vibrations can be either directly or indirectly influenced by several factors. These factors are categorised into two groups; namely, blast design parameters and geological factors.

Blast design is one of the key factors that influences the generation and propagation of ground vibrations. The design of a blast generally entails the following parameters: burden, spacing, timing, bench height, blasthole diameter, stemming, explosive column, and free face. Figure 2.2 provides an illustrative summary of these blast design parameters.

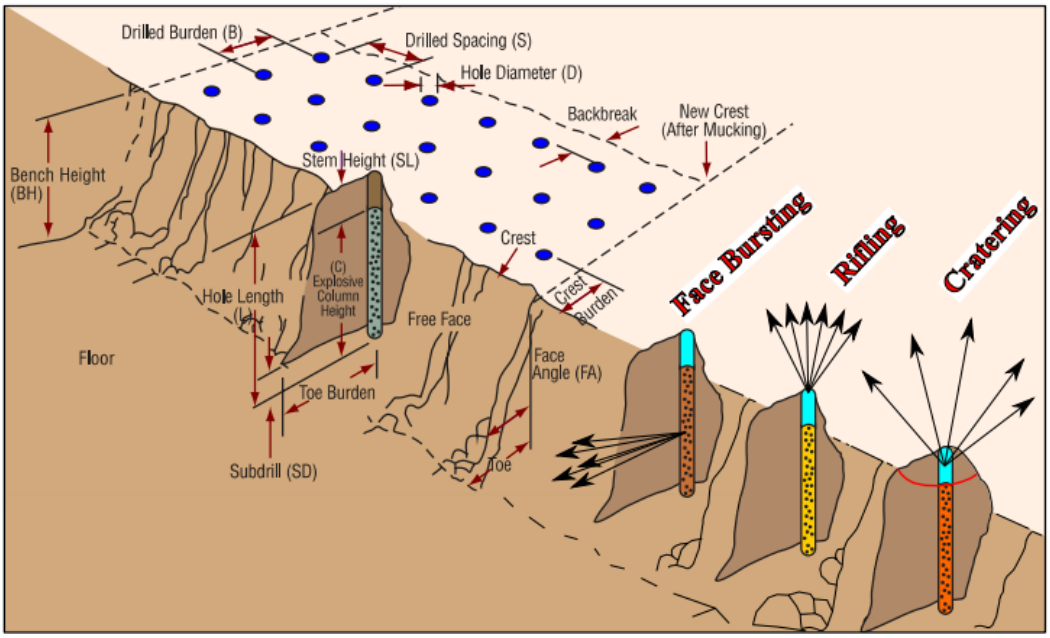

Figure 2.2: Blast design parameters (Hosseini et al., 2023)

It should be noted that not all blast design parameters equally influence ground vibrations. Several of these parameters have a direct effect on ground vibration while others have an indirect effect (see Table 2.1).

Table 2.1: An overview of how various blast parameters influence the control of ground vibrations (Dhekne, 2015)

Variables within the control of a blaster, [units]	**Effect on ground vibrations**		
	Significant	Moderate	Insignificant
Charge/delay, [kg]	X		
Delay interval, [ms]	X		
Spacing and burden, [m]		X	
Stemming (type and amount), [m]			X
Charge length and diameter, [m]			X
Angle of blasthole, [°]			X
Direction of initiation		X	
Total charge, [kg]			
Bare versus open detonating cord			X

Only the parameters that have a direct influence on ground vibration are discussed below.

2.2.2.1 Burden and spacing

Spacing is the distance between adjacent blastholes measured perpendicular to the burden (Sereme et al., 2019). Burden, on the other hand, is defined as the shortest distance between the nearest free face and the centre of the explosive charge (Yan et al., 2020).

While it is commonly assumed that spacing and burden affect blast-induced vibrations, research has indicated that their respective influence remains a subject of debate. As a case on point, Blair and Birney (1994) conducted a single blasthole experiment using two varying burdens to monitor the resulting peak particle velocity (PPV). They concluded that there was inadequate evidence to support the idea that burden affected ground vibration. However, based on a follow-up study, Blair (2015) reached the conclusion that burden influences ground vibrations. He argued that, from an energy perspective, the ground vibrations generated depend on the

length of the burden. In other words, the longer the burden the more the explosive energy is absorbed by the rock resulting in less vibration energy generated by the explosion. Another study conducted by Uysal et al. (2007) also supports the idea that blast-induced ground vibration can be influenced by the burden and spacing. This study was conducted at two different mines: Seyitomer Lignite Enterprise and Garp Lignite Enterprise. The aim was to investigate the vibrations caused by blasting. Their findings indicated a significant influence of burden on vibration levels while little was observed with spacing. In a contrasting experiment, Blair and Armstrong (2001) considered different burdens and measured the corresponding PPVs at various distances from the blast and for different volumes of explosives loaded across the rock mass. The two researchers noted that the relationship between PPV and distance was not clearly evident. Therefore, they concluded that ground vibration was not affected by burden.

2.2.2.2 Blasthole diameter

Blasthole diameter refers to the diameter of the hole drilled into the rock for the purpose of blasting. In mining, these holes are typically drilled into the rock face using specialized drilling equipment and are then filled with explosives. The diameter of the blasthole can therefore vary depending on the specific blasting operation and the desired result. Once selected for an operation, the hole diameter is rarely changed due to the restrictions imposed by the sizes of drill bits available. According to Blair (2010), blasthole diameters range between 0.05 m and 0.32 m. He also argued that this parameter has a significant effect on blast-induced ground vibrations.

Hu et al. (2014) conducted a rock blast test to investigate the effect of blasthole diameter on ground vibration. They discovered that the larger the blasthole diameter, the higher the magnitude of ground vibrations recorded. Furthermore, Afrasiabian et al. (2020) examined how the blast damage factor and blast design parameters affect ground vibration in a rock slope using dynamic blast loading. Their results were consistent with the findings

by Hu et al. (2014). The two studies mentioned above suggest that blast-induced vibration is significantly influenced by the diameter of the blast hole.

2.2.2.3 Blasthole depth

Blasthole depth refers to the length of the hole drilled into the rock to be blasted. The depth of the blasthole is determined by factors such as the depth of the commodity to be mined and the type and size of the machinery used. Relatively larger blasthole depths tend to result in lower ground vibrations as the explosive energy is dissipated in the form of body waves (Yan et al., 2020). In contrast, Worsey (1986) argued that reducing the blasthole depth can lead to a decrease in the level of vibration.

Another important point is that Yan et al. (2020) argued that there might be an optimal range for blasthole depth which has a high effect on ground vibrations. This is because Liu (2018) found that recorded ground vibrations were higher when their blasthole depth exceeded a certain critical length.

2.2.2.4 Explosive charge structure

Explosive charge structure refers to the specific arrangement of explosives within a blast hole designed to achieve optimal blasting results (Yan et al., 2020). Common charge structures include coupling and decoupling. Coupling involves placing the explosive charge in direct contact with the walls of the blasthole. When the explosive is tightly packed against the blasthole, the energy transfer to the surrounding rock is maximized. In contrast, decoupling involves introducing a gap, typically filled with inert material, between the explosive and the blasthole or the stemming.

The study of the impact of decoupling on ground vibrations started with Mel'nikov et al. (1979) and was later expanded by Fourney et al. (1981 & 2006). These researchers conducted theoretical analyses and experiments to understand the underlying mechanisms and effects of decoupling on ground vibrations. Their research demonstrated that decoupling can

significantly reduce ground vibrations caused by explosive blasts. By introducing a space or buffer between the explosive charge and the blasthole wall, the energy from the explosion is dissipated more effectively, leading to lower vibration levels. Further studies have built on this foundational work, exploring various aspects of decoupling, such as the optimal size and placement of air decks, the types of materials used for decoupling, and the effects on different geological formations. These advancements have contributed to the development of more precise and controlled blasting techniques.

For example, Blair (2004) experimentally compared decked and undecked single blastholes. The idea was to look at the effectiveness of air decking in disrupting blast waves to reduce blast vibrations. This research involved systematically analysing the performance of blastholes with and without air decks. His findings suggested that the anticipated benefits of air decking in mitigating blast vibrations might not be as straightforward as previously thought. Blair (2004) highlighted potential complexities and inconsistencies in how air decking interacts with blast waves. He then pointed out the need for further investigation into the conditions and parameters that influence its effectiveness.

In another study, Park and Jeon (2010) discovered that increasing the air decking coefficient at the bottom of blast holes effectively reduced blast vibrations. Through numerical analyses and field tests, their research demonstrated a clear relationship between the extent of air decking and the extent of vibration mitigation. Note here that air decking coefficient refer to the ratio of the length of the air space to the length of the explosive charge within the blast hole. By optimizing this ratio, Park and Jeon (2010) found that the energy released from the explosion was more effectively managed, resulting in less intense ground vibrations. This finding is significant for mining operations since controlling blast vibrations is crucial to minimizing their impact on nearby structures and reducing environmental disturbances. However, the length and extent of air decking used in a blasthole should be kept within a practical range. This helps in ensuring that the explosive

energy is utilised efficiently thereby controlling ground vibrations effectively. Figure 2.3 shows the difference between a conventionally charged blast hole and an air-decked blasthole for reference.

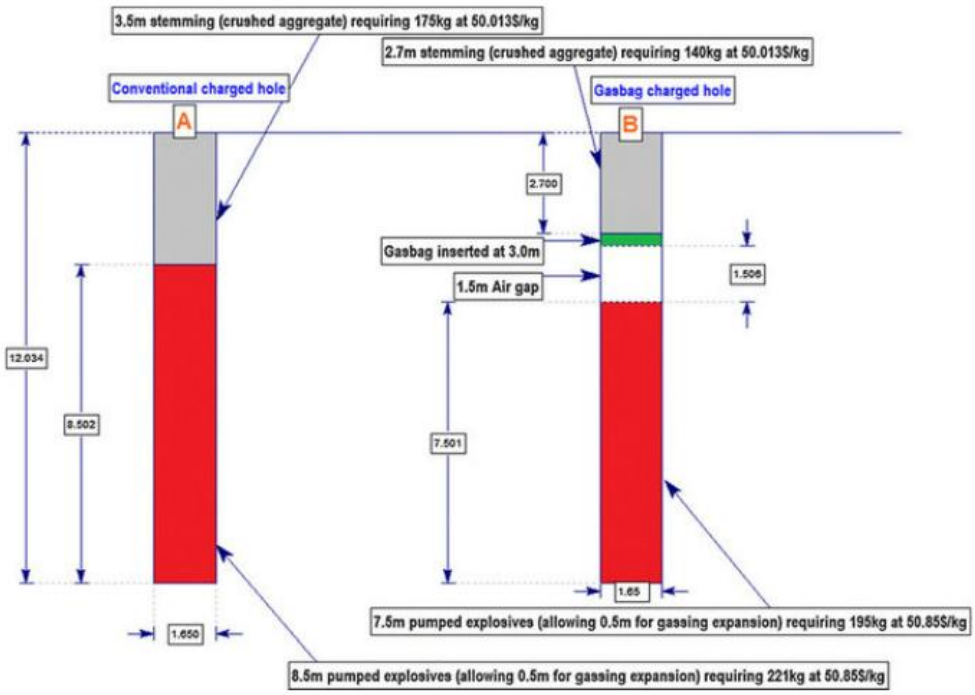

Figure 2.3: Comparison between a conventionally charged blasthole and an air-decked blasthole (Kabwe, 2017)

2.2.2.5 Stemming

Stemming entails covering the explosive column in a blasthole with an inert material (Mpofu et al., 2021). This practice helps to confine the explosive energy within the hole and improve the efficiency of the blast. Indeed, energy is channelled towards breaking the rock rather than allowing it to escape through the top of the hole. Stemming thus plays a crucial role in controlling blast-induced vibrations and enhancing rock fragmentation.

There are differing opinions on whether stemming plays a role in either generating or reducing blast-induced ground vibrations. According to Standards Australia (2006), the type and quantity of stemming do not significantly contribute to ground vibrations. Similar conclusions were

arrived at by Dhekne (2015) regarding the influence of stemming length and material over ground vibrations.

To sum up, inadequate stemming practices can contribute to ground vibration (Sereme et al., 2019). Stemming length plays a crucial role in controlling the generation of ground vibrations. Short stemming length may cause blowouts which may then lead to excessive vibrations (Rehman et al., 2021). On the other hand, excessive stemming length can increase ground vibrations (Sazid, 2014; Konya and Konya, 2018; Mpofu et al., 2021). And of note, Elevli and Arpaz (2010) reported a case where 13.1% of the estimated PPV was accounted for by stemming.

2.2.2.6 Properties of the explosive charge

Explosives possess distinct characteristics such as strength, density, and velocity of detonation (Ismail et al., 2024).

The strength of explosives speaks to the total work done by the gas produced by the explosion, while the density of the explosive is the mass of the explosive material per unit volume. The higher the amount of explosive material, the higher the density. The density is also related to the strength of the explosive. The two have a direct proportionality relationship; in other words, the denser the explosive, the higher its strength. When high-strength explosives are detonated, they tend to produce a large pressure wave which in turn generates great ground vibrations (Ismail et al., 2024).

The velocity of detonation (VOD) measures how quickly the shock wave travels through the explosive column in the hole. This velocity directly impacts explosive power making its measurement crucial. Indeed, VOD is used to assess the ability of explosives to generate pressure (Tete et al., 2016). This pressure helps propel the explosive gases to crack and break the rock further. Preis (2023) explained that higher VOD explosives produce high-frequency ground vibrations.

2.2.2.7 Delay blasting

Delay blasting, also known as timing, refers to the detonation of explosive charges at different times using predetermined delay intervals rather than all at once. This technique is crucial in balancing the effectiveness and safety of blasting operations. Explosive charges are set to detonate in a specific sequence which helps manage the direction and distribution of the explosive energy (Aldas and Ecevitoglu, 2008). Consequently, this reduces the intensity of the ground vibrations produced.

Delays are measured in milliseconds (ms); they can vary from a few milliseconds to several seconds. The precise timing depends on the specific goals of the blast and the characteristics of the material being blasted. By delaying the detonation of adjacent charges, the rock can fracture more effectively. This helps to prevent the superposition of stress waves which can subsequently amplify ground vibrations. Yan et al. (2020) argued that delay blasting reduces the quantity of explosive charge per delay compared to simultaneous initiation. This reduction limits the release of energy and effectively impacts ground vibration levels.

Studying the effect of short-delay timing on a blast, Rossmanith (2002) found that short-delay timing improves fragmentation and reduces ground vibration. Yan et al. (2020) further argued that delay blasting is an effective way to reduce ground vibrations. One can therefore propound that delay blasting influences ground vibrations. Indeed, concordant studies have reported that the level of vibrations produced by a blast can be reduced by using optimal delay intervals (see for example Shi and Chen, 2011; Wang et al., 2013; Qiu et al., 2018).

Shi and Chen (2011) carried out a field study aimed at examining the impact of delay timing on ground vibrations. To achieve this goal, the two researchers utilised the following blast delay times: 15 ms, 25 ms, 35 ms, and 40 ms. They then discovered that the optimal delay time corresponding to the highest reduction in ground vibration levels was 15 ms.

And in another study, Qiu et al. (2018) compared PPV values from two different blasts. In the first set of blasts, all blastholes were detonated simultaneously while in the second set, different delay times (0 ms, 8 ms, 13 ms, and 17 ms) were employed. The findings from the experimental showed that delay blasting produced lower ground vibrations compared to simultaneous initiation.

2.2.3 Free face and ground vibrations

A blast face or free face is the exposed surface of rock where blasting operations are conducted. The blast face is critical in determining the direction as well as the effectiveness of the blast. The blast face also influences factors such as fragmentation, muck pile shape, and overall blast efficiency (Ma et al., 2020).

Literature suggests that the presence of a free face can influence the propagation of ground vibrations. Ma et al. (2020) conducted a study to investigate the influence of the number of free faces on vibrations in underwater blasting. They found that when blasting a single free face, a significant portion of the blast energy is converted into vibration energy. And based on the empirical findings, they demonstrated that increasing the number of free faces can effectively reduce ground vibrations.

Wu et al. (2017) also analysed the impact of varying the number of free faces using wavelet analysis in conjunction with experimental data. They discovered that increasing the number of free faces can alter the distribution of vibrations across frequency bands, potentially resulting in higher-frequency energy in blasting vibrations.

2.2.4 Geological factors

Geological conditions play an important role in determining how rock masses respond to blasting vibrations. Classic properties of the rock such as its hardness, density, and structural integrity, affect the propagation of

energy from explosive blasts through the rock mass (Kuzu, 2008; Shi et al., 2016). For instance, softer rocks may absorb more vibration energy compared to harder ones thereby influencing the extent to which nearby structures and the surrounding environment are affected by the blast. To put it another way, rock hardness governs the attenuation law of blasting vibrations. The attenuation law of blasting vibrations refers to how vibrations weaken as they travel away from the blast site. Gutowski and Dym (1976) as well as Kim and Lee (2000) agree that ground vibrations dissipate as one moves away from the source. Geological factors such as the presence of fault lines, jointing, or varying layers within the rock can alter this attenuation process. Understanding these geological influences helps in predicting and controlling the spread of vibrations to minimize their impact on nearby infrastructure, communities, and the environment.

Nateghi (2011) monitored the reduction in the magnitudes of blast-induced vibrations. Corresponding PPVs were then recorded and compared from four distinct locations around the blasts. The study eventually reported notable variations in PPV attenuation across different rock units. This suggests that the geological characteristics of the rock formations influence how blast vibrations dissipate.

Hao et al. (2001) conducted a comprehensive study looking at the effects of joints on ground vibration propagation. The study was conducted on a site characterised by jointed rock formations. In terms of findings, the attenuation in stress waves was noted to vary significantly depending on their direction of propagation relative to the rock joints. Specifically, the attenuation of stress waves was found to be most rapid when the waves propagated in a direction perpendicular to the predominant joint set within the rock. This suggests that the rock joints effectively dissipate the energy of the stress waves when the waves encounter the joints head-on. Conversely, when the stress waves travelled parallel to the direction of the rock joints, the waves experienced the slowest rate of attenuation. This is an indication that the continuity of the rock joints in the parallel direction allows the stress waves to maintain their energy over a longer distance.

Wu et al. (1998) did a similar study to that of Hao et al. (2001) and produced comparable results. And in a different study, Simangunsong and Wahyudi (2015) discovered that PPV attenuates more rapidly in steeply dipping formations with multiple bedrock masses. This is because waves travel down and up the dip and therefore die down faster compared to when the waves travel along the strike.

Shi et al. (2016) demonstrated that the PPV of surface vibrations tends to be higher than that of underground vibrations at equivalent distances from the blast site. This difference suggests that variations in topography and in the properties of the rock formations significantly affect how blasting vibrations attenuate. Factors such as the surface terrain and the geological composition of the rock therefore play a crucial role in determining the spread and intensity of vibrations. Consequently, they should be considered when planning for safe blasting operations.

Finally, weather is another phenomenon that influences the propagation of ground vibrations through the rock mass. Hu et al. (2017) studied how blasting vibration attenuates in summer and in winter. The group of researchers found that that the attenuation rate of vibration was slower during winter compared to summer. This difference suggested that weather conditions in the form of temperature variations influence the mechanical behaviour and wave impedance properties of the materials through which the vibrations travel.

2.3 Empirical models of blast-induced ground vibrations

One of the first studies on blast-induced ground vibrations was conducted in the United States of America (USA) by a researcher named Rockwell. Rockwell (1927) undertook this study because of the growing concern over the blast-related damage to neighbouring structures. These structural damages were caused by ground vibrations and air blasts resulting from blasting activities from nearby quarries. This seminal study was later

followed by another one conducted by the United States Bureau of Mines (USBM) in 1935 – 1942. This subsequent study entailed an extensive investigation into the seismic effects of quarry blasting with the development of the damage criteria for residential structures. These criteria were based on the ground vibration acceleration of structures. The criteria were divided according to the vibration levels, where (Duvall and Fogelson, 1962):

- No damage was expected below 0.1g,
- “Caution” was to be applied between 0.1g – 1.0g, and
- Damage was almost certain above 1.0g.

Crandel (1949) also developed damage criteria based on vibration levels experienced by affected structures. These damage criteria were based on what he called the energy ratio. This ratio can be calculated by squaring the particle acceleration of the ground and dividing it by the squared frequency. He divided the energy ratios as follows:

- Ratios below 3 were deemed safe;
- Ratios between 3 and 6 required caution; and
- Ratios above 6 meant danger.

In 1949 – 1960, research on this subject started booming with experts and scholars from around the world showing interest in various states and organisations adopting different damage criteria (Fish,1951; Fish and Handcock, 1949; Morris and Westwater, 1953). For example, the Pennsylvania state, USA, adopted a damage criterion that uses the particle displacement of the structure to measure the damage caused. This criterion specified an allowable displacement of 0.03 inch (0.762 mm) as a safe limit. On the other hand, the states of New Jersey and Massachusetts, USA, both adopted damage criteria that specified an energy ratio of 1 as the allowable limit (Glasstone, 1950).

Next, Langefors et al. (1958) developed new damage criteria based on the velocity of motion of the ground at the house location. The criteria used four different levels of damage defined as follows:

- Level 1: 2.8 inches per second (in/s) – no noticeable damage
- Level 2: 4.3 in/s – fine cracks and fall of plaster
- Level 3: 6.3 in/s – cracking
- Level 4: 9.1 in/s – serious cracking

Finally, Duvall and Fogelsom (1962) reviewed all the damage criteria used then which were based on displacement, acceleration, and velocity. They subsequently found that velocity was the best parameter to use in the estimation of the damage experienced by residential structures. As such, the review study forms the backbone of the majority of PPV studies conducted to this day.

Over the years, researchers have developed empirical models to forecast the intensity of ground vibrations generated by blasting. These models enable one to predict ground vibrations before executing a blast. Blasting engineers can therefore explore way of reducing the environmental and structural effects of blasting, particularly in mining, construction, and quarrying. These empirical models were developed based on the inverse-power function descriptive of the seismic propagation law. Indeed, for the inverse power function, the peak particle velocity is given by a standard function of the form (Agrawal and Mishra, 2019):

$$PPV = K\,(SD)^{-\beta} \qquad (2.1)$$

Where PPV is the peak particle velocity

SD is the scaled distance as defined in the applicable Equations (2.2) to (2.5) below

K is a geological parameter characteristic of the rock mass

β is the attenuation coefficient characteristic of the site.

The values of K and β are both dependent on the choice of the predictor model given in Equations (2.2) – (2.5) below. Also, Equation (2.1) remains valid irrespective of how the scaled distance was calculated.

Among the various predictor models developed from Equation (2.1), the following are the most used for predicting blast-induced ground vibrations

(Bhagwat and Dey, 2016; Hasanipanah et al., 2015; Ongen et al., 2018; Ragam and Nimaje, 2018; Xue, 2019; Zhou et al., 2020):

- The United States Bureau of Mines model or USBM model
- The Langefors-Kihlstrom model
- The Ambraseys-Hendron model
- The Bureau of Indian Standards model or BIS model

The USBM model is the most widely accepted predictor model for ground vibrations compared to the others mentioned above due to its accuracy and suitability in terms of safety compliance (Khan et al., 2025). However, all four empirical models are good mathematical descriptions of the relationship between the peak particle velocity of ground vibrations and the scaled distance. The scaled distance is the only distinguishing factor amongst the above ground vibration models. It is calculated differently for each of the four empirical models. For example, in the USBM predictor model, scaled distance is calculated using the squared root scaled distance formula below (Xue, 2019):

$$SD_1 = \frac{R}{\sqrt{Q}} \qquad (2.2)$$

Where SD_1 is the scaled distance as defined for the USBM predictor model (m/kg$^{1/2}$)

R is the distance between blasting area and monitoring point (m)

Q is the maximum explosive charge per delay (kg).

The Ambraseys-Hendron model, on the other hand, uses the cubed-root scaled distance defined below (Xue, 2019):

$$SD_2 = \frac{R}{\sqrt[3]{Q}} \qquad (2.3)$$

Where SD_2 is the scaled distance as defined for the Ambraseys-Hendron predictor model (m/kg$^{1/3}$)

The Langefors-Kihlstrom model uses Equation (2.4) to calculate the scaled distance (Grobbelaar et al., 2020):

$$SD_3 = \frac{R^{1/3}}{\sqrt{Q}} \quad (2.4)$$

Where SD_3 is the scaled distance as defined for the Langefors-Kihlstrom predictor model ($m^{1/3}/kg^{1/2}$)

In contrast, the BIS predictor model uses Equation (2.5) to define the scaled distance (Xue, 2019):

$$SD_4 = \frac{R^{2/3}}{Q} \quad (2.5)$$

Where SD_4 is the scaled distance as defined for the BIS predictor model ($m^{2/3}/kg$)

All these four empirical models can be used to predict and control blast-induced ground vibrations by adjusting the amount of explosive charged per blast. The Langefors-Kihlstrom model is a bit more complex in application compared to the USBM model (Khan et al., 2025). The Langefors-Kihlstrom model is predominantly used in Scandinavian regions while the BIS model finds greater use in India and in areas with similar geologies to India's. In contrast, the USBM model is a bit more versatile in application compared to the other three models. It has been found to work in a wide variety of geological settings (Ghosh et al., 2024).

Let us talk about the USBM safe vibration limit curve. The USBM predictor model adopted the RI 8507 damage criteria to monitor ground vibrations and relate them to regulatory safety levels. This enabled the USBM team to develop the safe vibration limit curve illustrated in Figure 2.4. The curve helps one to predict the structural damage due to blasting that can result from exceeding these vibration limits.

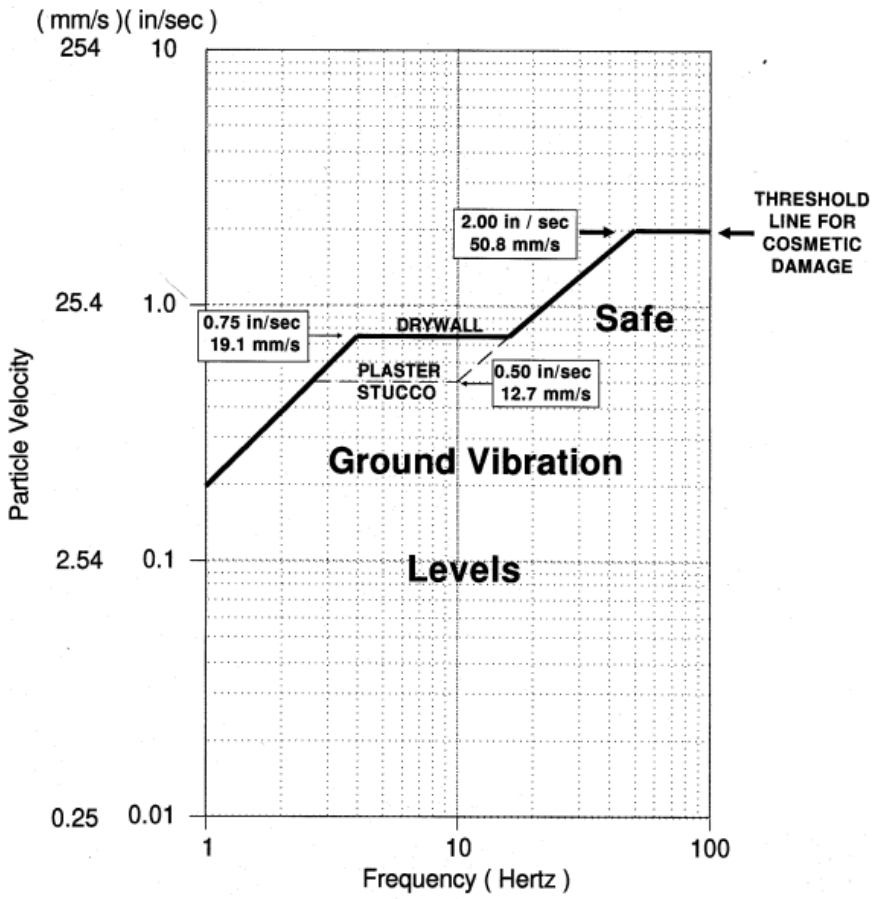

Figure 2.4: USBM safe vibration limit curve as per USBM RI 8507 standard (Siskind, 1980)

The limiting curve represents the ground vibration limits for cosmetic damage on residential structures. The maximum allowable PPV depends on the frequency of the vibration: the higher the frequency of the waves the higher the PPV value. And under normal circumstances, ground vibrations should not exceed 12.7 mm/s, but at higher frequencies, the limit can increase to 50 mm/s.

Although residential structures can withstand ground vibrations of up to 12.7 mm/s or higher when the frequency is high, humans are easily affected by much lower levels. Table 2.2 provides a summary of typical ground vibrations and corresponding human responses.

Table 2.2: Human response to vibration (Siskind, 1980)

Ground vibration level (mm/s)	Effects on humans
0.025 – 0.076	Imperceptible
0.076 – 0.254	Barely perceptible
0.254 – 0.762	Distinctly perceptible
0.762 – 2.540	Strongly perceptible
2.540 – 7.620	Disturbing
7.620 – 25.40	Very disturbing

Ground vibration levels between 0.76 and 2.54 mm/s are perceived by residential structures, but the probability of damage is almost non-existent. Levels in the range of 2.54 – 7.6 mm/s can be disturbing and levels above 7.6 mm/s can be very unpleasant, although they are unlikely to cause permanent structural damage.

Human sensory perception is also affected by frequency. The approximate human response curves are combined with the USBM limiting curve for damage in Figure 2.5. These curves slope in the opposite direction. In other words, humans are more tolerant to low frequency vibrations, i.e., frequencies below 10 Hz. To avoid damaging buildings, the USBM limiting curve should be applied. However, in order to limit the constant complaints from neighbours, vibrations should preferably be kept beneath the unpleasant as well as the intolerable curves.

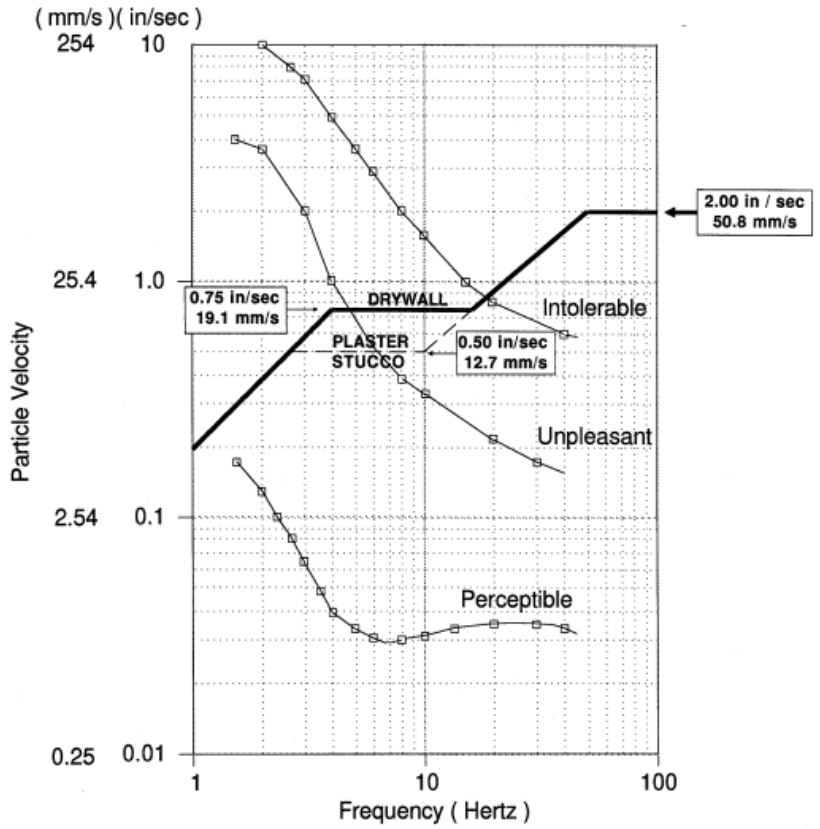

Figure 2.5: Human response curves compared with potential damaging limits (Siskind, 1980)

2.4 Stemming contrivances

Sazid (2014) detailed the historical development of stemming contrivances. He explained that the use of stemming contrivance dates back to the 19th century as shown in the timeline in Figure 2.6. The timeline clearly indicates the growing research interest in utilizing stemming devices to effectively contain explosive energy during blasting operations. Burgoyne et al. (1849) conducted an experiment where they used an iron plug to improve blasting results. The study did not yield noticeable benefits in terms of blast effectiveness or safety improvements.

Oct 06, 1874	*Kalmbach,*
Mar 16, 1915	*Tietig,*
Jul 02, 1946	*Lubelsky, and Walburn,*
Oct 03, 1959	*Householder,*
Aug 08, 1961	*Edney, and McGee,*
Oct 06, 1964	*Karpovich,*
Mar 16, 1965	*Griffith, and Wells,*
Dec 26, 1968	*Botes, V.J.,*
May 04, 1976	*Sanders, and Sanders*
Jul 05, 1988	*Worsey,*
Nov 24, 1998	*Skaggs,*
Aug 10, 1999	*Miller, and Brown,*
Nov 09, 1999	*Thomson,*
Apr 10, 2001	*Jenkins & Jenkins,*
Dec 04, 2001	*Bianchini,*
May 14, 2002	*Shann,*
Jan 07, 2003	*Fitzgibbon,*
Jul 24, 2003	*Andre,*
Mar 18, 2004	*Harcourt, and Eurich,*
Apr 20, 2006	*Robert, Cooper, and Arthur,*
Feb 19, 2008	*Kang,*
Aug 21, 2008	*Carroll,*
Dec 04, 2008	*John,*
Mar 26, 2009	*Dhooge,*
May 19, 2009	*Sorhus,*
Apr 06, 2010	*Gonjalez,*

Figure 2.6: A timeline depicting the historical development of stemming contrivances (Sazid, 2014)

Stemming plays a central role in controlling the level of ground vibrations produced during a blast. Stemming helps to confine the explosive energy within the blast hole ensuring that the energy is directed into breaking the surrounding rock rather than escaping through the blasthole opening (Rehman et al., 2021). This containment increases the efficiency and effectiveness of the blast, which in turn reduces the energy available for the generation of ground vibrations.

Figure 2.7 shows that during the detonation, the usage of the explosive energy is divided into 3 components: shockwave energy, heave energy, and wasted energy (Oates and Spiteri, 2021).

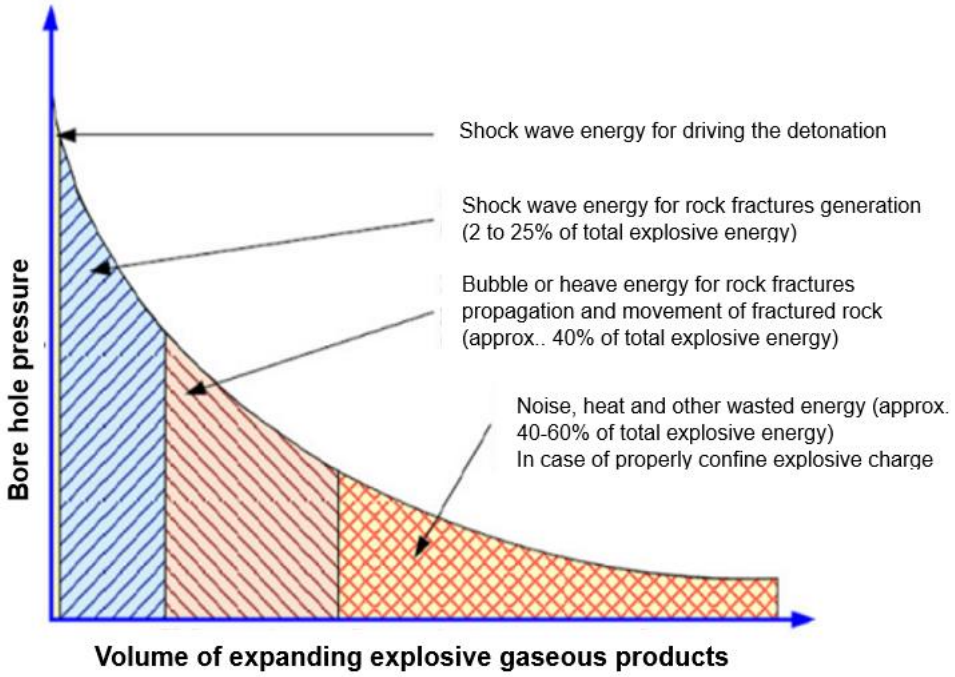

Figure 2.7: Partition of explosive energy during rock blasting (after Oates and Spiteri, 2021)

Shockwave energy is primarily responsible for initiating and propagating the shock wave through the explosive material and into the surrounding rock mass. This component of the explosive energy is the smallest of the three energy components. It typically constitutes 2 – 25% of the total explosive energy. It propels the detonation process through the explosive column and initiates cracks in the surrounding rock mass.

Heave energy refers to the energy expended in further cracking and breaking the rock through the explosion gases, lifting and displacing the rock mass surrounding the blast site. This energy is responsible for the physical displacement and movement of the fragmented rock material away from the blast zone. This component accounts for up to 40% of the entire explosive energy.

Wasted energy, the large component of the explosive energy, encompasses any portion of the explosive energy that does not contribute effectively to shockwave propagation or rock displacement. This can include energy losses due to inefficiencies in the explosive material itself, incomplete

combustion, or energy dissipation into the surrounding environment through factors like air blast, fly rock and/or ground vibration. This component accounts for about 40 – 60% of the explosive energy.

The law of conservation of energy states that energy cannot be created or destroyed, only converted from one form to another. During the detonation, a large portion of the energy is typically lost as heat, sound, and ground vibrations. It is believed that this wasted explosive energy can be redirected to break the rock more effectively. By refining the blasting process, the amount of wasted energy would be minimised and channelled towards breaking the rock. One of the ways that can be achieved is through the concept of blast energy containment which requires proper stemming.

The premature ejection of stemming material causes the loss of explosive energy and the rapid venting of gases into the atmosphere. This results in an air blast, that is, a shock wave generated by explosive detonation, often accompanied by forcefully ejected fly rock (de Graaf, 2013). During blasting, it is suggested that a significant amount of explosive energy escapes due to the premature ejection of stemming material which also leads to the venting of explosive gases into the atmosphere. Mpofu et al. (2021) argue that if this explosive energy can be contained within the blasthole for a longer duration, it could be expended more effectively in breaking the rock. Several researchers believe energy loss can be reduced by enhancing stemming techniques (e.g., Sazid et al., 2016; Rehman et al., 2021).

Oates and Spiteri (2021) explained that stemming helps with retaining the explosive energy that would otherwise be lost in unstemmed holes. Saharan et al. (2017) as well as Rehman et al. (2020) argued that in addition to stemming, the use of stemming plugs can greatly contribute to containing the blast energy within the blasthole. Stemming plugs are devices placed within the blasthole above the explosive charge. These plugs create a more effective seal within the blasthole, preventing the escape of gases and energy through the top of the blasthole (Sazid, 2014). By containing the explosive energy within the blasthole, stemming plugs force more of the

energy to go into the surrounding rock. This increased containment of energy ensures that a higher proportion of the explosive force contributes directly to breaking the rock, rather than being dissipated as heat, sound, and ground vibrations. By redirecting most of the available explosive energy towards rock breakage, less of the energy left would be converted into ground vibration.

Mpofu et al. (2021) conducted a study in which they assessed the effects of stemming practices on ground vibration and air blast. The study reported that poor stemming practices were one of the factors that led to the generation of high levels of ground vibration. Sazid et al. (2016) investigated the effect of confinement on the utilisation of explosive energy using a stemming plug known as SPARSH. They found that the stemming plugs increased the energy retention time within the blasthole fivefold. And in an earlier study, Sazid (2014) concluded that stemming plugs increase the energy retention time.

In another study, Rehman et al. (2021) conducted 6 full-scale production blast tests in which the effectiveness of three types of stemming plugs was evaluated. The stemming plugs included plastic moulded plugs, inflatable rubber balls, and cement mortar. Their respective performance was compared to the conventional stemming material with no plugs. The group of researchers discovered that blasting with any of the three plugs improved energy retention time and rock fragmentation while producing fewer boulders. However, amongst the three plugs, cement mortar was the most economical option and plastic moulded plug yielded the best fragmentation. The inflatable rubber plugs performed reasonably on both fragmentation and economically.

Lastly, Cevizci (2012) compared the ability of plaster stemming plugs against conventional stemming material to retain the explosive energy. In his findings, he reported that plaster stemming plugs increased the retention of energy within the blasthole thereby improving fragmentation.

2.5 Concluding remarks

The magnitude of blast-induced ground vibrations is the highest at the source of the blast. But vibrations dissipate as one move away from the said source. Ground vibrations can be influenced directly or indirectly by several factors. These include blasthole diameter, burden, blasthole depth, charge structure, stemming, and geological factors amongst others.

Blast diameter has been observed to incur higher levels of ground vibrations with larger blasthole diameters. On the other hand, it is still not clear how burden affects ground vibrations. Some researchers found that the longer the burden, the more explosive energy the rock absorbs, and the less vibrations are generated. Other researchers reported the opposite.

Regarding blasthole depth, some researchers believe that deeper blasthole hinders the generation of high-level vibrations. Other researchers also suggest the existence of an optimal range of blasthole depth with a correspondingly high effect on ground vibrations. Another group instead is of the view that there may be a critical blasthole depth beyond which ground vibration effects would be high.

In terms of decoupling, several studies have shown that decoupling can significantly reduce blast-induced ground vibrations. By the same token, one study highlighted that the use of air decking yielded inconclusive results in terms of reducing ground vibrations. Another further advised that increasing air decking at the bottom of the blastholes effectively reduces ground vibrations.

Talking about geological factors inherent to the rock mass, there exist several factors that directly influence ground vibrations. The hardness of the rock is one such factor. Indeed, soft rocks tend to absorb the vibration energy better thereby attenuating the waves and resulting in lower levels of vibrations reaching neighbouring structures. Geological discontinuities has also been found to influence the attenuation of ground vibrations through the rock mass.

Lastly, the quality of stemming is one of the most important factors that directly affect the generation of ground vibrations. This is where inert material is used to cover the explosive material after charging a blast to prevent the premature ejection of explosive energy and gases. The inert material traps the explosive energy and gases within the blasthole a bit longer. In doing so, the explosive energy and gases are channelled towards breaking the rock. Three stemming plugs were available in the literature: plastic moulded plugs, inflatable rubber balls, and cement mortar. Upon reviewing their respective performances, it was discovered that they all increase the energy retention time and contribute towards improved rock fragmentation as well as reduced boulders at varying degree. As such, there is merit in further investigating the use of stemming plugs in controlling ground vibrations. This is because most of the explosive energy is believed to be expended in rock fragmentation. Indeed, reported scientific investigations on the use of stemming plugs has so far been focused on improving rock fragmentation. But less attention has been paid towards considering their contribution to reducing ground vibrations. This study seeks to investigate the potential of stemming plugs to reduce ground vibrations.

Chapter 3 Experimental programme and data collection methodology

3.1 Introduction

The primary objective of this study is to determine the most suitable empirical model that describes the on-site vibration data produced at the selected quarry. This basically involves comparing the levels of ground vibrations generated with or without stemming plugs.

To address this, field experiments were conducted. The experiments were designed to assess the effectiveness of Varistem® stemming plugs in reducing blast-induced ground vibrations. Two blasting scenarios were implemented. The first set of blasting tests, referred to in this work as conventional blasting, entailed the use of aggregate material only for stemming. This set of experiments was used as a control. The second set, on the other hand, used a combination of aggregate material and Varistem® stemming plugs. Simply put, conventional blasts refer to experiments where the original blast design was executed by using only aggregates as stemming material. Varistem® blasts refer to the blast where both the aggregate stemming material and the Varistem stemming plugs were used together. In both cases, the same blast design was used with all blasting parameters kept constant except for the incorporation of the Varistem® stemming plugs. Blasting seismographs were employed to monitor the blast-induced ground vibrations produced in both scenarios for comparison in the subsequent chapters. There were two stations used for the monitoring the different production blasts conducted across the quarry; namely, Station A and Station B.

The subsequent sections cover the adopted data collection methodology as well as the equipment used in support of the test work.

3.2 Blast design

Blasting is the first step in the extraction of mineral resources. It plays a significant role in breaking down the rock mass from its in-situ state into smaller and manageable fragments that can easily be handled, transported, and processed (Bamford et al., 2021; Silva et al., 2017). However, the poor execution of a blast may lead to detrimental effects on the surrounding environment in the form of fly rock, air blast and ground vibrations (Mpofu et al., 2021). Proper care must be taken when designing and executing a blast to avoid or reduce these environmental effects. Table 3.1 summarised the blast design parameters used for the duration of the study.

Table 3.1: Adopted blast design

Average bench height	13.6 m
Blast-hole diameter	102 mm
Blast pattern	Staggered
Burden and spacing	2.8 m x 3.0 m
Stemming length	(28 x hole diameter = 2.86 m)
Average explosive mass per hole	±101.2 kg/hole
Technical powder factor	±0.87 kg/m^3
Stemming material	9.5 mm

A total of 27 production blasts were considered in this study, 12 of which constituted of the conventional blasts with the remaining 15 blasts being the Varistem® blasts. The conventional blast data were retrieved from the quarry's archived data while the Varistem® data was collected during the field experiment. The historical/archived data was collected before the adoption of the Varistem® stemming plugs.

Both scenarios employed the very same blast design to avoid any bias in the comparative analysis. The only varying factor between tests was the number of drilled blastholes per test conducted. This was done to keep up with the production demands of the quarry. To counter any vibration data bias that could arise from the varying blast-holes per test, an average

charge per delay of 102 kg was adopted for all tests. The same timing intervals (see Figure 3.1) were adopted for all the tests. The inter-spacing timing intervals were increasing from the front row to the back row by increments of 3 ms (inter-row timing interval). The first row would start with an inter-spacing timing of 6 ms, followed by the second row at 9 ms, the third row at 12 ms, and so on.

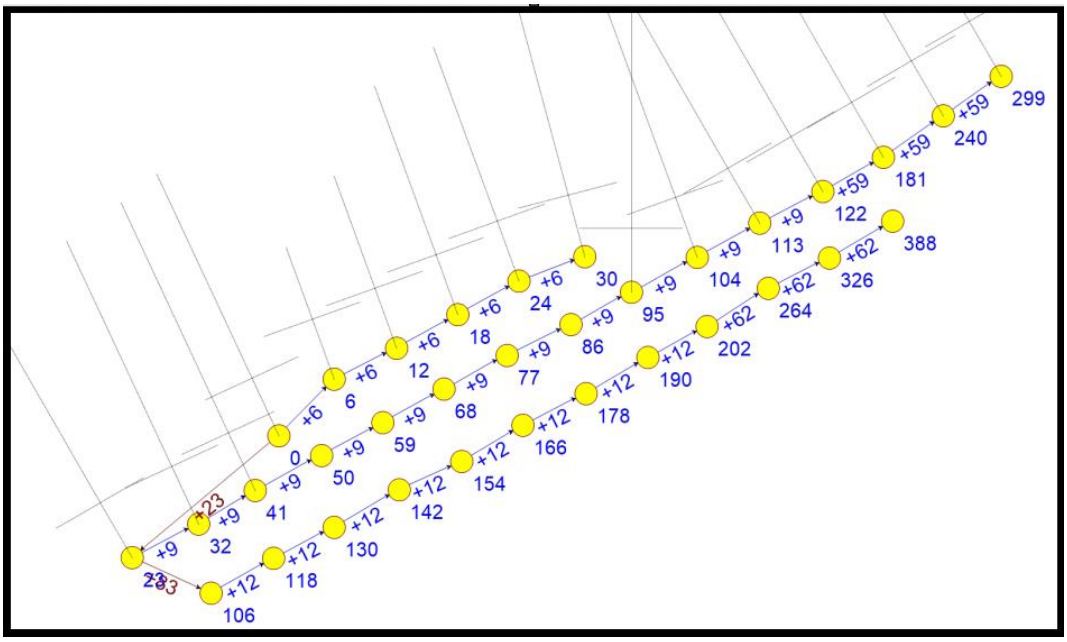

Figure 3.1: Blast pattern with timing intervals used at the Malandvule quarry

Each test took an average of 9 days from drilling to loading all the blasted material. The entire experimental study took 5 months to complete. There were no repeat tests conducted within the allocated timeframe of the study.

3.3 Data collection

A non-disclosure agreement was signed with the quarry in question to keep its name, location, maps, and other sensitive information confidential. Due to the required anonymity, it was decided to call the operation Malandvule Quarry. Suffice it to say that the quarry is situated in a busy area surrounded by amenities like public transport, a residential area, and a national highway.

Several specialised equipment was used to execute the various blasts as well as monitor and record the resultant blast-induced ground vibrations. Details are presented in the subsections below.

3.3.1 Drilling

Care must be taken during the drilling process as this influences the overall outcome of a blast. Gomes-Sebastiao and Graaf (2017) claim that poor drilling practices contribute to half of the problems experienced after a blast. This shows how important drilling accuracy is to the entire blasting process, which is why measures were taken to ensure quality drilling.

Malandvule quarry uses a Furukawa HCR1200 surface drill rig, which can drill blastholes of diameters between 76 mm and 102 mm, up to a depth of 22 m. To ensure accurate drilling, a Trimble Global Positioning System (GPS) was employed to locate the drilling points on the bench as dictated by the blast design. The design information would be given to the drill operator to execute who would then manoeuvre the drill rig (see Figure 3.2) to those points for drilling.

Figure 3.2: Surface drill rig (Source: Photo taken on site)

The operator would then set up the drill rig at the correct collar position of the blasthole and start drilling. The operator would also adjust drilling speeds and force depending on the type of rock the drill bit is penetrating at that point. The operator would then drill to the desired depth and move on to the next point. Finally, the blaster would follow up with a measuring tape (Figure 3.10) to confirm if the blastholes were drilled to the correct depth.

3.3.2 Electronic detonators and boosters

After the blasthole depth had been confirmed, C400 Trojan cast boosters (Figure 3.3a) were used along with the AXXIS Titanium electronic delay detonator (Figure 3.3b).

Figure 3.3: (a) C400 Trojan boosters and (b) AXXIS Titanium electronic delay detonator (Source: Photo taken on site)

The C400 Trojan cast boosters are made from high-quality Pentaerythritol tetranitrate (PETN), ensuring their reliability, consistency, and durability in various blasting environments. The booster is manufactured with an internal through-tunnel which allows easy insertion of the delay detonator and a second hole at the back end. The delay detonator is inserted on the front side of the cast booster (Figure 3.4a), pushed through the cast booster tunnel, inserted on another hole at the back (Figure 3.4b), and locked in position by pulling the detonating cord (Figure 3.4c). After the detonator was locked in, the booster was inserted into the bottom of the blasthole.

Figure 3.4: Booster-detonator with the insertion of the detonator done on the front side (a) and backside (b) of the booster; (c) Locking detonator in position before inserting in the blasthole (Source: Picture taken on site)

The electronic detonator is made up of three interconnected parts (BME, 2017): an aluminium case, a spool of wire, and a connector. The aluminium case encloses a fuse head, a printed circuit board, a primary charge, and a base charge. Both the base charge and primary charge contain PETN/RDX, a highly explosive chemical compound, and DDNP, a chemical compound used for initiating explosives in propellant primer devices respectively. The aluminium case is closed at one end, with the other end connected to a predetermined length of a tubular spool-configured wire with a connector at the end. The other end of the detonating cord is connected to a colour-coded connector clip (see Figure 3.5) which is used to connect the detonator to a harness wire. According to Cardu et al. (2013), electronic detonators can improve blasting results owing to their high precision and wide range of delays. They also claim that electronic detonators can reduce ground vibration when used correctly. This explains the standard operating protocols followed as described above.

Figure 3.5: Colour-coded connector clip (Source: Picture taken on site)

3.3.3 Charging explosives

The process of charging explosives commenced after placing the booster at the bottom of the blasthole. The quarry uses bulk emulsion explosives, a special highly concentrated water-in-oil emulsion. The explosive is made in a two-step process where a supersaturated solution of ammonium nitrate is emulsified together with oil materials into an emulsion explosive matrix (Zhang and Zhao, 2022). The emulsion explosive matrix is then sensitised, using a gassing solution. The gassing solution creates air bubbles within the explosive causing the explosive to expand in volume. The explosive manufacturing process is done at the site where the explosives are to be charged. The explosive components are mixed within the explosive truck, also known as the Mobile Manufacturing Unit or MMU (see Figure 3.6).

Figure 3.6: Explosive truck (Source: Picture taken on site)

An explosive truck is a specialised vehicle intended to house and transport bulk explosive components to the location where the explosive would be produced and deployed (Western Australian Government, 2023). This means that the emulsion components such as ammonium nitrate (AN), oil materials, and gassing solution are only mixed at the desired location just before they are pumped into the blasthole for safety reasons.

In terms of the work, the emulsion explosives were pumped using a hose pipe (Figure 3.8) that extended from the explosive truck. The mass of explosives charged per blasthole was poured as per the blast design. And before loading the blasthole, samples of the emulsion explosive mix were pumped into 200 ml transparent cups (Figure 3.7) to help monitor the gassing process.

Figure 3.7: Gassing process (Source: Photo taken on site)

Figure 3.8: Charging explosives (Source: Photo taken on site)

Gassing is the process of sensitising the emulsion explosive mix by incorporating a gassing solution (Alilovic and Reckzin, 2005). This causes the creation of air bubbles within the explosive mix followed by the expansion in the explosive volume over time (Mishra et al., 2018). This is why the mix was first pumped into the cups to monitor the volume expansion. Thereafter, the mix is then pumped into the blasthole up to a predefined volume less than the desired explosive volume. This is done to accommodate the explosive expansion process.

After pumping the explosive mix into the blast hole, the blaster would wait for approximately 15 min until the gassing process naturally stops. From there, the blaster would use a measuring tape (Figure 3.10) to confirm if the explosives expanded to the required level. If not, then the emulsion would either be added slowly if there was less than required or extracted if the blasthole was overcharged. Excess explosives are extracted using the honey sucker shown in Figure 3.9. This simple tool is made up of a PVC pipe fitted with a PVC ball valve at one end. When there is an explosive overcharge, the end without the fitting is forcefully inserted into the blasthole filled with explosives with the ball valve being open. This forces the explosive to fill into the PVC pipe. The operator then closes the valve and pulls the honey sucker out of the blasthole. Closing the valve creates a vacuum within the pipe that allows for the sucking of a small volume of explosives out of the blasthole.

Figure 3.9: Honey sucker (Source: Photo taken on site)

After the gassing process has been completed, there should be at least 2.5 m (measured from the collar position to the level of the explosive) left for stemming purposes. The quarry relies on a 2-bucket system where two 10-litre buckets of stemming material are used to fill the 2.5 m stemming length.

(a)

(b)

Figure 3.10: (a) Measuring tape (Better blasting, 2024); (b) Measuring the stemming length of each blasthole (Source: Photo taken onsite)

3.3.4 Varistem® stemming plugs

After the gassing process had been completed, the Varistem® stemming plugs (see Figure 3.11) were inserted into each blasthole with the help of a charging stick. Varistem® stemming plugs are high-strength polystyrene plugs that help trap explosive gases within the blasthole for long enough so that the associated energy is directed to the fracturing the rock mass (Rehman et al., 2020). These plugs are manufactured through a process known as dip moulding, which makes them develop flexibility and high tear strength (ERG Industrial, 2023). These two mechanical properties are aimed at improving the effectiveness of the Varistem® stemming plugs. Indeed, during the detonation, a shockwave is released which exerts a force on the Varistem® plug. This force pushes the plug into the stemming material which then creates a temporary pressure seal within the blast-hole. The seal forces the explosive energy and gases to penetrate through the microfractures of the surrounding rock mass thereby weakening it.

Figure 3.11: Varistem® plugs of diameter 102 mm (Source: Photo taken on site)

Varistem® stemming plugs are supplied by ERG Industrial. Plugs with a diameter of 102 mm were used in line with the blast design presented earlier in Table 3.1. Figure 3.12 illustrates the process involved in the installation of the Varistem® stemming plug into the blasthole.

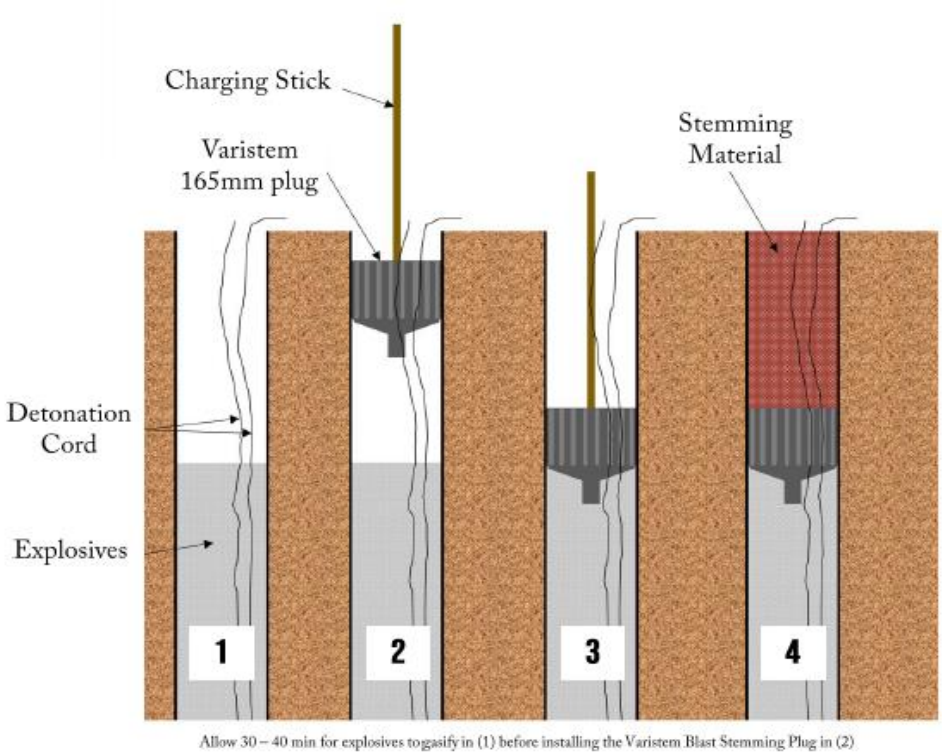

Figure 3.12: Illustration of the process of installing a Varistem® stemming plug (ERG Industrial, 2020)

3.3.5 Stemming material

After the Varistem® stemming plug had been inserted, the stemming process could commence. Mpofu et al. (2021) define stemming as the process of placing an inert material at the top of explosives charged in a blasthole. Stemming therefore helps contain the blast energy and the explosive gases generated during detonation for the effective breakage of the rock mass (Cevizci, 2012).

Stemming can be done using various materials including drill cuttings, clay, sand, and crushed aggregates (Oates and Spiteri, 2021). According to Mpofu et al. (2021), stemming material should have a high density and a high shear strength to be more effective. In one empirical study, Oates and Spiteri (2021) found that crushed aggregates are one of the most effective stemming materials. Mpofu et al. (2021) added that crushed aggregates are cost-effective and can be produced on site to a desirable size. The

Malandvule quarry which is the subject of the present research study uses the crushed aggregates shown in Figure 3.13 for stemming as they are readily produced on-site.

Figure 3.13: Crushed aggregates (Source: Photo taken on site)

The crushed aggregates used for stemming have an average size of 10 mm and are poured into the blasthole using 10-litre buckets. In terms of operating protocols, as the stemming material was being poured into the blasthole, another crew member was busy tamping the material using a tamping pole (see Figure 3.14). Note that tamping is the process whereby the charged stemming material is consolidated into the blasthole by repeated compaction.

Figure 3.14: Tamping of stemming material (Source: Photo taken on site)

Figure 3.15: Blast-hole stemmed to the collar level (Source: Photo taken on site)

3.3.6 AXXIS Titanium logger

An AXXIS Titanium logger is a portable device used to scan the unique identification (UID) of each detonator connector clip and then allocate a delay period to the scanned connector clip. As shown in Figure 3.16, the AXXIS Titanium logger used in this research study features a user-friendly touchscreen interface and a numeric keypad. This allows users to input detonator firing times and connector IDs. The device serves as a stand-

alone tool for blasters to program delays. It can also be seamlessly integrated with BLASTMAP, the equipment software, for enhanced functionality. After the stemming process had been completed, the blaster deployed on site used the AXXIS Titanium logger to scan the electronic detonator connectors. Effectively, the blaster placed the connector clip copper contacts on the logger metal terminals (see Figure 3.17) and allocate the necessary delays as per the blast design specifications.

Figure 3.16: The logger used to program the timing of the detonators on site (Source: Photo taken on site)

Figure 3.17: Illustration of how the connector of the electronic detonator is scanned (Source: Photo taken on site)

After the delay periods had been allocated to all detonators, the delay information was then transferred to the blasting box using the logger. This was done by connecting the logger to the blasting box through a cable.

3.3.7 AXXIS Titanium harness wire

After all the connectors of the electronic detonators had been allocated their respective delays, the harness wire in Figure 3.18 was rolled out across the bench.

Figure 3.18: AXXIS Titanium harness wire (Source: Photo taken on site)

This was done to simplify the process of connecting the connector clips of the electronic detonators to the harness wire as shown in Figure 3.19. The certified blaster had to open the detonator connector clip, connect the harness wire to the connecting points of the clip, and then close the connector clip to fix the wires together. All the detonators were connected in this manner through the harness wire. Finally, the wire was rolled to where the blasting box was placed.

Figure 3.19: How to connect the detonator connector clip to surface wire – (Left) Opening the connector clip; (Centre) Connecting the wire; (Right) Closing the connector clip (Source: Photo taken on site)

3.3.8 Blasting box

The harness wire which was now connected to all the electronic detonators was then connected directly to an AXXIS Titanium blasting box (see Figure 3.20). This was done to establish a connection between the blasting box and the electronic detonators to be initiated. Two AXXIS Titanium boxes were used at the quarry, with one configured as a slave box (blasting box) and the other as a master box (blaster box). The blasting box was directly connected to the harness wire while the blaster box was connected to the blasting box via a wireless connection. The slave box was placed at a line-of-sight distance of about 500 m from the production bench while the master box was placed at about 1000 m away from the slave box.

Figure 3.20: AXXIS Titanium Blasting box (Source: Photo taken on site)

Operating the blasting box is straightforward. It involves dual rotary switches that allow one to power it on, set it to standby mode, and establish communication channels for initiating the actual blast. Dual-directional communication (or two-way communication) had to be established between the blasting box and the detonators. However, prior to the blast, all detonators were thoroughly checked by the blasting box through an electronic interrogation process to ensure clean connectivity. After all this, the actual detonation was then initiated via wireless communication thereby connecting the blaster box to the blast block itself.

After the blasting box had been connected to the detonators through the harness wire, the logger was used to communicate the timing data to the blasting box which generated a one-time PIN. The PIN was used to establish a connection between the slave blasting box and the master blasting box. This activated the master box and made it ready to initiate the blast.

3.3.9 Antenna

The AXXIS Titanium long-range electromagnetic transmitter (ET) plate antenna in Figure 3.21 was used to boost the signal between the blasting box and the blaster box. The antenna was connected to the blasting box via

a cable. The antenna works within a line-of-sight distance that ranges between 1500 m and 5000 m. On the other hand, the blaster box was placed under the blasting shelter and connected to a short-range antenna.

Figure 3.21: The AXXIS Titanium long-range electromagnetic transmitter plate antenna (Source: Photo taken on site)

Both antennas consist of metal conductors designed to transmit and receive radiofrequency (RF) waves. The short-range antenna was used as a transmitter while the long-range ET plate antenna was used as a receiver. The operational principle of this setup is such that when it is time to blast, the blaster would press the firing button. The blaster box would respond by generating RF waves which would be transmitted by the short-range antenna and received by the long-range ET plate antenna. The RF waves would then be converted to electrical signals within the ET plate antenna and transmitted to the blasting box. The blasting box would finally interpret these signals as a blasting command and execute the blast.

3.3.10 Blasting seismograph

A seismograph is a specialised device used for measuring and recording both blast-induced ground and air vibrations. Seismographs are generally

equipped with two sensors: one measuring the ground waves (geophone) and the other measuring the airwaves (microphone).

In the case of the Malandvule quarry, a NOMIS Mini Supergraph seismograph was used to monitor both ground and air vibrations. This specific model has a standard triaxial geophone to monitor ground vibrations ranging between 0 mm/s and 254 mm/s for a ±3% error. This NOMIS seismograph also has a frequency response that ranges between 2 Hz and 400 Hz.

Figure 3.22: NOMIS Mini Supergraph seismograph (Source: Photo taken on site)

To get accurate readings for ground vibrations, the geophone was firmly fixed into the ground. This was done by pushing the geophone spikes (see Figure 3.23) into the ground thereby providing a good coupling between the ground and the spikes. The seismographs were set up 30 min before the blast to ensure that there was enough time to complete of the safety protocols for the blast. This was also to allow the electronics within geophone sensors to stabilise before the monitoring process could begin.

Figure 3.23: Geophone spikes (Source: Photo taken on site)

To this end, both the geophone and the microphone had to be connected to the seismograph before the device could be turned on. Note that the geophone had to be firmly fixed in position before the equipment could be turned on. This was done to prevent any movement of the geophone sensor that may produce inaccurate results. It is also important to say that during the installation of the geophone, the blaster had to make sure that the arrow on top of the geophone transducer (see Figure 3.24) points towards the blast. This helped the transducer to understand the direction of the vibration waves and allowed the accurate recording of incoming vibration data.

Figure 3.24: Geophone transducer arrow (Source: Photo taken on site)

Lastly, the Seismograph was set to Self-trigger mode. This mode of operation is intended for scenarios where data gathering is needed for a brief and precise timeframe. This mode typically last up to 60 s and captures the entire digital waveform for potential printing or analysis at a later stage. It also allows one to set predetermined vibration trigger levels that would enable the equipment to automatically turn on and record the activity for a specified time and then store the data. Once it is done recording, the equipment returns to standby mode, awaiting the next event that surpasses the trigger threshold. The NOMIS seismograph used in this study was calibrated to self-trigger at 0.25 mm/s. It was calibrated at that value to help the seismograph start recording the vibrations before they could be perceived by humans.

The following section focuses on how the recorded data was processed.

3.4 Data processing

After the seismograph was done recording each blast event, the blaster would connect it to a computer. Installed on the dedicated computer is the SuperGraphics software, which was supplied along with the Mini-Supergraph seismograph. This specialised software allows the computer to download the raw data from the seismograph. Once files are downloaded, they are stored in a subdirectory of the SuperGraphics directory. These files contain all relevant user data such as the company name, seismograph location, date and time, operator, and all the recorded vibration data and signal waveforms. The collected blasting data was exported to a Microsoft® Excel® spreadsheet for easy access, analysis and interpretation. Two categories of blasting data were available, i.e., blasts with and without stemming plugs as explained at the beginning of this chapter in Section 3.1.

3.4.1 Empirical modelling of the PPV data collected

Several empirical models of ground vibrations were used to make sense of the contribution of the stemming plugs to blast-induced ground vibrations. These models have two fundamental parameters: the maximum explosive charge per delay Q and the distance R between the blasting area and the monitoring site. The empirical models also contain two site-specific parameters: K and β. The two parameters are dependent mainly on the geological and geo-mechanical factors of the site as well as the specific blasting design used. Table 3.2 shows the four empirical models of ground vibrations used to probe the blast data collected. Note that the table is a summary of the review work covered in Section 2.3.

Table 3.2: List of empirical models used to analyse the data collected on site

Model name and reference	**Equation**
USBM (Duvall and Fogelson, 1962)	$PPV = K\left(\frac{R}{Q^{0.5}}\right)^{-\beta}$
Langefors-Kihlstrom (1978)	$PPV = K\left(\frac{R^{1/3}}{\sqrt{Q}}\right)^{-\beta}$
BIS (1973)	$PPV = K\left(\frac{R^{2/3}}{Q}\right)^{-\beta}$
Ambraseys-Hendron (1968)	$PPV = K\left(\frac{R}{Q^{1/3}}\right)^{-\beta}$

For all the equations in Table 3.2, PPV represents the peak particle velocity (mm/s); Q is the maximum explosive charge per delay (kg); R is the distance from the blast area to the monitoring station (m); K and β are site-specific coefficients which were calculated by means of regression analysis.

Khandelwal and Singh (2006) stated that ground vibrations can be influenced by factors such as the geological properties of the site as well as the blast design and explosives used. The empirical models in Table 3.2 specifically speak to the blast design captured in the maximum explosive Q charge per delay and the distance R between the blasting area and the monitoring site. In contrast, the combined effects of the geomechanical

properties and the remaining blast design parameters are accounted for by the two coefficients K and β. According to Hossaini and Sen (2004), K and β are somehow descriptive of the type of explosives used and the geomechanical properties of the rock mass.

To better understand the contribution of the stemming plugs in reducing ground vibrations, the empirical models in Table 3.2 were employed along with the necessary input data collected during the blast tests. These equations were used to curve-fitted to the data to allow the following:

- A comparison and ranking of the four models in terms of how best each describes the on-site ground vibration data generated with or without stemming plugs.
- A comparison of the levels of blast-induced ground vibrations recorded with and without Varistem® stemming plugs.

The four empirical predictor models in Table 3.2 were ranked in terms of their performance using the following evaluation metrics:

- Mean Absolute Error (MAE)
- Coefficient of determination (R^2)
- Root Mean Squared Error (RMSE).

When it came to highlighting the contribution of the Varistem® plugs, statistical hypothesis testing was employed to compare PPV values produced with and without stemming plugs. The success rate and significance of the comparison were ascertained at the confidence level of 95% commonly used in engineering research.

A brief overview of the hypothesis testing as was carried out in this research study is presented in the following subsections.

3.4.2 Applying Student's t-distribution test

Statistical hypothesis testing was resorted to in this work to determine if the Varistem® stemming plugs contribute towards the reduction of blast-

induced ground vibrations. This was done by assessing whether a statistical difference in PPVs at a 95% significance existed between blasting with or without stemming plugs. This is represented as follows:

$$\begin{cases} H_0: \mu = 8.48\ \mathrm{mm/s} \\ H_1: \mu \neq 8.48\ \mathrm{mm/s} \end{cases} \tag{3.5}$$

Where $H_0: \mu \geq 8.48\ \mathrm{mm/s}$ is the null statement stating no difference between conventional and Varistem® blasts while $H_1: \mu < 8.48\ \mathrm{mm/s}$ is the alternative statement.

A two-tailed test was conducted since this section seeks to establish whether there is a difference between Varistem® and conventional PPVs. Student's t-distribution was assumed to describe the PPV data (MacFarland and Yates, 2021). This is because the standard deviation of both conventional and Varistem® blasts was unknown a priori and their respective sample sizes were below 30 blasts.

3.4.3 Presentation of the ground vibration data collected

For this study, the data and associated results were mostly presented in tabular, mathematical, and graphical formats. Indeed, the raw data corresponding to the ground vibrations recorded from the seismographs were presented in tables while empirical models were expressed mathematically. The PPV data was then processed through empirical modelling and presented graphically.

3.4.4 Customisation of the statistical test

The best empirical model for the PPV data was used for statistical testing. Chapters 4 and 5 later shows that the BIS model was selected as the best model. The BIS model applied to conventional and Varistem® PPV data was then subjected to Student's t-test. This statistical test was to establish whether the Varistem® PPVs were significantly different to the conventional

PPVs. The BIS model was used as a substitute for actual data because it was easier to compare the estimated values of K and β corresponding to conventional and Varistem® blasting respectively.

3.5 Challenges and limitations of the study

Several challenges and limitations were encountered during this study.

First, there was very limited time to collect enough data as required by the research objectives set out for this study without disturbing production very much. One was hoping to get a chance to also collect data for the conventional blast as well but was only limited to historical data. This is because of safety concerns and regulatory requirements not to exceed 134 decibels (dB) of air blast amongst others.

Another limitation was that the quarry restricted access to the geological and geomechanical data. This limited the study in terms of looking at the propagation of ground vibration waves through different rock formations before reaching the monitoring stations. Some blastholes also took more explosives than anticipated, which could be the result of explosives flowing into wider cracks and pockets than filling the blasthole. This resulted in the uneven distribution of explosives that led to the generation of higher ground vibrations. And in some cases, the blaster would go ahead with overcharged or undercharged blast-holes while trying to catch up with the blasting schedule. These discrepancies would also translate into inconsistent intensities of the ground vibration generated during the blast.

Finally, the rainy weather was another challenge. Some drill holes would be filled with mud and water caused by rain making it difficult to clean them before the explosives could been charged. Consequently, less explosives were loaded when the blasthole was not cleaned properly with undesirable outcomes.

Chapter 4 Modelling the blast-induced ground vibrations with and without stemming plugs

4.1 Introduction

This chapter focuses on analysing the data collected in Chapter 3. Input data such as the distance between the blast area and the seismograph location as well as the maximum charge per delay were used in processing the vibration data. The scaled distance method was employed along with four empirical ground vibration models covered in Section 3.4.1 to make sense of the collected data. The peak particle velocities (PPVs) for both the conventional and the Varistem® blasts were plotted and analysed for qualitative trends. The two set of PPV data were then compared to see whether the Varistem® blast can consistently induce lower PPV levels than the conventional blast.

The subsequent sections present the results extracted from the raw data collected in Chapter 3 as well as the outcome of the empirical modelling.

4.2 Recorded vibration data

This section presents the relevant vibration data collected before and after blasting. The data collected before the blast includes the distance from the blast and the maximum charge weight per delay. On the other hand, the data collected after the blast includes PPV, scaled distance, and seismographs. All this data can be extracted from the seismograph report. The said report is divided into five sections as shown in Section 4.2.1. This information is presented below to give an overall view of the type of data produced by the seismograph.

4.2.1 Vibration data report

4.2.1.1 Report heading

The first section of the report shows the user data of the report (see Figure 4.1). It states the location of the seismograph, the date on which the event was recorded, the distance between the blast and the seismograph, the maximum weight charge per delay, and the scaled distance. The scale distance was calculated using the USBM equation.

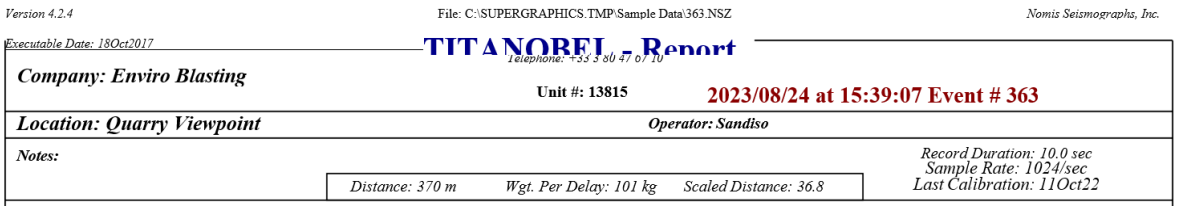

Figure 4.1: All user data (Source: Malandvule Quarry)

4.2.1.2 Seismic table

Table 4.1 exemplifies the seismic data expressed as PPV and frequency and recorded by the seismograph during a specific blast. The PPV is presented as a vector with the corresponding radial component, transverse component, and vertical component. Each component also comes with its corresponding frequency. Table 4.1 finally indicates the vector sum of the three components and their frequencies.

Table 4.1: Seismic data of a recorded blast (Source: Malandvule Quarry)

Seismic

Gain: 1 Trigger: 1.016 mm/s ▽ Vector Sum: 3.19 mm/s @ 16.52 Hz

Channel	Radial	Transverse	Vertical
○ Velocity (mm/s)	1.778	1.778	2.889
Frequency (Hz)	22.20	28.40	16.50
Trigger >>> Peak	198.2	450.2	460.9

4.2.1.3 Air blast table

The third section of the report contains the air blast data (see Table 4.2). The table states the magnitude of the air pressure in kilopascals (kPa), its value recorded in decibels linear (dBL), and the corresponding frequency.

Table 4.2: Air blast data (Source: Malandvule Quarry)

Air

Gain: 1 Air Trigger: 125 dBL

Measurement	**Value**	Trigger >>> Peak	
		1090.8	
kPa	.1394		
dBL	**136.9**		
Hz	4.1		

4.2.1.4 Seismic scale graph

The fourth section of the report is dedicated to the seismic scale graphs of the various PPV components and the corresponding air blast. As illustrated in Figure 4.2, the first three graphs represent the radial (labelled R on the y-axis), transverse (T), and vertical (V) components of the PPV signal while the last graph denotes the air blast (A). The small circle on each of the four seismic graphs points out the maximum PPV or air blast value recorded during the blast.

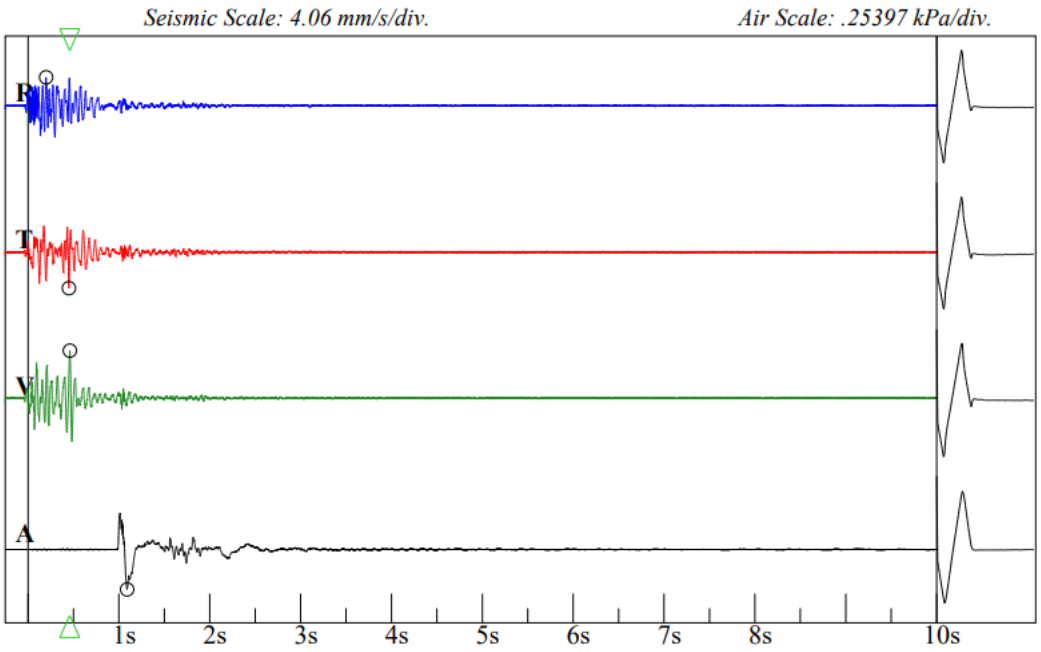

Figure 4.2: Seismic scale graph (Source: Malandvule Quarry)

4.2.1.5 USBM model graph

The last section presents the USBM model diagram. As shown in Figure 4.3, this is a log-log plot of the PPV as a function of frequency. The diagram also shows the limit line that PPV should not exceed to avoid any structural damage to nearby buildings. One may refer to Figure 2.4 and Section 2.3 of the literature review, i.e., Chapter 2, for a detailed presentation of this concept. Lastly, several coloured alphabets show the varying magnitudes of the PPV components as recorded by the seismograph. In this case, it can be noted that all labelled data points are below the limit Z-shaped line suggesting that safe blasting was performed.

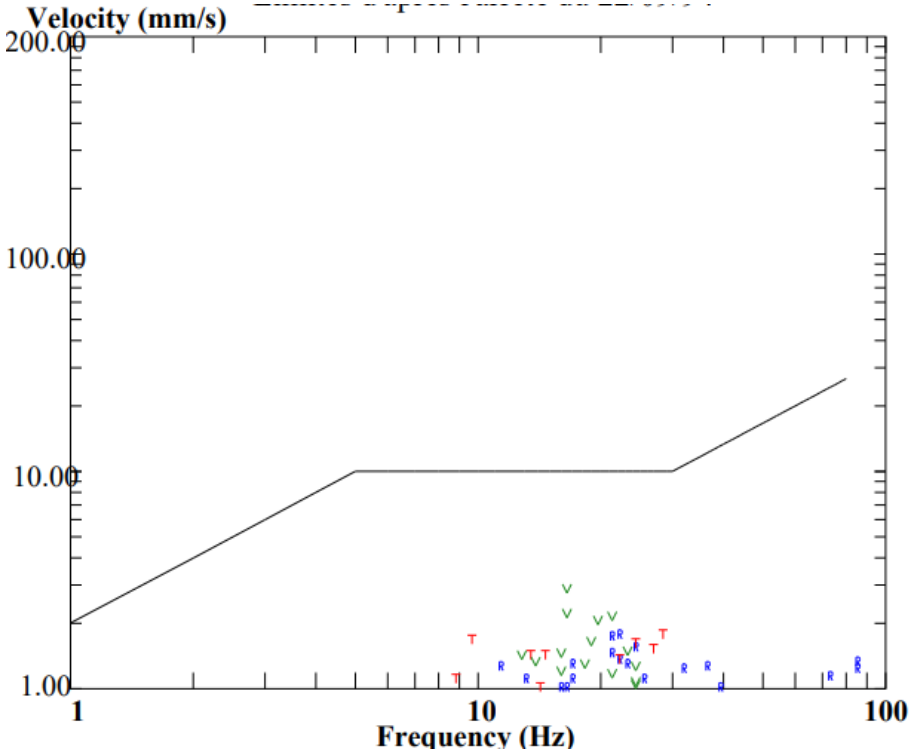

Figure 4.3: USBM model diagram (Source: Malandvule Quarry)

4.2.2 Historical data retrieved from the Quarry's archives

Historical data was retrieved from the archives of the quarry to form what is referred to in this work as conventional blast data, i.e., blasts done without the use of the Varistem® plugs. This data was comprised of data collected prior to the implementation of the Varistem® plugs as part of stemming practices. The information also came in the form of seismic reports like that presented in Section 4.2.1.

Table 4.3 provides a summary of the data extracted from all the historical data reports.

Table 4.3: Conventional blast vibration data

Blast #	Station A			Station B		
	R (m)	Q (kg)	PPV (mm/s)	R (m)	Q (kg)	PPV (mm/s)
1	325	366.8	14.57	345	366.8	8.24
2	341	65.0	3.63	293	65.0	7.14
3	360	61.0	4.36	465	61.0	3.98
4	258	75.0	7.20	585	75.0	3.89
5	352	319.3	7.24	315	319.3	7.34
6	320	70.0	4.14	430	70.0	4.62
7	305	309.2	11.07	420	309.2	5.92
8	186	386.5	14.66	295	386.5	8.10
9	209	100.0	7.68	660	100.0	3.83
10	220	368.6	12.96	345	368.6	6.63
11	215	95.0	7.87	620	95.0	3.54
12	330	105.0	6.32	470	105.0	5.43

4.2.3 Data collected during the actual on-site trials

The Varistem® blast data refers to the data collected with the implementation of the Varistem® stemming plugs. The corresponding ground vibration data was collected on-site using the seismographs as detailed in Section 3.4.

After each blast, a seismograph report that is similar to the illustrative report described in Section 4.2.1 was produced. The data extracted from all the reports generated for each blast were processed and populated as shown in Table 4.4.

Table 4.4: Varistem® blast vibration data

Blast #	Station A			Station B		
	R (m)	Q (kg)	PPV (mm/s)	R (m)	Q (kg)	PPV (mm/s)
1	411	90	2.82	327	90	3.62
2	370	478.7	3.65	322	478.7	5.05
3	235	419.2	3.8	456	419.2	4.12
4	151	82	3.17	553	82	2.77
5	220	479.9	4.18	392	479.9	3.81
6	128	106	3.73	585	106	3.23
7	320	475.4	3.65	585	475.4	4.65
8	470	111	2.45	286	111	3.95
9	168	490.7	5.59	312	490.7	4.18
10	383	517	4.27	540	517	4.27
11	215	262	3.88	427	262	3.88
12	434	374.7	3.73	314	374.7	4.93
13	265	434.0	3.78	299	434.0	5.58
14	210	592.7	4.66	110	592.7	6.36
15	250	364.4	4.5	342	364.4	4.13

4.3 Empirical modelling of historical ground vibration data

Four empirical models of ground vibration were employed to determine the most suitable for the Malandvule quarry because of their widely accepted use (Bhagwat and Dey, 2016; Hasanipanah et al., 2015; Ongen et al., 2018; Ragam and Nimaje, 2018; Xue, 2019; Zhou et al., 2020). The scaled distance of each model (i.e., SD_1, SD_2, SD_3, SD_4) was calculated following their respective definitions in Equations (2.2) to (2.5). This was applied to the data in Table 4.3 while the resultant scaled distances and their peak particle velocities were interpreted graphically. Figures 4.4 – 4.11 show the resulting plots per empirical model and monitoring station produced from the historical data only.

4.3.1 Curve-fitting with the USBM model

The squared root scaled distance formula in Equation (2.2) was used to calculate the scale distance SD_1. This scaled distance was then used along with the corresponding measured historical PPV to determine the site-specific parameters K and β. The empirical model was used on the data sets collected from both the stations, Station A and Station B.

Figure 4.4 depicts the variation of PPV values with the corresponding scaled distances SD_1 as was recorded at Station A before the advent of the Varistem® plugs. In contrast, Figure 4.5 shows similar types of results at Station B.

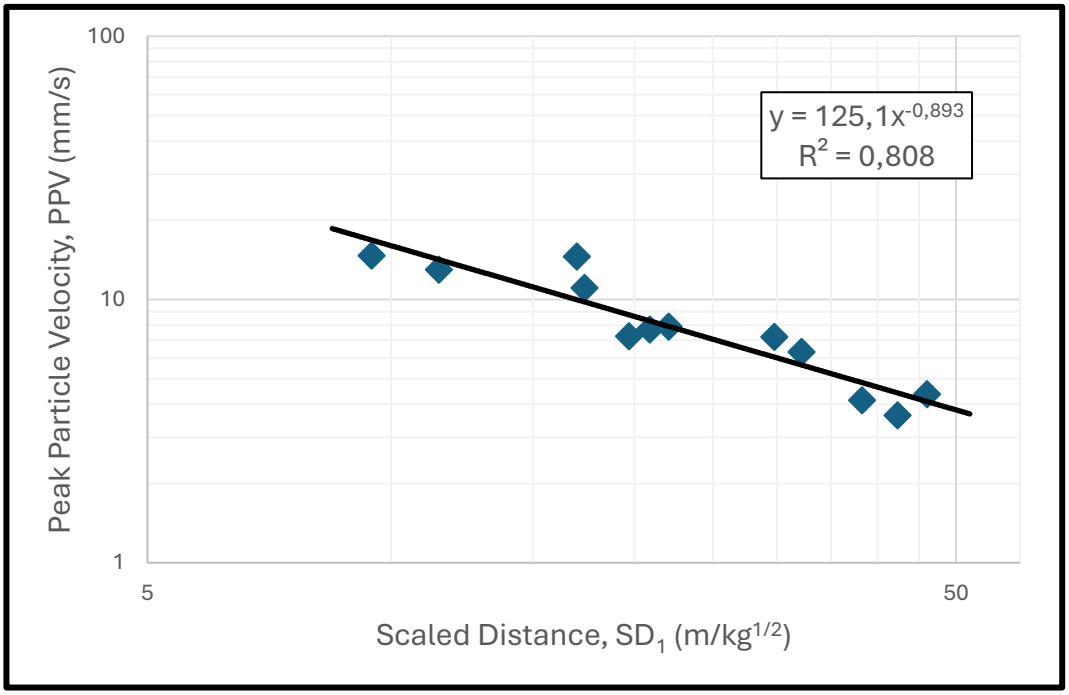

Figure 4.4: Nonlinear regression of the historical Peak Particle Velocity (PPV) vs Scaled Distance (SD) using the USBM model (i.e., Equation 2.2) at Station A

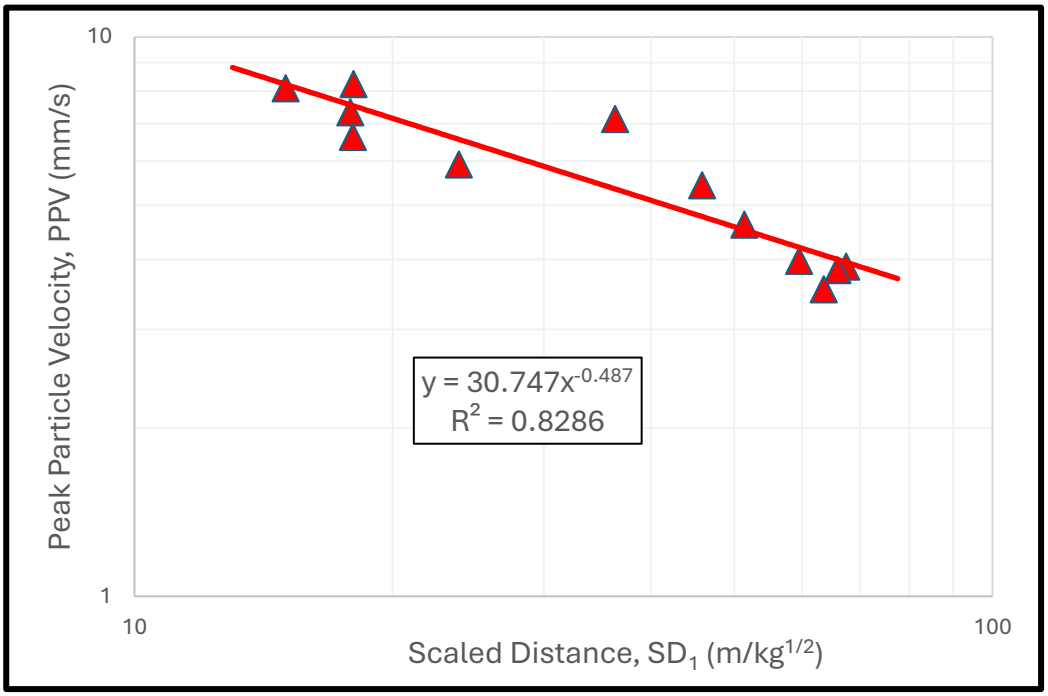

Figure 4.5: Nonlinear regression of historical PPV vs SD using the USBM model (i.e., Equation 2.2) at Station B

The visual comparison of Figure 4.4 and Figure 4.5 suggests that the farthest a monitoring station is, the higher the K and β values become. The value of R^2 is higher at Station B than at Station A. This is an indication that the USBM model describes the data from the closest station better than it does for the farther Station A.

4.3.2 Curve-fitting with the Ambraseys-Hendron model

The cubed-root scaled distance in Equation (2.3) was used to calculate the scaled distance for the Ambraseys-Hendron model. The resultant scaled distance was used along with the site-recorded PPV to determine the curve-fitting parameters descriptive of this empirical model for both monitoring stations, see Figures 4.6 and 4.7.

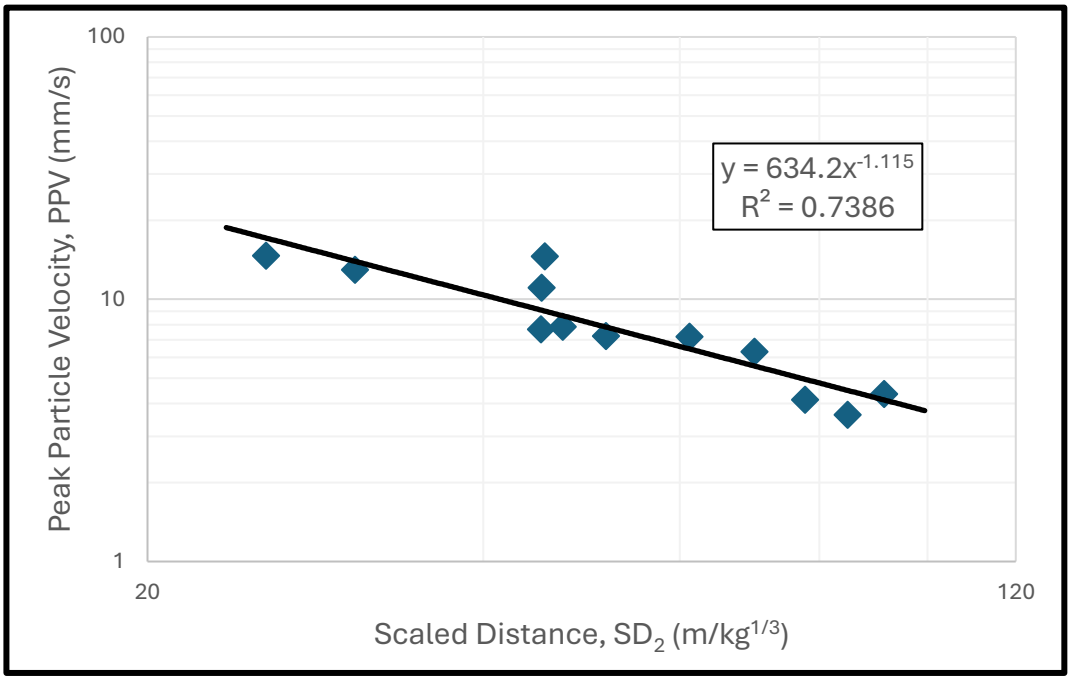

Figure 4.6: Nonlinear regression of historical PPV vs SD using the Ambraseys-Hendron model (i.e., Equation 2.3) at Station A

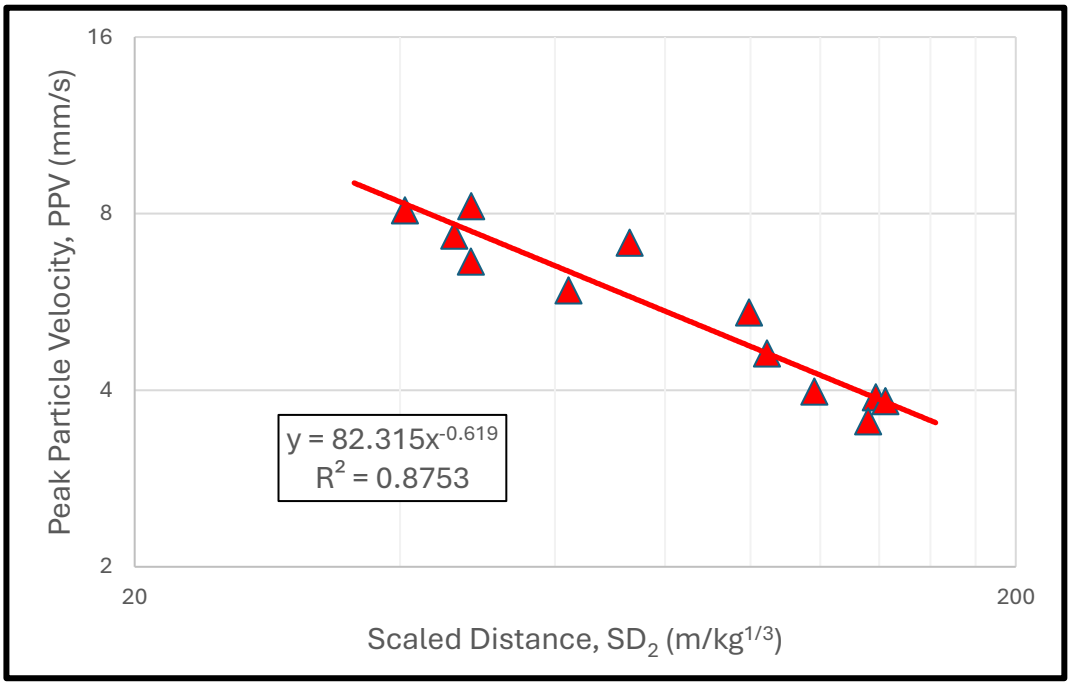

Figure 4.7: Nonlinear regression of historical PPV vs SD using the Ambraseys-Hendron model (i.e., Equation 2.3) at Station B

It seems as if the trend observed with the USBM model is also valid for the Ambraseys-Hendron model. And although the models are different in structure, they seem to behave the same.

4.3.3 Curve-fitting with the Langefors-Kihlstrom model

Equation (2.4) was used to calculate the scaled distance for the Langefors-Kihlstrom model. A similar method to that used in the previous two empirical models was also applied to produce similar graphs for this model. These are given by Figures 4.8 and 4.9.

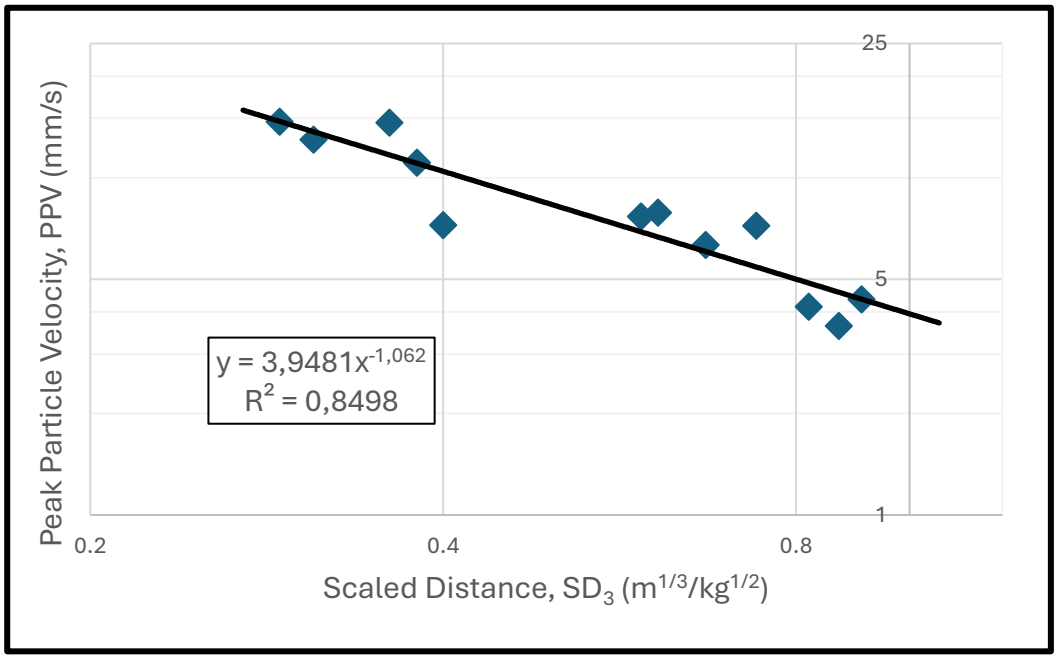

Figure 4.8: Nonlinear regression of historical PPV vs SD using the Langefors-Kihlstrom model (i.e., Equation 2.4) at Station A

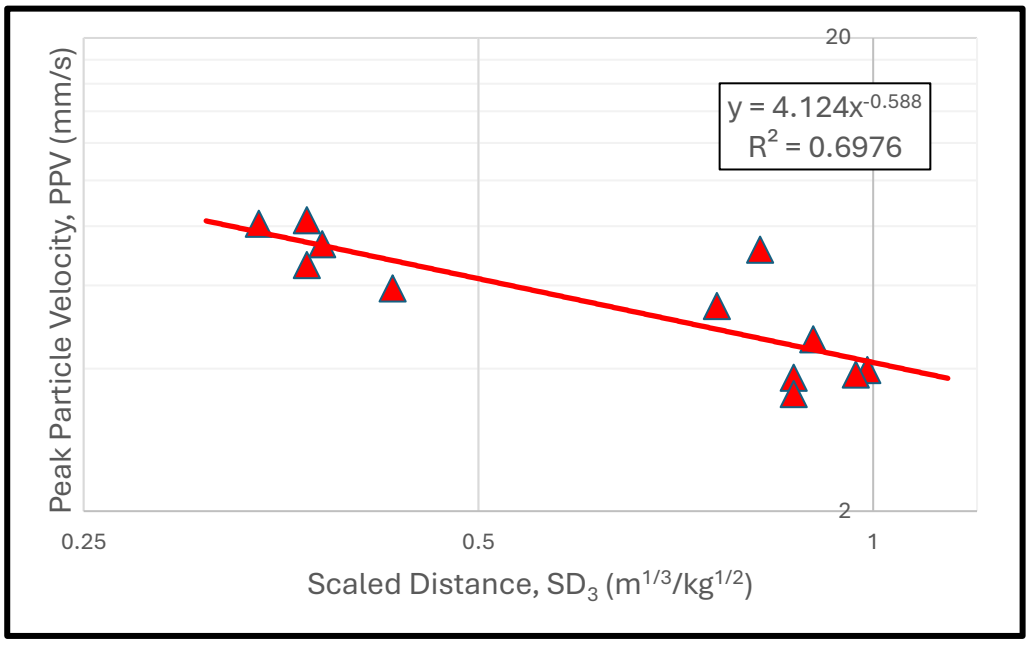

Figure 4.9: Nonlinear regression of historical PPV vs SD using the Langefors-Kihlstrom model (i.e., Equation 2.4) at Station B

An interesting and rather peculiar observation is made with the Langefors-Kihlstrom model. Differently to the models presented in Sections 4.3.2 and 4.3.3, the K value seems to be lower for Station A compared to Station B. However, the β value still shows similar behaviour to the one observed in Figures 4.4 and 4.5. Another interesting observation is that the R^2 value is lower for the closest station, i.e., Station B. This means that the Langefors-Kihlstrom model seems to describe the data well at the farthest station, Station A, as opposed to the scatter observed at Station B.

4.3.4 Curve-fitting with the BIS model

The scaled distance for this model was calculated using Equation (2.5). Here also, this scaled distance was used along with the corresponding PPV to plot their relationship at the two monitoring locations as shown in Figures 4.10 and 4.11 respectively.

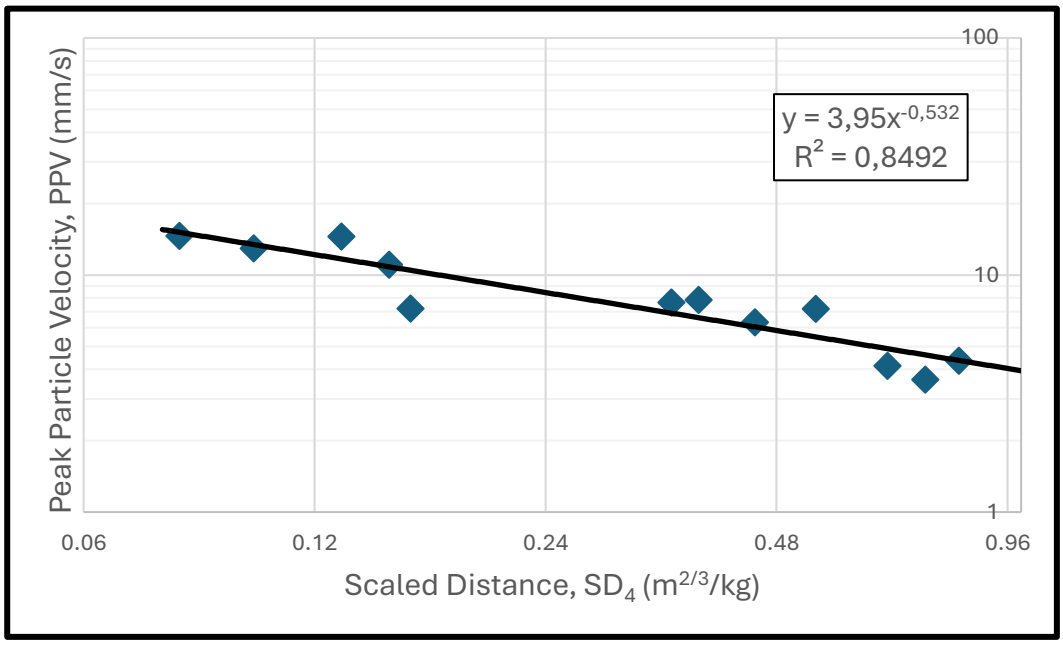

Figure 4.10: Nonlinear regression of historical PPV vs SD using the BIS model (i.e., Equation 2.5) at Station A

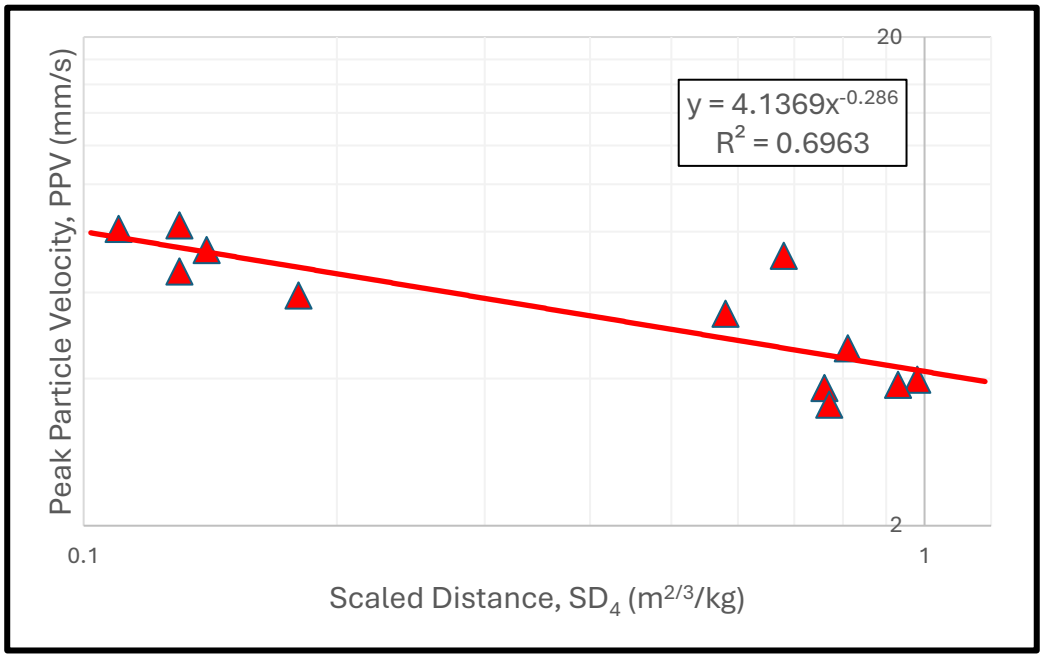

Figure 4.11: Nonlinear regression of historical PPV vs SD using the BIS model (i.e., Equation 2.5) at Station B

The trend observed in the previous Section 4.3.3 is also observed in Figure 4.10 and Figure 4.11. In other words, the USBM and the Ambraseys-

Hendron models depicted a similar trend and, in the same way, the Langefors-Kihlstrom and the BIS models behaved similarly.

4.3.5 Summary of the curve-fitted site parameters produced from the historical ground vibration data

Table 4.5 provides a summary of the estimated parameters characteristic of the quarrying site for all four empirical models considered and according to the seismograph locations. These site-specific parameters (i.e., K and β) were found by means of nonlinear regression. Table 4.5 also states the coefficients of determination (R^2) for the four empirical models used.

Table 4.5: Estimates of the curve-fitted site parameters and corresponding coefficients of determination for the conventional ground vibration data

Model name	Seismograph location	K	β	R^2
USBM (Duvall and Fogelson, 1962)	Station A	125.1	0.893	0.808
	Station B	30.7	0.487	0.829
Ambraseys and Hendron (1968)	Station A	634.2	1.115	0.739
	Station B	82.3	0.619	0.875
BIS (IS6922), 1973	Station A	3.95	0.532	0.849
	Station B	4.1	0.286	0.696
Langefors and Kihlstrom (1978)	Station A	3.9	1.062	0.850
	Station B	4.1	0.588	0.698

It can be noted that both the BIS and the Langefors-Kihlstrom models predict PPV better when the monitoring station is located farther away from the blasting area. On the other hand, the USBM and the Ambraseys-Hendron models respond relatively poorly when ground vibrations are monitored farther away from the blasting area. The β value seems to behave in the same manner regardless of the model used. Indeed, β seems to increase as one moves farther away from the source. Interestingly, there

seems to exist an inverse relationship between the K-factor and the corresponding value of R^2 for all four models. Indeed, the lower the K-factor, the higher the value of R^2 is.

4.4 Empirical modelling of ground vibration levels after incorporating stemming plugs

This section presents the data collected with the use of Varistem® stemming plugs. Here also, this data was extracted from seismic reports similar to those described in Section 4.2.1 The data called Varistem® data in this dissertation is summarised in Table 4.4. Note that the Varistem® ground vibration data is also reported for the two stations; namely, the farthest Station A and closest Station B.

In terms of empirical modelling, both the distance and weight charge data were first used to calculate the various scale distances as was done in Section 4.3. Thereafter, the resulting scaled distances (i.e., SD_1, SD_2, SD_3, SD_4) were used along with their corresponding PPVs to plot the relevant graphs. Figures 4.12 – 4.19 in the subsections below show the resulting curve-fits and data plots per empirical model and monitoring station produced from the Varistem® ground vibration data.

4.4.1 Describing the Varistem® ground vibration data using the USBM model

The scaled distance SD_1 was calculated the same way as was done in Section 4.3.1, i.e., Equation (2.2). This scaled distance was then used with the relevant PPV data to produce Figures 4.12 and 4.13 as monitored in Station A and Station B respectively.

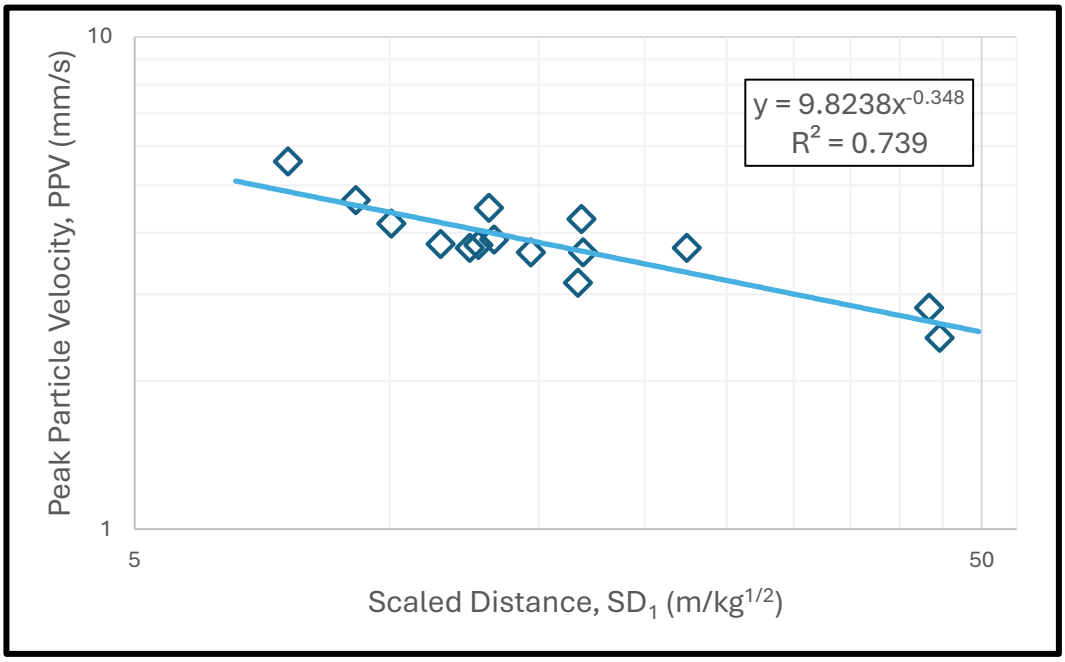

Figure 4.12: Nonlinear regression of Varistem® PPV vs SD using the USBM model (i.e., Equation 2.2) at Station A

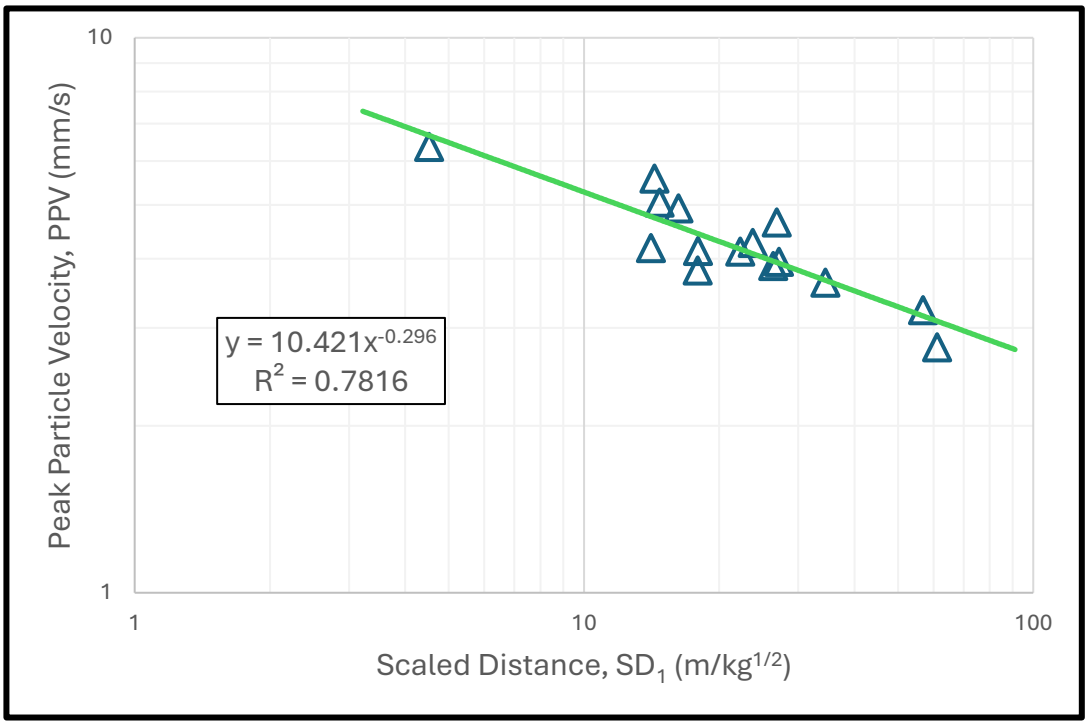

Figure 4.13: Nonlinear regression of Varistem® PPV vs SD using the USBM model (i.e., Equation 2.2) at Station B

It can be seen from Figures 4.12 and 4.13 that the closer the monitoring station is to the blast area, the higher the K-factor and the lower the β value.

Also, the model works better when the monitoring station is closer as is reported by the higher value of R^2 at the closest Station B.

4.4.2 Describing the Varistem® ground vibration data using the Ambraseys-Hendron model

Here, Equation (2.3) was used to calculate the scale distance of the Ambraseys-Hendron model. Figures 4.14 and 4.15 show PPV plotted against the scaled distance, SD_2, at Station A and Station B respectively.

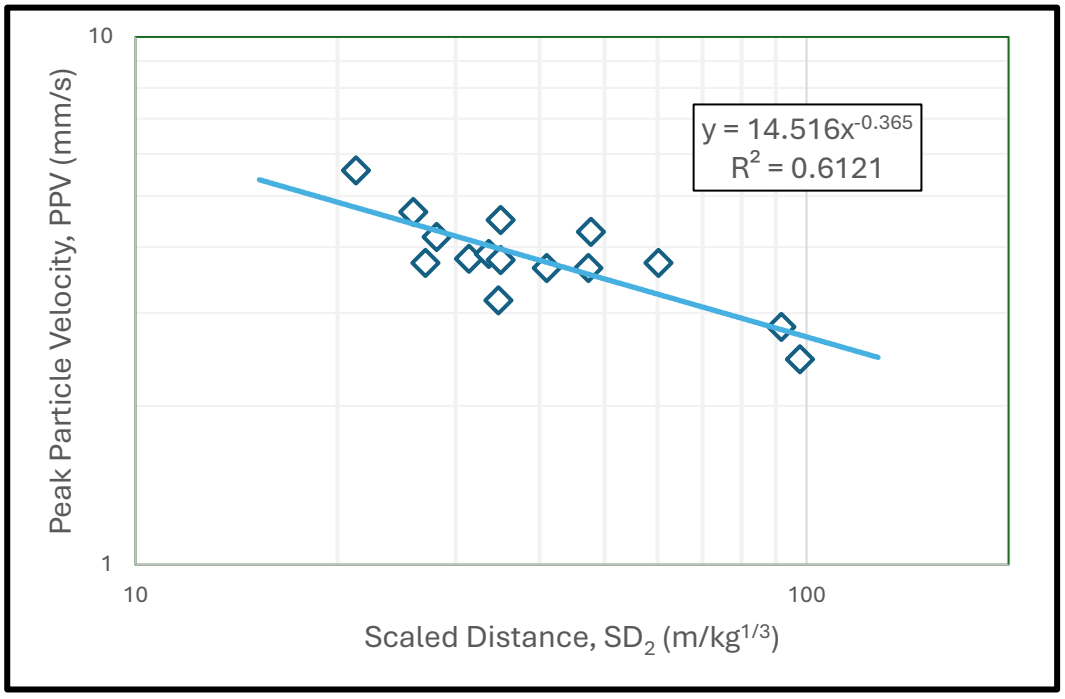

Figure 4.14: Nonlinear regression of Varistem® PPV vs SD using the Ambraseys-Hendron model (i.e., Equation 2.3) at Station A

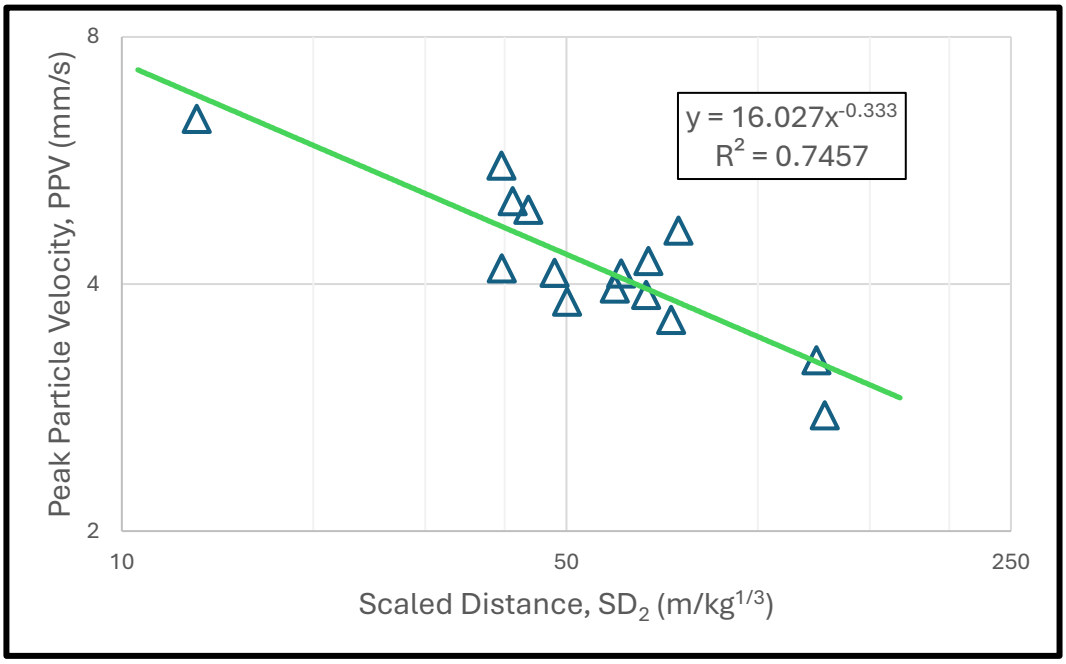

Figure 4.15: Nonlinear regression of Varistem® PPV vs SD using the Ambraseys-Hendron model (i.e., Equation 2.3) at Station B

As alluded to in Section 4.3.2, the Ambraseys-Hendron model seems to follow a similar trend to the one displayed by the USBM model. Indeed, the Ambraseys-Hendron model also describes the data better for the station located closer, Station B, as opposed to the farther station.

4.4.3 Describing the Varistem® ground vibration data using the Langefors-Kihlstrom model

The scaled distance, SD_3, for the Langefors-Kihlstrom model was calculated using Equation (2.4). The resultant scaled distance and corresponding PPV were then plotted to produce Figures 4.16 and 4.17 representative of the data collected at Station A and Station B respectively.

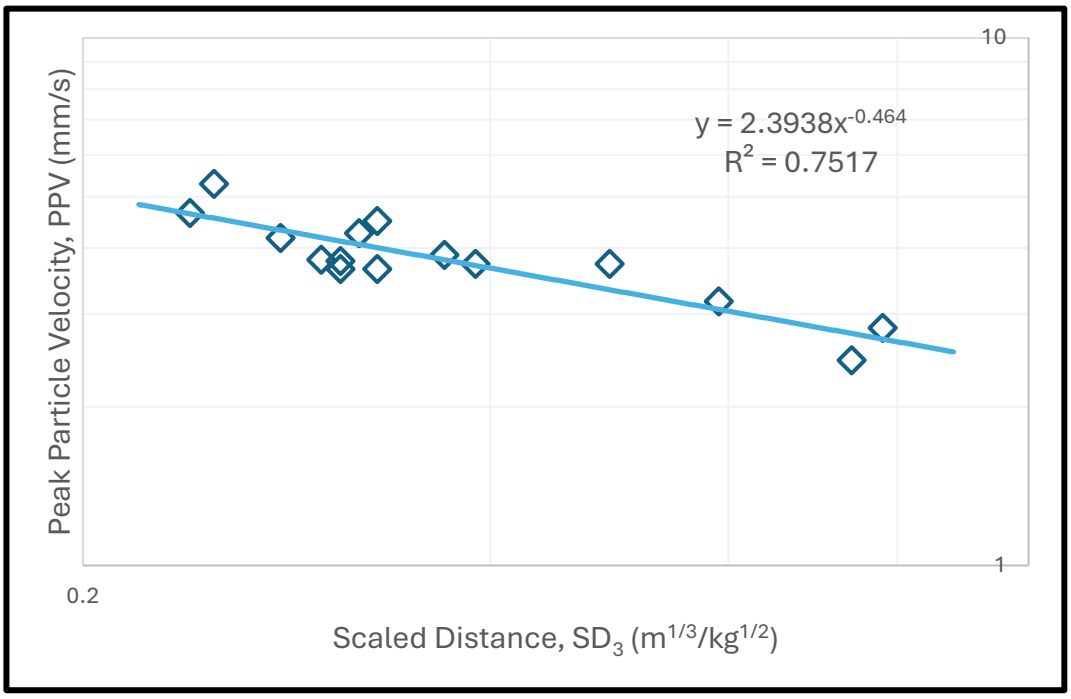

Figure 4.16: Nonlinear regression of Varistem® PPV vs SD using the Langefors-Kihlstrom model (i.e., Equation 2.4) at Station A

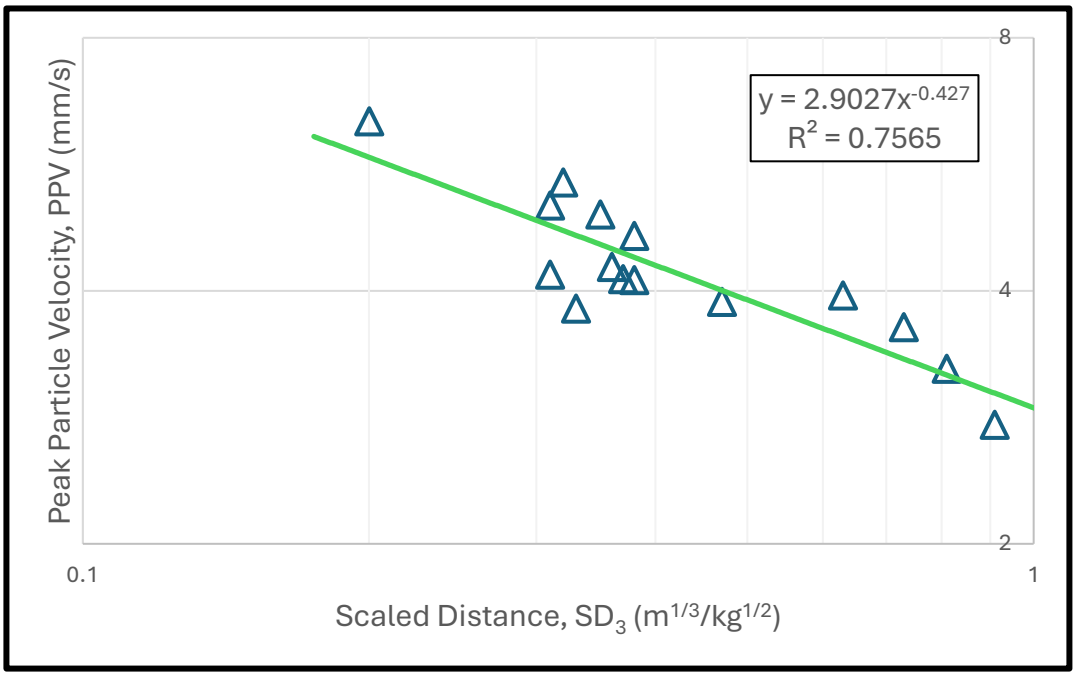

Figure 4.17: Nonlinear regression of Varistem® PPV vs SD using the Langefors-Kihlstrom model (i.e., Equation 2.4) at Station B

In this case, the Langefors-Kihlstrom model seems to display similar traits as both the USBM and the Ambraseys-Hendron models. Indeed, the

qualitative comparison of analyses and conclusions made in Section 4.3.1, 4.3.2, and 4.3.3 suggests that the three empirical models lead to similar conclusions when describing the Varistem® ground vibration data.

4.4.4 Describing the Varistem® ground vibration data using the BIS model

Figures 4.18 and 4.19 are graphical representations of the scaled distance, SD_4, as per the BIS model plotted against corresponding PPV for the two monitoring stations. The scale distance for this model was calculated using Equation (2.5).

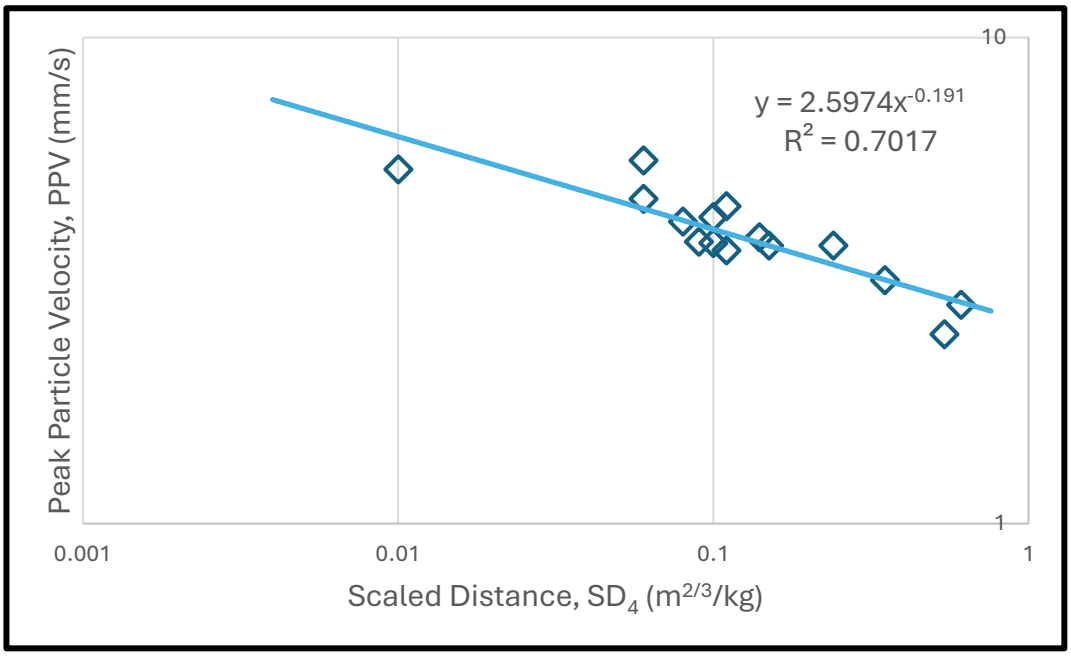

Figure 4.18: Nonlinear regression of Varistem® PPV vs SD using the BIS model (i.e., Equation 2.5) at Station A

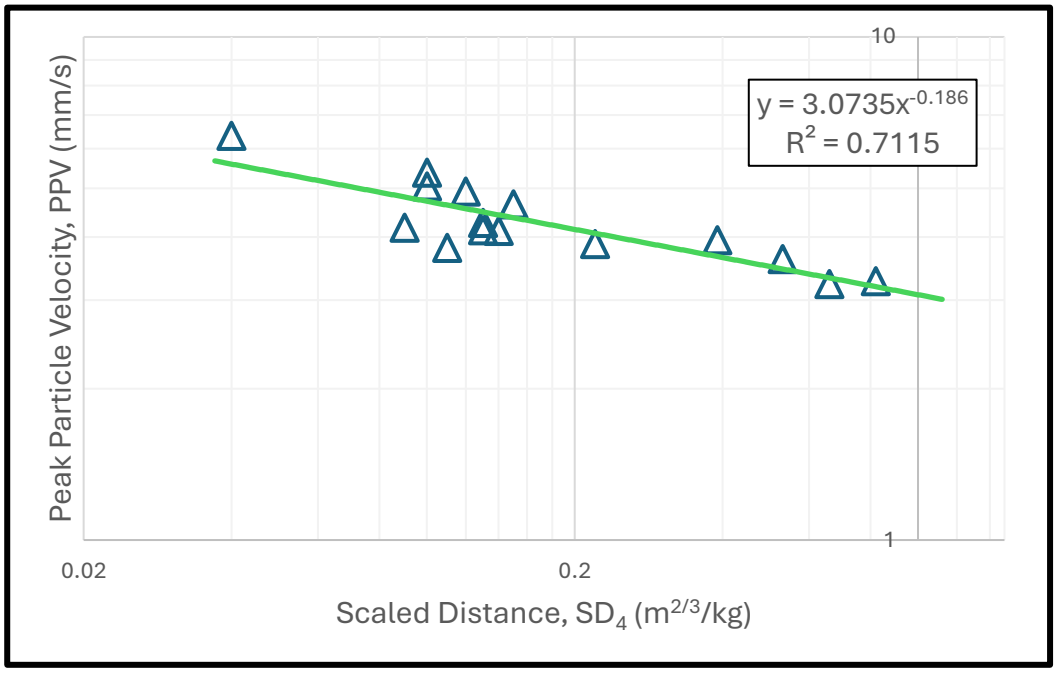

Figure 4.19: Nonlinear regression of Varistem® PPV vs SD using the BIS model (i.e., Equation 2.5) at Station B

Interestingly so, The BIS model also exhibited similar behaviour to the other three regardless of their differences. The R^2 value for the BIS model is almost equal for both stations, meaning that the distance from the station to the source of the blast does not significantly affect the performance of the BIS model.

4.4.5 Summary of the curve-fitted site parameters produced from the Varistem® ground vibration data

Table 4.6 gives a summary of the estimated site-specific parameters (i.e., K and β) for all four empirical models and at the two seismograph locations. These parameters were derived from the Varistem® data in Table 4.4.

By and large, the USBM and the Ambraseys-Hendron models produced comparable values of K and β. In the same way, the Langefors-Kihlstrom and the BIS models yielded similar K and β values.

Table 4.6: Estimates of the curve-fitted site parameters and corresponding coefficients of determination for the Varistem® ground vibration data

Model name	Seismograph location	K	β	R^2
USBM (Duvall and Fogelson, 1962)	Station A	9.8	0.348	0.739
	Station B	10.4	0.296	0.782
Ambraseys and Hendron (1968)	Station A	14.5	0.365	0.612
	Station B	16.0	0.333	0.746
BIS (IS6922), 1973	Station A	2.6	0.191	0.702
	Station B	2.9	0.186	0.712
Langefors and Kihlstrom (1978)	Station A	2.4	0.464	0.752
	Station B	2.9	0.427	0.757

4.5 Summarised findings

A set of blast field trials was conducted on the possibility of using the Varistem® stemming plugs to reduce blast-induced ground vibrations. This then enabled the comparison of the level of blast-induced ground vibrations produced with and without Varistem® stemming plugs. A total of 27 production blasts was considered, 12 blasts were collected from historical blasts where conventional stemming without Varistem® plugs was standard practice while the remaining 15 blasts were conducted on site using the stemming plugs as a later adoption by the quarry. In both cases, aggregates were employed as stemming material.

Two NOMIS Mini Supergraph seismographs were used to monitor the blast events and record ground vibrations. These seismographs were positioned in two different locations; namely, Station A and Station B. Station B was located closer to the blasting area while Station A was a bit further away. The ground vibration data recorded by the two seismographs was then used for analysis. Four empirical predictor models (i.e., USBM, Ambraseys-Hendron, Langefors-Kihlstrom, and BIS) were curve-fitted to the data. Comparative analysis was applied to contrast the data recorded for Station

A and Station B while qualitatively assessing the performance of each empirical model.

For the historical/conventional data, the visual comparison of the USBM model suggested that the further the monitoring station is, the higher the K and β values become. The value of R^2 was higher for Station B compared to Station A. The Ambraseys-Hendron model also showed a similar trend to that of the USBM model although the two models are different. However, the Langefors-Kihlstrom model seemed to behave differently. The K value became lower when moving farther away from the blasted bench while the β value showed a similar trend to that observed with the USBM model. When coming to R^2, the Langefors-Kihlstrom model seemed to describe the data better at Station A than at Station B. This is demonstrated by the higher value of R^2 at the farthest station. Finally, it was noted that the BIS model displayed a trend similar to that seen with the Langefors-Kihlstrom model.

After looking at the conventional data, the analysis went on to interrogating the Varistem® ground vibration data. The same approach used with the conventional ground vibration data was adopted for the Varistem® data. And interestingly, all four empirical predictor models displayed a similar trend in contrast to what was noted for the conventional data. Moreover, higher K-factor and lower β value corresponded to a monitoring station closer to the blast area, i.e., Station B. The R^2 value was also higher suggesting that with the Varistem® stemming plugs, all four models work better when the monitoring station is closer.

In summary, after comparing the results from both conventional and Varistem® ground vibration data, the following conclusions can be made:

- The β value decreases for all four models tested as one moved closer to the blasting area. This means that vibrations die down slowly closer to the source and faster far away from it.
- The coefficient of determination R^2 was higher at the closest station suggesting better prediction ability of all models closer to the source.

Chapter 5 Contribution of stemming plugs to reducing blast-induced ground vibrations

5.1 Introduction

This chapter primarily focuses on ranking the four empirical ground vibration models presented in Chapter 4. The idea is to determine the best-performing model as a function of the location of the monitoring station. Thereafter, the ground vibration results obtained with and without the incorporation of the Varistem® stemming plugs are compared. This is to ascertain whether the introduction of the Varistem® stemming plugs can potentially reduce blast-induced ground vibrations. Statistical methods were employed for the purpose as presented in the sections below.

5.2 Ranking the performance of the empirical models

In this section, all four empirical models (i.e., USBM, Ambraseys-Hendron, Langefors-Kihlstrom, and BIS) are ranked according to how best they describe the site data in Tables 4.3 and 4.4. Their performance was assessed using the following statistical metrics:

- Mean Absolute Error (MAE)
- Coefficient of Determination (R^2)
- Root Mean Squared Error (RMSE)

These metrics were chosen because of their popularity (Nguyen et al., 2019; Hasanipanah et al., 2015; Ragam and Nimaje, 2018; Khandelwal and Singh, 2009; Xue, 2019). They were calculated in Microsoft® Excel® using both measured and modelled data as follows:

$$RMSE = \sqrt{\frac{1}{n}\sum_{i=1}^{n}(y_i - \hat{y}_i)^2} \quad (5.1)$$

$$MAE = \frac{1}{n}\sum_{i=1}^{n}|y_i - \hat{y}_i| \quad (5.2)$$

$$R^2 = 1 - \frac{\Sigma_i(y_i - \hat{y}_i)^2}{\Sigma_i(y_i - \bar{y})^2} \quad (5.3)$$

where n is the total number of data; y_i is the measured value; $\hat{y}_i$ is the predicted value and $\bar{y}$ is the mean of measured values.

For a good model, R^2 should be closer to 1 while both RMSE and MAE should approach 0. The conventional and the Varistem® PPV data were used to evaluate the performance of each empirical model.

Tables 5.1 and 5.2 list the models according to how best they describe the collected PPV data with the best model on top and the worst is the lowest row of the table.

Table 5.1: Ranking metrics for the selected empirical ground vibration models regressed against the historical/conventional blast data

	MAE	**RMSE**	**R^2**
Langefors-Kihlstrom model	1.050	1.467	0.850
BIS model	1.089	1.472	0.849
USBM	1.248	1.694	0.808
Ambraseys-Hendron model	1.430	1.990	0.739

The model ranking in Table 5.1 was conducted using the conventional PPV data only. Accordingly, the Langefors-Kihlstrom model yielded the lowest values of MAE (1.050 as opposed to 1.089, 1.248, and 1.430) and RMSE (1.467 versus 1.472, 1.694, and 1.990) while it yielded the highest value of R^2 (0.850 versus 0.849, 0.808, and 0.739).

By applying the same performance criterion for all models, it can easily be deduced from Table 5.1 that the BIS model is the second best-rated model followed by the USBM model. And the worst-performing model is the Ambraseys-Hendron model.

Table 5.2: Ranking metrics for the selected empirical ground vibration models regressed against the Varistem® blast data

	MAE	**RMSE**	R^2
Langefors-Kihlstrom model	0.287	0.357	0.752
USBM model	0.319	0.374	0.739
BIS Model	0.324	0.455	0.702
Ambraseys-Hendron model	0.368	0.455	0.612

A similar criterion was applied to rank the empirical models against the Varistem® PPV data. It is interesting to note in Table 5.2 that the models produced fairly comparable performance when the Varistem® ground vibration data was used. However, the Langefors-Kihlstrom model was deemed the best, closely followed by the USBM, then, by the BIS, and lastly, by the Ambraseys-Hendron models. This is because the Langefors-Kihlstrom model produced arguably the lowest MAE (0.287), the lowest RMSE (0.357), and the highest R^2 (0.752).

In essence, irrespective of the fact that conventional or Varistem® data is used, the Langefors-Kihlstrom model outperforms the other three. This indicates that the Langefors-Kihlstrom model work well for the Malandvule quarry and may therefore be used for simulation work going forward.

5.3 Comparison between peak particle velocities generated with and without Varistem® plugs

It was noted in Chapter 4 that the coefficient of determination R^2 was lower at Station A and higher at Station B. This could have been caused by the

presence of the shear zone shown in Figure 5.1 which is located between Station A and the blasting area.

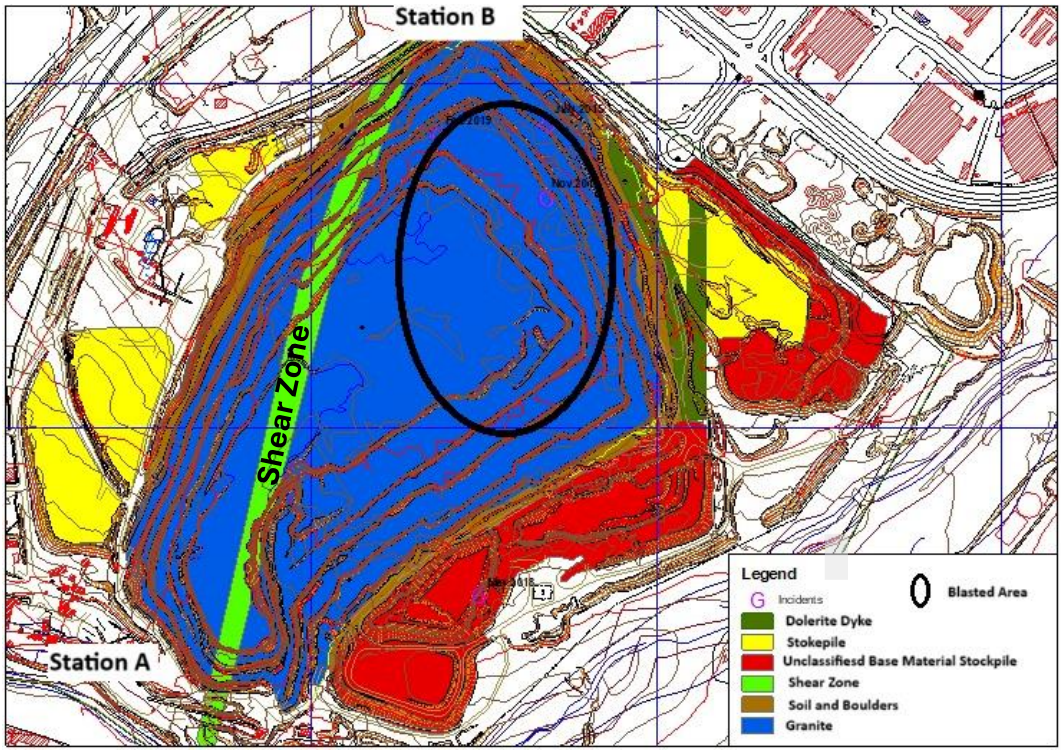

Figure 5.1: Geological makeup of the quarry (Source: Malandvule Quarry)

The presence of the shear zone, as labelled in Figure 5.1, can affect the propagation and attenuation of the explosive energy in the form of vibration waves, refer to Section 2.2.4 and Zhu et al. (2011) for further details. Several studies highlighted that the propagation of wave energy is affected by geological discontinuities such as shear zones, cracks, joints, and faults (Bard and Thomas, 1999; Zhang et al., 2024). These discontinuities affect the propagation and attenuation rate of the vibration waves with a potentially pronounced effect on the recorded ground vibrations.

Another cause for the low coefficient of determination R^2 at Station A could be attributed to its close location to the primary crusher. Indeed, the ground vibration waves generated by the blast could be experiencing interference from the vibrations generated by the primary crusher. This could be destructive and lead to the seismograph picking up lower vibration amplitudes.

The second observation was that the attenuation coefficient factor β in Equations (2.2) to (2.5) was higher at the farthest station and lower at the closest station. This attenuation coefficient β measures the rate at which the vibration wave intensity diminishes as the waves propagate through the rock mass (Liu et al., 2022). The attenuation of ground vibration waves may be caused by the geometrical spreading of the waves, the internal friction of the rock, and scattering during propagation. In this case study, the empirical evidence tends to suggest that the attenuation rate of the vibration waves increases with distance. This is supported by the review covered in Section 2.2.4, where geological factors were reported to increase the internal friction of the ground thereby increasing the wave attenuation coefficient. By looking at Figure 5.1, one can see that there is a shear zone between Station A and the blasting area. The presence of this zone increases the internal friction of the ground thereby resulting in a higher attenuation coefficient β within and in the vicinity. Figure 5.2 provides visual evidence of this natural jointing of the rock mass at the quarry.

Figure 5.2: Jointing of the rock mass at the quarry (Source: Malandvule Quarry)

Figure 5.2 shows how jointed the rock mass in an around the quarry is. And according to Hao et al. (2001), joints can directly influence the propagation and attenuation of ground vibration waves. Their study highlighted that the attenuation rate of the vibration waves increases when the waves propagate perpendicularly to the predominant rock joint set. In contrast, the wave attenuation factor β decreases when the waves propagate parallel to the direction of the joint set. Since the attenuation coefficient is high at station A, it is possible that that the recorded waves propagated in a direction perpendicular to that of the joint set.

5.4 Comparison between conventional and Varistem® peak particle velocities using the BIS model

One of the study objectives was to compare the peak particle velocities of the conventional and the Varistem® blast data. This was to establish whether the Varistem® stemming plugs contribute to reducing blast-induced ground vibrations.

In this section, conventional PPV was compared with Varistem® PPV. Both were plotted against the scaled distance defined accordingly to the BIS model (i.e., Equation 2.5). The BIS model was picked over the other models because it was found to be the best-performing model for both the historical and Varistem® data as demonstrated earlier in Section 5.2.

5.4.1 Comparison between conventional and Varistem® blasts against scaled distance as monitored at Station A

Figure 5.3 shows the comparison between the Varistem® and the conventional PPV as monitored from Station A. The visual inspection of Figure 5.3 suggests that there is potential for the Varistem® plug to reduce blast-induced ground vibration levels. The inference stems from the fact that the line chart corresponding to the Varistem® data visually appears to lie

below the conventional PPV line. Coincidentally, as highlighted in Section 2.3, the ground vibration safety limit underpinned by the USBM safe vibration limit curve is 12.7 mm/s at lower frequencies. This safety limit threshold as per the USBM RI 8507 standard (Siskind, 1980) was adopted by the quarry as the recommended limit. It can therefore be noted that 25% of the conventional PPV data points exceed the safety limit while all the Varistem® PPV data points fall below it.

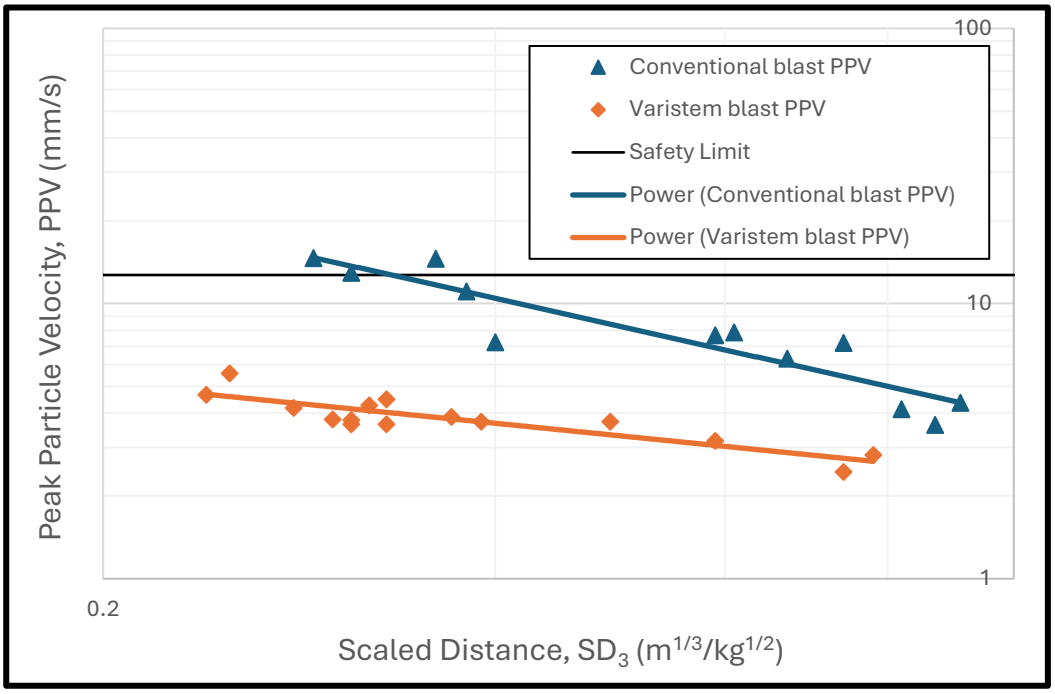

Figure 5.3: Comparison between the Varistem® and the conventional PPVs against the scaled distance as per Equation (2.5) for monitoring Station A

5.4.2 Comparison between conventional and Varistem® blasts against scaled distance as monitored at Station B

Figure 5.4 depicts the comparison between the conventional PPV and the Varistem® PPV. These were plotted against the scaled distance, SD_4, as monitored from Station B. A similar trend noted in Figure 5.3 appears in Figure 5.4 as well. The line chart for Varistem® PPV data appears to be lower than the conventional PPV line. In addition to this, both the Varistem® and the conventional PPV line charts are below the safety limit line. By

visually inspecting Figure 5.4, one can see the potential of Varistem® stemming plugs towards reducing ground vibration levels.

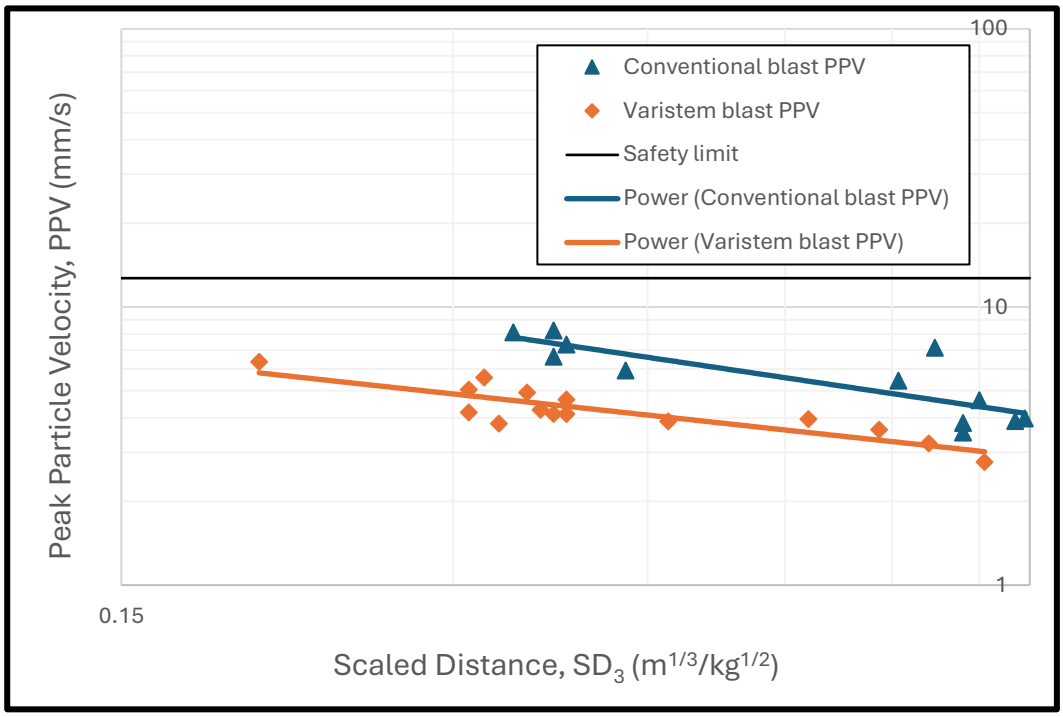

Figure 5.4: Comparison between the Varistem® and the conventional PPVs against the scaled distance as per Equation (2.5) for monitoring Station B

According to Gutowski and Dym (1976) as well as Kim and Lee (2000), ground vibrations dissipate as one moves away from the blast source (also refer to Section 2.2.4 for additional details). It then makes sense why the ground vibrations at Station B, the farthest station, both lie below the safety limit while at the closer Station A, some of the PPV points lie above it.

Finally, both Figures 5.3 and 5.4 provides empirical evidence of the potential of Varistem® stemming plugs in reducing vibrations induced during a blast. To confirm this, statistical hypothesis testing is conducted next.

5.4.3 Student's t-testing of Varistem® versus conventional peak particle velocities

In this section, hypothesis testing was employed to quantitatively confirm the behaviour reported in both Figures 5.3 and 5.4. The statistical test was

performed by comparing the Varistem® and the conventional PPVs. The alternative hypothesis in this case was that Varistem® PPV is lower than the conventional one as seen in both Figures 5.3 and 5.4. Student's t-test was employed for the purpose.

Tables 5.3 and 5.4 present the outcome of Student's t-test at Station A and Station B respectively.

Table 5.3: Two-sample t-test assuming unequal variances at Station A

	Conventional PPV	*Varistem® PPV*
Mean	8.48	3.86
Variance	15.48	0.57
Observations	12	15
Hypothesized Mean Difference	0	
Df	12	
t Stat	4.00736	
P(T<=t) one-tail	0.00087	
t Critical one-tail	1.78229	
P(T<=t) two-tail	0.00174	
t Critical two-tail	2.17881	

According to Table 5.3, the mean of the conventional PPV (8.48 mm/s) is much higher than that of the Varistem® one (3.86 mm/s). It is also worth noting that the P-value for the one-tail test (0.00087) is significantly lower than 0.05. This means that the Varistem® PPV is lower than the conventional PPV at a 95% confidence level. It is therefore warranted that the Varistem® stemming plug contribute to containing the explosive energy thereby lowering the blast-induced ground vibrations.

Table 5.4: Two-sample t-test assuming unequal variances at Station B

	Conventional PPV	*Varistem® PPV*
Mean	5.72	4.30
Variance	3.05	0.82
Observations	12	15
Hypothesized Mean Difference	0	
Df	16	
t Stat	2.55465	
P(T<=t) one-tail	0.01060	
t Critical one-tail	1.74588	
P(T<=t) two-tail	0.02120	
t Critical two-tail	2.11991	

Table 5.4 also depicts a similar trend to that reported in Table 5.3. The P-value at 0.01060 on the one-tail test is lower than 0.05. Therefore, the null hypothesis is rejected. This means that the Varistem® PPV is not equivalent to the conventional PPV at a 95% confidence level. This can be seen by how the mean PPV for the Varistem® blast (4.30 mm/s) is lower than that of the conventional blast (5.72 mm/s). By looking at these elements, one can conclude that there is enough evidence to infer that the mean PPV produced with the Varistem® plugs is significantly lower than the conventional PPV mean.

All in all, the statistical test supports the visual presentation of the PPV data shown in both Figures 5.3 and 5.4. According to Tables 5.3 and 5.4, Varistem® stemming plugs play a significant role in reducing blast-induced ground vibrations at both stations.

5.5 Comparing peak particle velocities generated with and without Varistem® plugs by bootstrapping

Bootstrapping, another robust statistical method, was employed to confirm whether the conclusion reached in Section 5.4 is valid. The bootstrapping

technique generally requires the resampling of both the Varistem® and the conventional PPV data.

To this end, resampling was performed using the Microsoft® Excel® software for 20 runs. As a result of this, 20 new PPV data sets were generated from the original conventional PPV data. This was followed by calculating the mean PPVs of each of the 20 data sets, which resulted in a new 20-point data set of mean PPVs. This new 20-point data set was used to calculate its mean PPV and standard deviation for later PPV comparison. A similar procedure was conducted for the Varistem® data set collected from Station A. Eventually, both the conventional and Varistem® PPV data sets were represented by their new mean PPV and standard deviations calculated from their respective data distributions. From the conventional data set, a mean PPV of 8.72 mm/s was calculated with a standard deviation of 0.99 mm/s. conversely, a mean PPV of 3.89 mm/s with a standard deviation of 0.18 mm/s was generated for the Varistem® data set.

The resampled data was probed to understand its distribution. Figures 5.5 and 5.6 show the distributions for the resampled conventional and Varistem® data respectively.

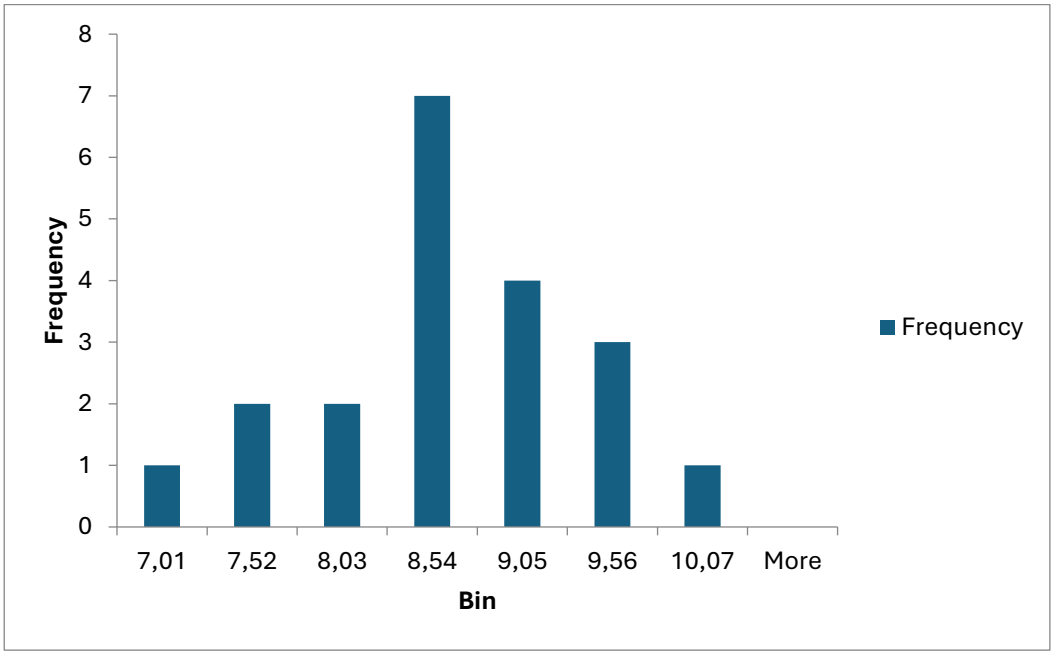

Figure 5.5: Distribution of the resampled conventional ground vibration data

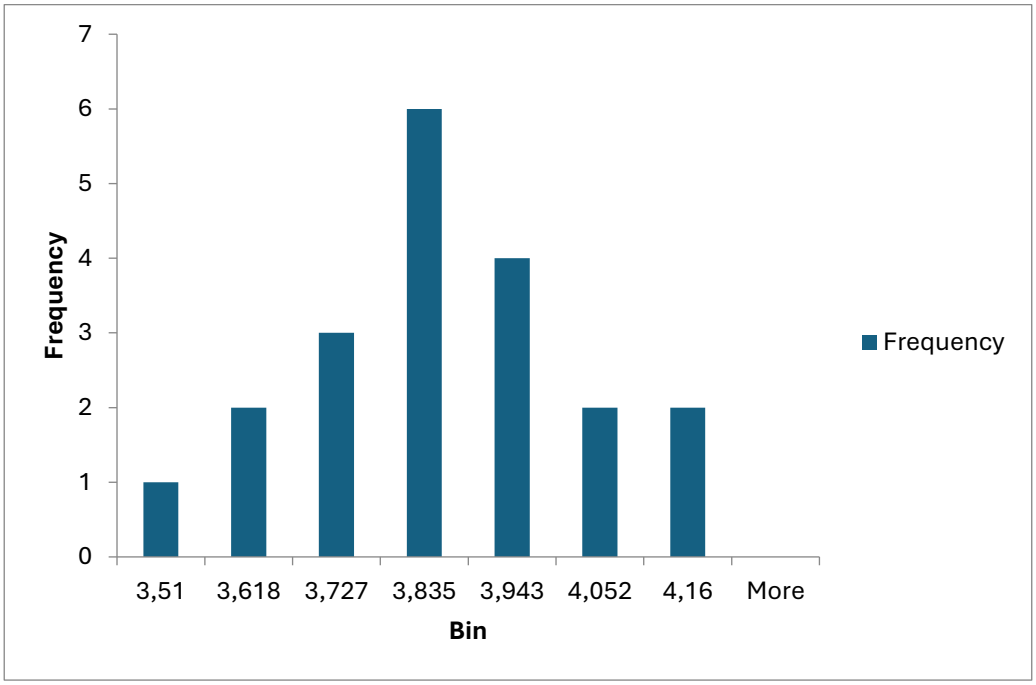

Figure 5.6: Distribution of the resampled Varistem® ground vibration data

Figures 5.5 and 5.6 show that the resampled conventional and Varistem® data sets are fairly symmetrical and close to normally distributed. This means that 2σ (i.e., twice the standard deviation) is equivalent to the 95% confidence interval. As such, the following mean and confidence intervals can be inferred on the population PPV values:

- For conventional PPV data: 8.72 mm/s ± 2 x 0.99 ≈ ±1.98 mm/s
- For Varistem® PPV data: 3.89 mm/s ± 2 x 0.18 ≈ 3.89 ± 0.36 mm/s

Therefore, the population ranges for the two PPV data sets can be quoted as follows:

- For conventional PPV data, 6.74 ≤ PPV ≤ 10.7 mm/s
- For Varistem® PPV data, 3.53 ≤ PPV ≤ 4.25 mm/s

Based on the above, the 95% confidence intervals corresponding to the conventional and the Varistem® data do not overlap. As such, it can be confirmed that the Varistem® PPV is statistically and significantly lower than the conventional PPV. In other words, if the experiments were repeated 100

times, both the conventional and Varistem® PPVs would only be similar in no more than 5 occasions.

Finally, the minimum PPV value for the conventional data (6.74 mm/s) was compared with the maximum PPV value for the Varistem® data (4.25 mm/s). The two PPVs were used to calculate the contribution of stemming plugs to reducing blast-induced ground vibrations as $\frac{(6.74-4.25)}{6.74} \times 100$ = 36.94%. Therefore, the Varistem® stemming plugs may be expected to reduce the level of ground vibrations by almost 37%.

5.6 Significance of the findings

This section provides a summary of the potential contribution of the Varistem® stemming plug to reduce the intensity of blast-induced ground vibrations. Looking at the work covered in the chapter, one can conclude that there is significant evidence to that end. This is demonstrated in Figures 5.3 and 5.4 where the Varistem® PPV line chart lies below the conventional PPV line. In Figure 5.3, the conventional PPV data also stretches above the 12.7 mm/s USBM regulatory limit while all the Varistem® PPV data points lie entirely below the regulatory limit. This meant that some of the conventional blasts exceeded the USBM regulatory limit while all the Varistem® blasts stayed within the recommended safe limit.

In terms of reducing blast-induced ground vibrations, Student's t-test was used to examine the contribution of the Varistem® plugs. Tables 5.3 and 5.4 show the results of the t-test where the mean conventional PPV (8.48 mm/s) is much higher than that of the Varistem® one (3.86 mm/s). For closest Station A, the P-value of 0.00174 was found which is below the 0.05 threshold. Considering both the PPV mean and the P-value, it is evident that the Varistem® PPV is significantly lower than the conventional PPV at a 95% confidence. Table 5.4 also shows a similar trend to the one seen in Table 5.3. Indeed, the mean conventional PPV (5.72 mm/s) was found to be higher than that of the Varistem® data (4.30 mm/s). Similarly, with the

corresponding P-value of 0.02120 being less than the threshold 0.05, the rejection of the null hypothesis is warranted. Therefore, the Varistem® PPV for both stations were deemed significantly lower than the conventional PPV at 95% confidence level. This further supports the assertion that the Varistem® stemming plugs play a significant role in reducing ground vibration levels.

A step further was taken to confirm this outcome. Bootstrapping was performed on the measured PPV for both the conventional and the Varistem® blasts. This enabled one to generate the 95% confidence interval representing the inherent variations of the two PPV data sets relative to the conventional and the Varistem® blasts respectively. These ranges were compared and found not to overlap which suggests that the two PPV populations are different. In addition to this, the one-sided t-test confirmed the fact that the Varistem® PPV was lower than the conventional PPV. Finally, the two ranges of variability at 95% confidence level were used to quantify the effect of the Varistem® plugs. Based on the estimation, it was found that the stemming plugs can yield up to 36.94% reduction in ground vibrations. So, until further data is made available, one can confidently say that the incorporation of the Varistem® stemming plugs reduces the level of blast-induced ground vibrations by 37%.

Chapter 6 Conclusion and recommendations

6.1 Introductory summary

The main objective of this research study was to appraise the potential of the Varistem® stemming plugs towards reducing blast-induced ground vibrations. Ground vibrations were measured under two different stemming conditions. A total of 27 production blasts were considered, with 12 of them retrieved from the historical archives of the quarry while the remaining 15 were generated during the field test work. The 12 blasts were conventional blasts that were conducted before the quarry adopted the Varistem® stemming plugs. These blasts were only stemmed with aggregate material. The other 15 blasts were stemmed with a combination of both the aggregate material and the Varistem® stemming plugs. All blasts (i.e., conventional and Varistem®) were monitored and recorded from two fixed stations; namely, Station A and Station B. Station B was located closer to the blasting area while Station A was located relatively farther. The blasts were monitored using portable NOMIS Supergraph seismographs. These specialised seismographs were installed before conducting any blast to help monitor the vibration levels. Four empirical predictor models of peak particle velocity (PPV) were then used to analysis the ground vibration data. There are the United States Bureau of Mines (USBM) model, the Ambraseys-Hendron model, the Langefors-Kihlstrom model, and the Burean of Indian Standards (BIS) model. The models were ranked according to how best they individually described the data collected at both stations. The Langefors – Kihlstrom model was found to be the most suitable empirical predictor model for the Malandvule quarry.

Next, blast-induced ground vibrations generated with and without Varistem® stemming plugs were compared. This was done to establish whether the Varistem® stemming plugs contributed to reducing the level of ground vibrations generated through blasting activities. Student's t-

distribution was employed to help with comparing the conventional and the Varistem® PPVs. Bootstrapping was also applied to the recorded PPV values for both the Varistem® and the conventional blasts. The resampled data was further used to generate the values of the PPV populations for both the conventional and the Varistem® blasts. Overall, the Varistem® stemming plugs was found to reduce the level of blast-induced ground vibrations.

6.2 Effects of incorporating the Varistem® stemming plugs

The objectives of the present research study were to firstly determine the most suitable empirical predictor model that would describe the on-site ground vibration data produced with and without the Varistem® stemming plugs. Secondly, the research was aimed at comparing the level of ground vibrations generated under similar blasting conditions but done with and without Varistem® stemming plugs.

In terms of the first objective, the four empirical predictor models were ranked using the following metrics: the Mean Absolute Error (MAE), the Root Mean Squared error (RMSE), and the coefficient of determination (R^2). The analysis revealed that the most suitable predictor model was the Langefors-Kihlstrom model, followed by the either the USBM or BIS model, and lastly, by the Ambraseys-Hendron model.

In terms of the second objective, the level of blast-induced ground vibrations generated with and without the Varistem® stemming plugs were compared. The corresponding PPV data, referred to in this work as the Varistem® data and the conventional or historical data, was recorded by the two seismographs each placed at a different monitoring station. At the closest Station A, 25% of the conventional blasts exceeded the recommended USBM regulatory limit of 12.7 mm/s. The incorporation of the Varistem® stemming plugs resulted in all the blasts recorded at the same location falling below the regulatory limit. A visual representation of the comparison

showed that the Varistem® PPV line chart plotted against the Langefors-Kihlstrom-based scale distance was lower than the conventional PPV line. This highlighted the potential of the Varistem® stemming plugs to reduce the level of blast-induced ground vibrations.

This potential of the Varistem® stemming plugs was probed by statistical methods. Student's t-test was performed on the PPV data and found that the Varistem® PPV was significantly lower than the conventional PPV. The t-test conducted at Station A showed that the mean conventional PPV (8.48 mm/s) was higher than the mean Varistem® counterpart (3.86 mm/s). In addition to this, the P-value (0.00174) at this station was lower than 0.05. This meant that the conventional and the Varistem® PPVs were statistically different with the Varistem® PPV being lower than the conventional PPV. The t-test at the farthest Station B also showed that the mean conventional PPV (5.72 mm/s) was higher than the Varistem® velocity (4.30 mm/s). The corresponding P-value (0.02120) was also lower than 0.05. Coupling the P-value with the PPVs at this station led to the conclusion that the Varistem® PPV was significantly lower than the conventional PPV.

As a confirmatory analysis, bootstrapping was conducted to resample the recorded conventional and Varistem® PPV data. This new data was used to determine the PPVs of the populations for both the conventional and Varistem® blasts. From there, the 95% confidence intervals were generated to describe the centrality and spread of the PPVs for the population corresponding to the conventional and Varistem® blasts respectively. Statistical testing then highlighted that the Varistem® ground vibrations was lower than the conventional ones. The statistical ranges of the PPV populations finally were compared for any overlap. Since the ranges did not overlap, it was concluded that Varistem® and conventional blasts were statistically different. And perhaps the most important point to make is that the Varistem® stemming plugs were estimated to contribute to reducing blast-induced ground vibrations by almost 37%.

6.3 Recommendations for future work

According to the reviewed literature, the explosive energy partition shows that about 2 – 25% of the explosive energy is employed towards breaking the rock with the rest of the energy being wasted through various forms.

Since Varistem® stemming plugs are designed to trap this explosive energy for some time within the blasthole, it may be required in future to measure the average amount of energy that the plugs can redirect toward breaking the rock.

Since Varistem® stemming plugs are quite new in the market, it may be required to do a cost – benefit analysis to see if adopting the plugs may have any financial benefit as well.

Since this study used historical conventional blast data along with field collected Varistem blast data to assess the contribution of Varistem® stemming plugs towards reducing ground vibrations, it may be required to conduct a study where experiments with and without stemming plugs are conducted under identical blasting parameters to ensure a more precise comparison of their effects.

Lastly, since this scope of this study was limited to one quarry, the performance of Varistem® stemming plugs on other surface mining operations extracting coal, gold, or platinum amongst others should be explored. This will provide a fuller view of the contribution of the Varistem® plugs in terms of rock fragmentation, ground vibrations, air blast, and fly rock to name but a few.

References

Afrasiabian, B., Ahangari, K., Noorzad, A., 2020. Study on the effects of blast damage factor and blast design parameters on the ground vibration using 3D discrete element method. Innovative Infrastructure Solutions, vol. 5, no. 37, pp. 1 – 14

Agrawal, A., 2017. The effect of back rows delay timing and size of blast on fragmentation and muckpile shape parameters. Masters Dissertation, Indian Institute of Technology, Dhanbad

Agrawal, H., Mishra, A., 2019. Modified scaled distance regression analysis approach for prediction of blast-induced ground vibration in multi-hole blasting. Journal of rock Mechanics and geotechnical Engineering, vol. 11, no. 1, pp. 202 – 207

Aldas, G., Ecevitoglu, B., 2008. Waveform analysis in mitigation of blast-induced vibrations. Journal of Applied Geophysics, vol. 66, pp. 25 – 30

Alilovic, I., Reckzin, E., 2005. Methods of gassing emulsion explosives and explosives produced thereby. United States of America, Patent US6855219B2, February 15, 2005.

Bamford, T., Esmaeili, K., Schoellig, A.P., 2021. A deep learning approach for rock fragmentation analysis. International Journal of rock Mechanics and Mining Sciences, vol. 45, pp. 1 – 13

Bard, P., Thomas, J. R., 1999. Wave propagation in complex geological structures and their effects on strong ground motion. In: E. Kausel, G. Manolis. Wave motion in earthquake engineering. Southampton, UK: WIT Press. pp. 38 – 95

Betterblastting, 2024. Better blasting. [Online] Available at: https://betterblasting.ca/products/measuring-tapes/ [Accessed on 18 November 2024]

Bhagwat, V.P., Dey, K., 2016. Comparison of some blast vibration predictors for blasting in underground drifts and some observations. Journal of the Institution of Engineers (India): Series D, vol. 97, no. 1, pp. 33 – 38

Blair, D., 2004. Charge weight scaling laws and the superposition of blast vibration waves. International Journal for Blasting and Fragmentation, vol. 8, no. 4, pp. 221 – 239

Blair, D., 2010. Seismic radiation from an explosive column. Geophysics, vol. 75, no. 1, pp. 55 – 65

Blair, D., 2015. Wall control blasting. 11th International Sympossium on Rock Fragmentation by Blasting, The Australasian Institute of Mining and Metallurgy, pp. 13 – 26, Sydney, 24 August 2015

Blair, D., Armstrong, L., 2001. The influence of burden on blast vibration. International Journal for Blasting and Fragmentation, vol. 5, no. 1, pp. 108 – 129

Blair, D.P., Birney, B., 1994. Vibration signatures due to single blastholes fired in the Charlotte Deeps. ICI Confidential Report, United States of America

BME, 2017. AXXIS detonator. [Online] Available at: https://bme.co.za/wp-content/uploads/2020/11/MSDS-AXXIS-GII-Detonator-2017.pdf#:~:text=The%20electronic%20detonator%20assemblies%20consist%20of%203%20parts,base%20charge%20consists%20of%20DDNP%20and%20PETN%2FRDX%20respectively [Accessed on 06 September 2023]

Burgoyne, J.F., 1849. Rudimentary treatise on the blasting and quarrying of stone for building and other purposes. J. Weale, London

Cardu, M., Giraudi, A., Oreste, P., 2013. A review of the benefits of electronic detonators. REM – Revista Escola de Minas, International Engineering Journal, vol. 3, no. 66, pp. 375 – 382

Cevizci, H., 2012. A newly developed plaster stemming method for blasting. Journal of the Southern African Institute of Mining and Metallurgy, vol. 112, no. 12, pp. 1071 – 1078

Crandell, F., 1949. Ground vibrations due to blasting and its effects upon structures. Journal of Boston Society of Civil Engineers, pp. 222 – 245

De Graaf, W., 2013. Surface mining explosives. *Explosives Engineering*: University of Pretoria. pp. 3.10 – 3.19.

Dhekne, P., 2015. Environmental impacts of rock blasting and their mitigation. International Journal of Chemical, Environmental and Biological Sciences, vol. 3, no. 1, pp. 46 – 50

Duvall, W.I., Fogelson, D.E., 1962. Review of criteria for estimating damage to residences from blasting vibrations. Report of Investigations 5968, United States Bureau of Mines, Michigan

Elevli, B., Arpaz, E., 2010. Evaluation of parameters affected on the blast induced ground vibration (BIGV) by using relation diagram (RDM). Acta Montanistica Slovaca, vol. 15, no. 4, pp. 261 – 268

ERG Industrial, 2023. How does Varistem® improve energy retention and utilization?. [Online] Available at: https://ergindustrial.com/how-does-varistem-work/ [Accessed 28 August 2023]

Fish, B., 1951. Seismic vibrations from blasting. Mine and Quarry Engineering, vol. 17, no. 5 pp. 145 – 148

Fish, B., Handcock, J., 1949. Short delay blasting. Mine and Quarry Engineering, vol. 15, pp. 339 – 343

Fourney, W., Barker, D., Holloway, D., 1981. Model studies of explosive well stimulation techniques. International Journal of Rock Mechanics and Mining Sciences and Geomechanics Abstracts, vol. 18, no. 2, pp. 113 – 127

Fourney, W., Bihr, S., Leiste, U., 2006. Borehole pressures in an air decked situation. International Journal for Blasting and Fragmentation, vol. 10, no. 1, pp. 47 – 60

Ghosh, S., Behera, C., Mishra, M. K., 2024. Prediction of blast-induced ground vibration using multivariate statistical analysis in the opencast chromite mines of the Indian State of Odisha. Sādhanā, vol. 49, no. 2, pp. 1 – 12

Glasstone, S., 1950. The effects of nuclear weapons. Washington DC: United States atomic energy commission.

Gomes-Sebastiao, G., Graaf, W.D, 2017. An investigation into the fragmentation of blasted rock at Gomes Sand. Journal of the Southern African Institute of Mining and Metallurgy, vol. 117, no. 4, pp. 321 – 328

Grobbelaar, M., Molea, T., Durrheim, R., 2020. Measurement of air and ground vibrations produced by explosions situated on the earth's surface. Journal of the Southern African Institute of Mining and Metallurgy, vol. 120, no. 9, pp. 521 – 530

Gutowski, T., Dym, C., 1976. Propagation of ground vibration: A review. Journal of Sound and Vibration, vol. 49, no. 2, pp. 179 – 193

Hagan, T.N., 1977. Rock breakage by explosives. Proceedings of the 6th Colloquium. Stockholm, Sweden, 22–26 August 1977. Gasdynamics of explosions and Reactive Systems, pp. 329 – 340.

Hao, H., Wu, Y., Ma, G., Zhou, Y., 2001. Characteristics of surface ground motions induced by blasts in jointed rock mass. Soil Dynamics and Earthquake Engineering, vol. 21, no. 2, pp. 85 – 98

Hasanipanah, M., Monjezi, M., Shahnazar, A., Armaghani, D.J., Farazmand, A., 2015. Feasibility of indirect determination of blast induced ground vibration based on support vector machine. Measurement, vol. 75, pp. 289 – 297

Hossaini, M.F., Sen, G.M., 2004. Effect of explosive type on particle velocity criteria in ground vibration. Journal of Explosives Engineering, vol. 21, no. 4, pp. 34 – 36

Hosseini, S., Poormirzaee, R., Gilani, S., Jiskani, I.M., 2023. A reliability-based rock engineering system for clean blasting: Risk analysis and dust emissions forecasting. Springer-Verlag GmbH, Germany

Hu, L., Ding, S., Xu, R., Han, F., Wu, C., 2014. Effect of blasthole diameter on blasting vibration. Mining Technology Journal, vol. 5, pp. 144 – 147

Hu, Y., Liu, M., Wu, X., Zhao, G., Li, P., 2018. Damage-vibration couple control of rock mass blasting for high rock slopes. International Journal of Rock Mechanics and Mining Sciences, vol. 103, pp. 137 – 144

Hu, Y., Wu, X., Zhao, G., Li, P., Sun, P., 2017. Investigation of safety control for rock blasting excavation under cold condition. Chinese Journal of Geotechnical Engineering, vol. 39, no. 11, pp. 2139 – 2146

Ismail, A.M., Ibrahim, A.M., Hassnien, S., 2024. Evaluation of blast-induced vibration effects on buildings: Case Study. IOSR Journal of Engineering (IOSRJEN), vol. 14, no. 4, pp. 50 – 64

Kabwe, E., 2017. Improving collar zone fragmentation by top air-deck blasting technique. Geotechnical and Geological Engineering, vol. 35, no. 1, pp. 157 – 167

Khandelwal, M. (2010). Evaluation and prediction of blast-induced ground vibration using support vector machine. International Journal of Rock Mechanics and Mining Sciences, vol. 47, no. 3, pp. 509 – 516.

Khandelwal, M., Singh, T., 2006. Prediction of blast induced ground vibrations and frequency in opencast mine: A neural network approach. Journal of Sound and Vibration, vol. 289, no. 4 – 5, pp. 711 – 725

Khan, M.F.H., Hossain, M.J., Ahmed, M.T., Monir, M.U., Rahman, Md.A., Sweety, T.S., Akash, F.A., Shovon, S.M., 2025. Ground vibration effect evaluation due to blasting operations. Heliyon, vol. 11, no. 2, pp. 1 – 25

Kim, D.S., Lee, J.S., 2000. Propagation and attenuation characteristics of various ground vibrations. Soil Dynamics and Earthquake Engineering, vol. 19, no. 2, pp. 115 – 126

Konya, C., Konya, A., 2018. Effect of hole stemming practices on energy efficiency of comminution. In Energy Efficiency in the Minerals Industry. Green Energy and Technology, Springer, Cham, pp. 31 – 53

Kumar, R., Choudhury, D., Bhargava, K., 2016. Determination of blast-induced ground vibration equations for rocks using mechanical and geological properties. Journal of Rock Mechanics and Geotechnical Engineering, vol. 8, no. 3, pp. 341 – 349

Kuzu, C., 2008. The importance of site-specific characters in prediction models for blast-induced ground vibrations. Soil Dynamics and Earthquake Engineering, vol. 28, no. 5, pp. 405 – 414

Langefors, U., Kihlstrom, B., Westerberg, H., 1958. Ground vibration in blasting. Water Power, vol. 10, pp. 335 – 338, 390 – 395, 421 – 424

Liu, R., 2018. Influence of different burial depth on blasting vibration. Wuhan University of Science and Technology (in Chinese).

MacFarland, T., Yates, J.M., 2021. Using R for biostatistics. Springer, Cham, pp. 141 – 240

Ma, C., Wu, L., Zhou, Y., Wang, Y., Sun, M., 2020. Influence of free face numbers on energy distribution characteristics of blast vibration signal in underwater drilling blasting. In IOP Conference Series: Earth and Environmental Science, IOP Publishing, vol. 560, no. 1, p. 012076, 3 – 5 July 2020, Lanzhou, China

Mel'nikov, N., Marchenko, L., Zharikov, I., Seinov, N., 1979. A method of enhanced rock breaking by blasting. Soviet Mining Science, vol. 15, no. 6, pp. 565 – 572

Mishra, A.K., Rout, M., Singh, D.R., Jana, S.P., 2018. Influence of gassing agent and density on detonation velocity of bulk emulsion explosives. Geotechnical and Geological Engineering, vol. 36, no. 1, pp. 89 – 94

Morris, G., Westwater, R., 1953. Damage to structures by ground vibrations due to blasting. The Engineer, pp. 116 – 118

Mpofu, M., Ngobese, S., Maphalala, B., Roberts, D., Khan, S., 2021. The influence of stemming practice on ground vibration and air blast. Journal of the Southern African Institute of Mining and Metallurgy, vol. 121, no. 1, pp. 1 – 10

Nateghi, R., 2011. Prediction of ground vibration level induced by blasting at different rock units. International Journal of Rock Mechanics and Mining Sciences, vol. 48, pp. 899 – 908

Noren-Cosgriff, K., Ramstad, N., Neby, A., Madshus, C., 2020. Building damage due to vibration from rock blasting. Soil Dynamics and Earthquake Engineering, vol. 138, pp. 1 – 13

Nguyen, H., Bui, X.N., Tran, Q.H., Mai, N.L., 2019. A new soft computing model for estimating and controlling blast-produced ground vibration based on hierarchical K-means clustering and cubist algorithms. Applied Soft Computing Journal, vol. 77, no. 1, pp. 376 – 386

Oates, T., Spiteri, W., 2021. Stemming and best practice in the mining industry: A literature review. Journal of the Southern African Institute of Mining and Metallurgy, vol. 121, no. 8, pp. 415 – 426

Ongen, T., Karakus, D., Konak, G., Onur, A.H., 2018. Assessment of blast-induced vibration estimation models. Journal of African Earth Sciences, vol. 145, pp. 267 – 273

Park, D., Jeon, S., 2010. Reduction of blast-induced vibration in the direction of tunneling using an air-deck at the bottom of a blasthole. International Journal of Rock Mechanics and Mining Sciences, vol. 47, pp. 752 – 761

Preis, E., 2023. Velocity of detonation (VoD) explained. [Online] Available at: https://ergindustrial.com/velocity-of-detonation-vod-explained/ [Accessed on 21 December 2024]

Qiu, X., Shi, X., Gou, Y., Zhou, J., Chen, H., Huo, X., 2018. Short-delay blasting with single free surface: results of experimental tests. Tunnelling and Underground Space Technology, vol. 74, pp. 119 – 130

Ragam, P., Nimanje, D.S., 2018. Evaluation and prediction of blast-induced peak particle velocity using artificial neural network: A case study. Noise and Vibration worldwide, vol. 49, no. 3, pp. 111 – 119

Rehman, A.U., Emad, M., Khan, M., 2021. Improving the environmental and economic aspects of blasting in surface mining by using stemming plugs. Journal of the Southern African Institute of Mining and Metallurgy, vol. 121, no. 7, pp. 369 – 378

Rehman, A.U., Emad, M.Z., Khan, M.U., 2020. Role of ergonomics in the selection of stemming plugs for surface mining operations. Archives of Mining Sciences, vol. 65, no. 1, pp. 59 – 70

Rockwell, E.H., 1927. Vibrations caused by quarry blasting and their effect on structures. Rock Products, vol. 30, no. 3, pp. 58 – 61

Rossmanith, H.P., 2002. The use of Language diagrams in precise initiation blasting. Part I: Two interacting blastholes. Trade Journal, vol. 6, no. 1, pp. 104 – 136

Saharan, M., Sazid, M., Singh, T., 2017. Explosive energy utilization enhancement with air-decking and stemming plug, ‘SPARSH’. Symposium of the International Society for Rock Mechanics, vol. 191, pp. 1211 – 1217, 20 June 2017, Ostrava, Czech Republic

Sazid, M., 2014. Investigating the role of effective stemming in engineering blasting operations for open-pit mines. PhD thesis, Indian Institute of Technology, Bombay

Sazid, M., Saharan, M., Singh, T., 2016. Enhancement of the explosive energy utilization with the application of new stemming contrivance. International Journal of Innovative Science and Modern Engineering (IJISME), vol. 4, no. 2, pp. 1 – 5

Sereme, B., Mpofu, M., Roberts, D., Ngobese, S., Lumbwe, T., 2019. Monitoring of blasting and determination of optimal stemming. Unpublished Report, Coaltech Research Association, Johannesburg

Shi, X., Chen, S., 2011. Delay time optimization in blasting operations for mitigating the vibration-effects on final pit walls' stability. Soil Dynamics and Earthquake Engineering, vol. 31, no. 8, pp. 1154 – 1158

Shi, X., Qiu, X., Zhou, J., Huang, D., Chen, X., Gou, Y., 2016. A comparative study of ground and underground vibrations induced by bench blasting. Shock and Vibration, vol. 2016, no. 1, pp. 1 – 9

Silva, J., Amaya, J., Basso, F., 2017. Development of a predictive model of fragmentation using drilling and blasting data in open pit mining. Journal of the Southern African Institute of Mining and Metallurgy, vol. 117, no. 11, pp. 1089 – 1094

Simangunsong, G.M., Wahyudi, S., 2015. Effect of bedding plane on prediction blast-induced ground vibration in open pit coal mines. International Journal of Rock Mechanics and Mining Sciences, vol. 79, no. 1, pp. 1 – 8

Siskind, D., Stagg, M., Kopp, J., Dowding, C., 1980. Structure response and damage produced by ground vibration from surface mine blasting. Report, US Department of Interior Office of Surface Mining, Pittsburgh

Standards Australia, 2006. Explosives – Storage and use. Sydney, 2 February 2006

Tete, A.D., Deshmukh, A., Yerpude, R., 2016. Design and implementation of electronic sensor for velocity-of-detonation measurement of cartridge

explosive and comparison with Dautriche Method. International Journal of Mining and Mineral Engineering, vol. 7, no. 2, pp. 113 – 125

Uysal, O., Arpaz, E., Berber, M., 2007. Studies on the effect of burden width on blast-induced vibration in open-pit mines. Environmental Earth Sciences Journal, vol. 53, no. 3, pp. 643 – 650

Wang, Z., Fang, C., Chen, Y., Cheng, W., 2013. A comparative study of delay time identification by vibration energy analysis in millisecond blasting. International journal of Rock mechanics and Mining Sciences, vol. 60, pp. 389 – 400

Western Australian Government, 2023. What is a mobile processing unit (MPU)?. [Online] Available at: https://www.dmp.wa.gov.au/Dangerous-Goods/What-is-a-mobile-processing-14377.aspx [Accessed 28 August 2023]

Worsey, P., 1986. Understanding vibrations from multi-hole blasts using short delay periods. Journal of Explosives Engineering, vol. 3, pp. 25 – 28

Wu, C., Xu, R., Zhang, Q., 2017. Influence of free surface on energy distribution characteristics of blasting vibration. Explosion and Shock waves, vol. 37, no. 6, pp. 907 – 914

Wu, Y., Hao, H., Zhou, Y., Chong, K., 1998. Propagation characteristics of blast-induced shock waves in a jointed rock mass. Soil Dynamics and Earthquake Engineering, vol. 17, no. 6, pp. 407 – 412

Xue, X., 2019. Neuro-fuzzy based approach for prediction of blast-induced ground vibration. Applied Acoustics, vol. 152, no. 10, pp. 73 – 78

Yan, Y., Hou, X., Fei, H., 2020. Review of predicting the blast-induced ground vibrations to reduce impacts on ambient urban communities. Journal of Cleaner Production, vol. 260, no. 4, p. 121135

Ye, Z., Yang, J., Yao, C., Zhang, X., Jiang, S., Zhou, C., 2023. Attenuation characteristics of shock waves in drilling and blasting based on viscoelastic

wave theory. International Journal of Rock Mechanics and Mining Sciences, vol. 171, no. 4, pp. 1 – 14

Yuana, W., Su, X., Wang, W., Wen, L., Chang, J., 2019. Numerical study of the contributions of shock wave and detonation gas to crack generation in deep rock without free surfaces. Journal of Petroleum Science and Engineering, vol. 177, pp. 699 – 710

Zhang, K.M., Zhao, H.R., 2022. Perspectives in the stability of emulsion explosive. Advances in Colloid and Interface Science, vol. 307, p. 102745

Zhang, Y., Zhu, J., Xu, H., Han, D., Bao, W., 2024. Examining theoretical applicability of displacement discontinuity model to wave propagation across rock discontinuities. *Journal of Rock Mechanics and Geotechnical Engineering.*

Zhou, J., Asteris, P.G., Armaghani, D.J., Pham, B.T., 2020. Prediction of ground vibration induced by blasting operations through the use of the Bayesian network and random forest models. Soil Dynamics and Earthquake Engineering, vol. 139, pp.1 – 12

Zhu, J.B., Perino, A., Zhao, G.F., Barla, G., Li, J.C., Ma, G.W., Zhao, J., 2011. Seismic response of a single and a set of filled joints of viscoelastic deformational behaviour. Geophysical Journal International, vol. 186, no. 3, pp. 1315 – 1330

Appendices

Annexure A

Seismograph reports received from the quarry.

Varistem blast Reports

Conventional blast Reports

Annexure B

These are the Scaled Distance calculation for each model.

Station A

Ambraseys Model – Station A

R (m)	*Q (kg)*	*SD*
411	*90*	*91.71*
370	478.7	*47.30*
235	419.2	*31.40*
151	82	*34.76*
220	479.9	*28.10*
128	106	*27.05*
320	475.4	*41.00*
470	111	*97.80*
168	490.7	*21.30*
383	517	*47.72*
215	262	*33.60*
434	374.7	*60.20*
265	434.04	*35.00*
210	592.7	25.00006
250	364.4	*35.00*

BIS Model – Station A

R (m)	*Q (kg)*	*SD*
411	*90*	0.61
370	478.7	0.11
235	419.2	0.09
151	82	0.35
220	479.9	0.08

128	106	0.24
320	475.4	0.10
470	111	0.54
168	490.7	0.06
383	517	0.10
215	262	0.14
434	374.7	0.15
265	434.04	0.10
210	592.7	0.06
250	364.4	0.11

Langefors Model – Station A

R (m)	*Q (kg)*	*SD*
325	*366.84*	0.36
341	65	0.87
360	61	0.91
258	75	0.74
352	319.3	0.40
320	70	0.82
305	309.2	0.38
186	386.5	0.29
209	100	0.59
220	368.6	0.31
215	95	0.61
330	105	0.67

USBM Model – Station A

R (m)	*Q (kg)*	*SD*
411	*90*	43.32
370	478.7	16.91

235	419.2	11.48
151	82	16.68
220	479.9	10.04
128	106	12.43
320	475.4	14.68
470	111	44.61
168	490.7	7.58
383	517	16.84
215	262	13.28
434	374.7	22.42
265	434.04	12.72
210	592.7	8.63
250	364.4	13.10

Station B

Ambraseys Model – Station B

R (m)	*Q (kg)*	*SD*
327	*90*	*72.97*
322	478.7	*41.16*
456	419.2	*60.93*
553	82	*127.29*
392	479.9	*50.07*
585	106	*123.61*
585	475.4	*74.96*
286	111	*59.51*
312	490.7	*39.56*
540	517	*67.28*
427	262	*66.73*
314	374.7	*43.55*
299	434.04	*39.49*

110	592.7	*13.10*
342	364.4	*47.88*

BIS Model – Station B

R (m)	*Q (kg)*	*SD*
327	*90*	0.53
322	478.7	0.10
456	419.2	0.14
553	82	0.82
392	479.9	0.11
585	106	0.66
585	475.4	0.15
286	111	0.39
312	490.7	0.09
540	517	0.13
427	262	0.22
314	374.7	0.12
299	434.04	0.10
110	592.7	0.04
342	364.4	0.13

Langefors Model – Station B

R (m)	*Q (kg)*	*SD*
345	*366.84*	0.37
293	65	0.82
465	61	0.99
585	75	0.97
315	319.3	0.38
430	70	0.90
420	309.2	0.43

295	386.5	0.34
660	100	0.87
345	368.6	0.37
620	95	0.87
470	105	0.76

USBM Model – Station B

R (m)	*Q (kg)*	*SD*
345	*366.84*	18.01
293	65	36.34
465	61	59.54
585	75	67.55
315	319.3	17.63
430	70	51.39
420	309.2	23.89
295	386.5	15.01
660	100	66.00
345	368.6	17.97
620	95	63.61
470	105	45.87

Annexure C

These Excel® spreadsheets have the SD vs PPV plots produced from the Quarry's historical Conventional data.

Station A – Conventional PPV data

For Ambraseys Model – Station A

	A	B	C
1	SD	Measured PPV	Modelled PPV
2	45.4	14.57	9.01
3	84.81	3.63	4.49
4	91.45	4.36	4.13
5	61.18	7.2	6.46
6	51.5	7.24	7.83
7	77.65	4.14	4.95
8	45.1	11.07	9.07
9	25.53	14.66	17.11
10	45.03	7.68	9.09
11	30.68	12.96	13.94
12	47.12	7.87	8.64
13	69.95	6.32	5.56

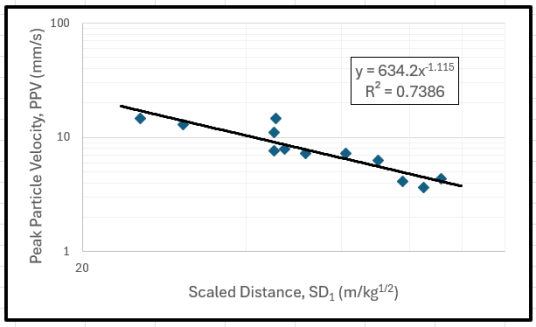

For BIS Model – Station A

SD	Measured PPV	Modelled PPV
0.13	14.57	11.69
0.75	3.63	4.60
0.83	4.36	4.36
0.54	7.2	5.48
0.16	7.24	10.47
0.67	4.14	4.89
0.15	11.07	10.84
0.08	14.66	15.14
0.35	7.68	6.90
0.1	12.96	13.45
0.38	7.87	6.61
0.45	6.32	6.04

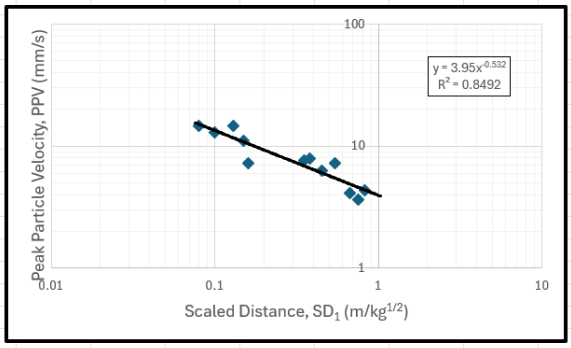

For Langefors Model – Station A

SD	Measured PPV	Modelled PPV
0.36	14.57	11.68
0.87	3.63	4.58
0.91	4.36	4.36
0.74	7.2	5.44
0.4	7.24	10.45
0.82	4.14	4.87
0.38	11.07	11.03
0.29	14.66	14.70
0.59	7.68	6.91
0.31	12.96	13.69
0.61	7.87	6.67
0.67	6.32	6.04

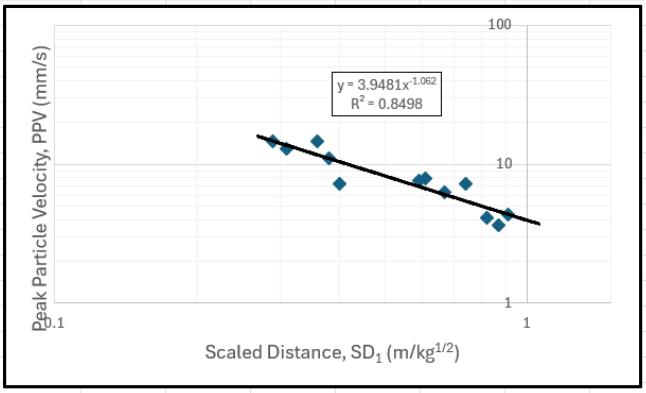

For USBM Model – Station A

SD	Measured PPV	Modelled PPV
16.97	14.57	9.98
42.3	3.63	4.42
46.01	4.36	4.10
29.79	7.2	6.04
19.7	7.24	8.74
38.25	4.14	4.83
17.35	11.07	9.79
9.46	14.66	16.82
20.9	7.68	8.29
11.46	12.96	14.17
22.06	7.87	7.90
32.2	6.32	5.63

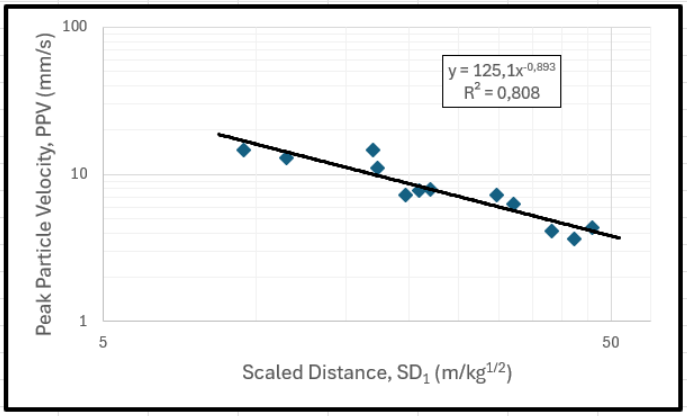

Station B – Conventional PPV data

For Ambraseys Model – Station B

SD	Measured PPV	Modelled PPV
48.19	8.24	7.48
72.87	7.14	5.79
118.13	3.98	4.29
138.72	3.89	3.89
46.09	7.34	7.69
104.34	4.62	4.64
62.11	5.92	6.39
40.5	8.1	8.33
142.19	3.83	3.83
48.12	6.63	7.48
135.88	3.54	3.94
99.62	5.43	4.77

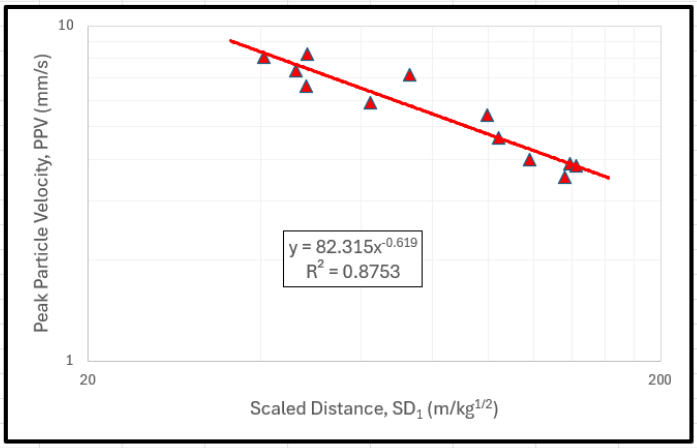

For BIS Model – Station B

SD	Measured PPV	Modelled PPV
0.13	8.24	7.41
0.68	7.14	4.62
0.98	3.98	4.16
0.93	3.89	4.22
0.14	7.34	7.26
0.81	4.62	4.39
0.18	5.92	6.76
0.11	8.1	7.78
0.76	3.83	4.47
0.13	6.63	7.41
0.77	3.54	4.46
0.58	5.43	4.83

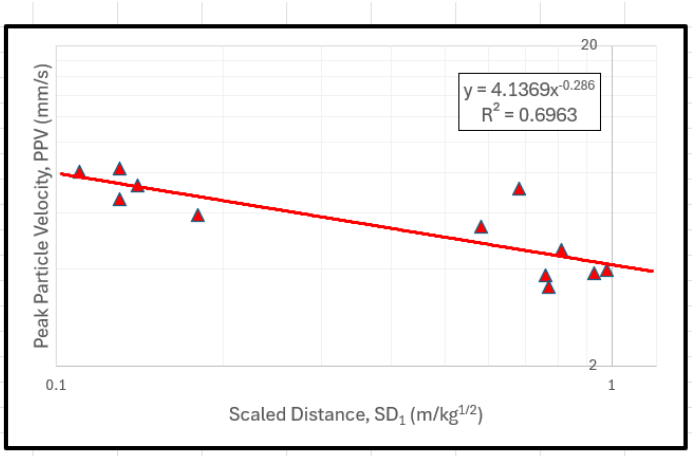

For Langefors Model – Station B

SD	Measured PPV	Modelled PPV
0.37	8.24	7.40
0.82	7.14	4.63
0.99	3.98	4.15
0.97	3.89	4.20
0.38	7.34	7.28
0.9	4.62	4.39
0.43	5.92	6.77
0.34	8.1	7.78
0.87	3.83	4.48
0.37	6.63	7.40
0.87	3.54	4.48
0.76	5.43	4.85

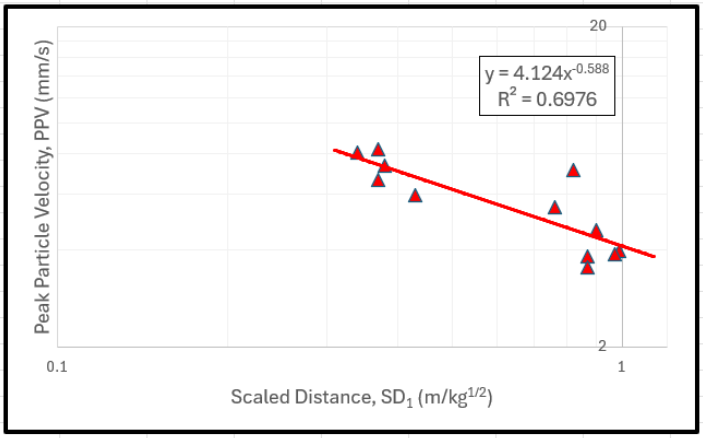

For USBM Model – Station B

SD	Measured PPV	Modelled PPV
18.01	8.24	7.52
36.34	7.14	5.34
59.54	3.98	4.20
67.55	3.89	3.95
17.85	7.34	7.56
51.39	4.62	4.51
23.89	5.92	6.56
15.01	8.1	8.22
66	3.83	4.00
17.97	6.63	7.53
63.61	3.54	4.07
45.87	5.43	4.77

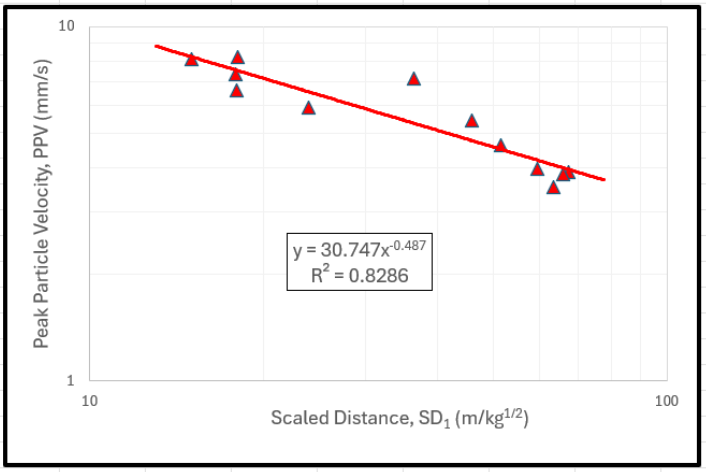

These Excel® spreadsheets have the SD vs PPV plots produced from the Quarry's Varistem® data.

Station A – Varistem® PPV data

Ambraseys Model – Station A

SD	PPV	Modelled PPV
91.71	2.82	2.79
47.3	3.65	3.55
31.4	3.8	4.13
34.76	3.17	3.98
28.1	4.18	4.30
27.05	3.73	4.36
41	3.65	3.74
97.8	2.45	2.73
21.3	5.59	4.75
47.72	4.27	3.54
33.6	3.88	4.02
60.2	3.73	3.25
35	3.78	3.97
25.95	4.66	4.42
35	4.5	3.97

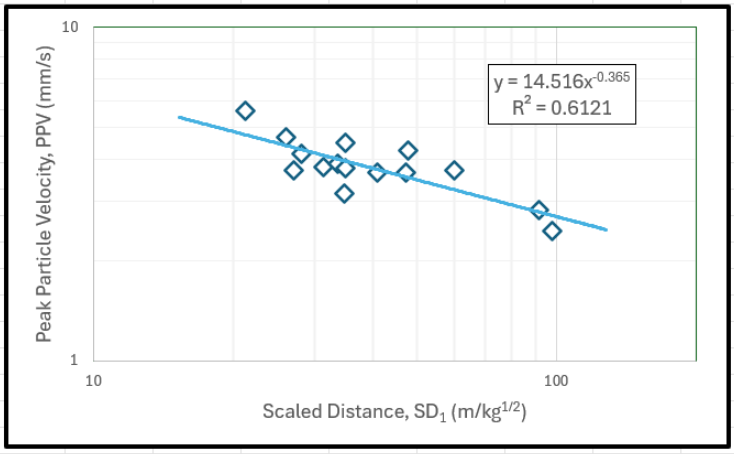

BIS Model – Station A

SD	PPV	Modelled PPV
0.61	2.82	2.85
0.11	3.65	3.96
0.09	3.8	4.11
0.35	3.17	3.17
0.08	4.18	4.21
0.24	3.73	3.41
0.01	5.35	6.26
0.54	2.45	2.92
0.06	5.59	4.45
0.1	4.27	4.03
0.14	3.88	3.78
0.15	3.73	3.73
0.1	3.78	4.03
0.06	4.66	4.45
0.11	4.5	3.96

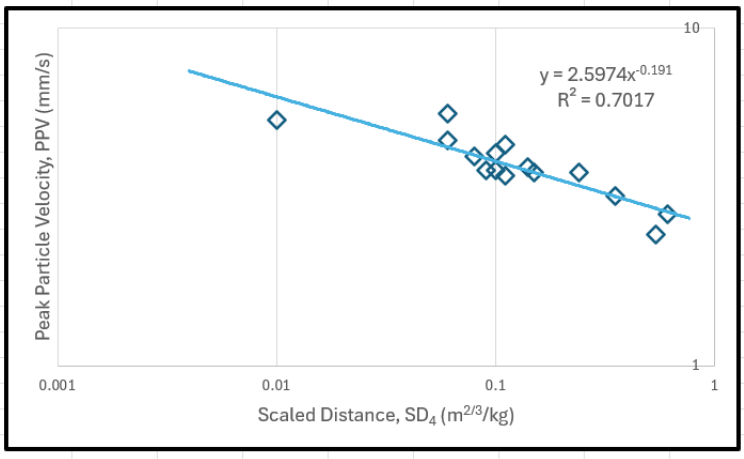

Langefors Model – Station A

SD	PPV	Modelled PPV
0.78	2.82	2.69
0.33	3.65	4.00
0.3	3.8	4.19
0.59	3.17	3.06
0.28	4.18	4.32
0.49	3.73	3.33
0.31	3.65	4.12
0.74	2.45	2.75
0.25	5.29	4.55
0.32	4.27	4.06
0.37	3.88	3.80
0.39	3.73	3.71
0.31	3.78	4.12
0.24	4.66	4.64
0.33	4.5	4.00

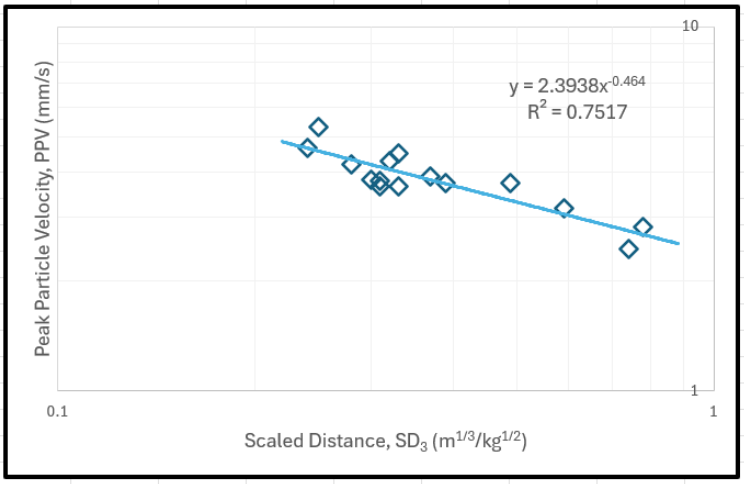

USBM Model – Station A

SD	PPV	Modelled PPV
43.32	2.82	2.65
16.91	3.65	3.67
11.48	3.8	4.20
16.68	3.17	3.69
10.04	4.18	4.40
12.43	3.73	4.09
14.68	3.65	3.86
44.61	2.45	2.62
7.58	5.59	4.85
16.84	4.27	3.68
13.28	3.88	3.99
22.42	3.73	3.33
12.72	3.78	4.05
9.12	4.66	4.55
13.1	4.5	4.01

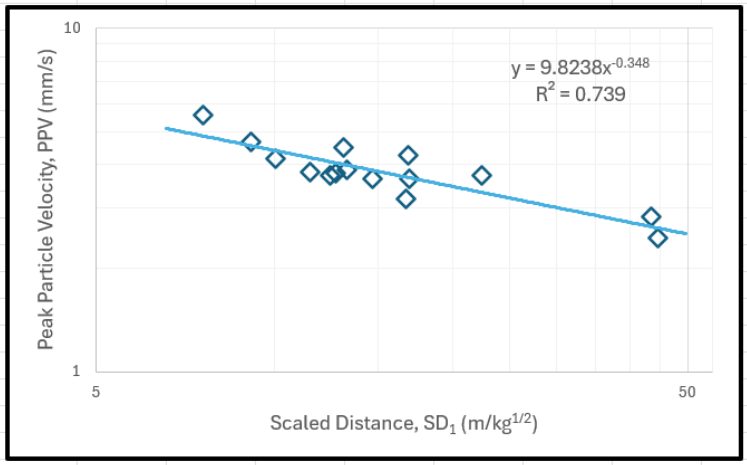

Station B – Varistem® PPV data

Ambraseys Model – Station B

SD	PPV	Modelled PPV
72.97	3.62	3.84
41.16	5.05	4.65
60.93	4.12	4.08
127.29	2.77	3.19
50.07	3.81	4.35
123.61	3.23	3.22
74.96	4.65	3.81
59.51	3.95	4.11
39.56	4.18	4.71
67.28	4.27	3.95
66.73	3.88	3.96
43.55	4.93	4.56
39.49	5.58	4.71
13.1	6.36	6.80
47.88	4.13	4.42

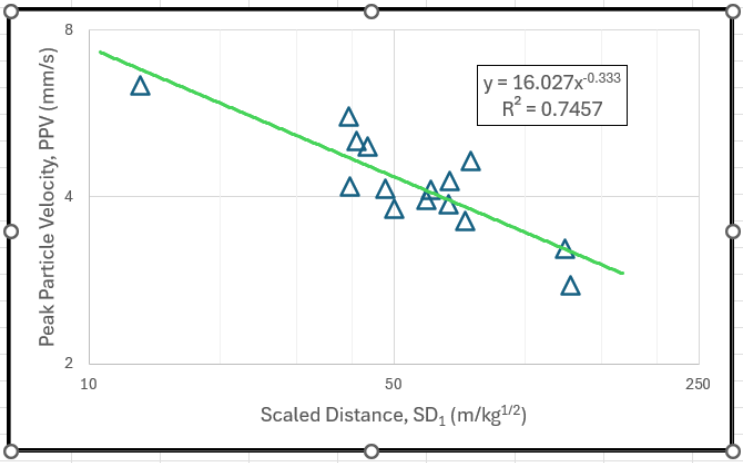

BIS Model – Station B

SD	PPV	Modelled PPV
0.53	3.62	3.32
0.1	5.05	4.75
0.14	4.12	4.42
0.82	3.27	3.03
0.11	3.81	4.65
0.66	3.23	3.17
0.15	4.65	4.36
0.39	3.95	3.55
0.09	4.18	4.86
0.13	4.27	4.49
0.22	3.88	4.01
0.12	4.93	4.57
0.1	5.38	4.75
0.04	6.36	5.78
0.13	4.13	4.49

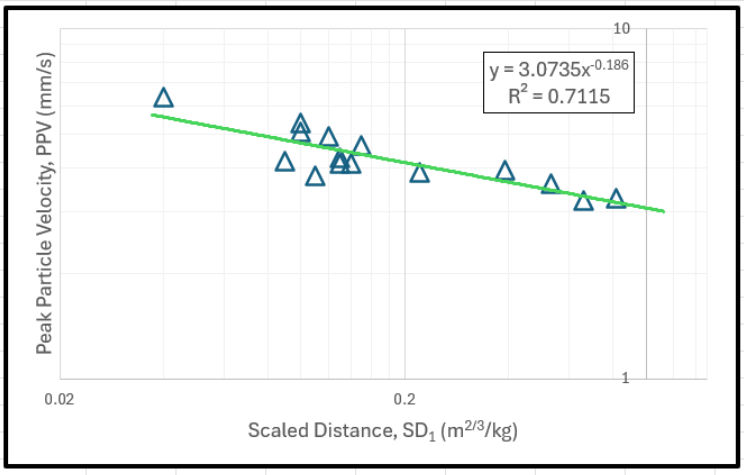

Langefors Model – Station B

SD	PPV	Modelled PPV
0.73	3.62	3.32
0.31	5.05	4.80
0.38	4.12	4.40
0.91	2.77	3.02
0.33	3.81	4.68
0.81	3.23	3.18
0.38	4.65	4.40
0.63	3.95	3.54
0.31	4.18	4.80
0.36	4.27	4.50
0.47	3.88	4.01
0.35	4.93	4.56
0.32	5.38	4.74
0.2	6.36	5.80
0.37	4.13	4.45

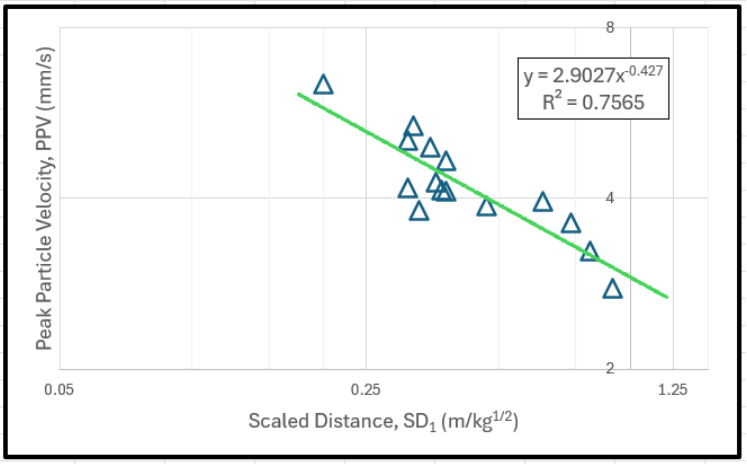

USBM Model – Station B

SD	PPV	Modelled PPV
34.47	3.62	3.65
14.72	5.05	4.70
22.27	4.12	4.16
61.07	2.77	3.09
17.89	3.81	4.44
56.82	3.23	3.15
26.83	4.65	3.94
27.15	3.95	3.92
14.08	4.18	4.76
23.75	4.27	4.08
26.38	3.88	3.96
16.22	4.93	4.57
14.35	5.58	4.74
4.52	6.36	6.67
17.92	4.13	4.44

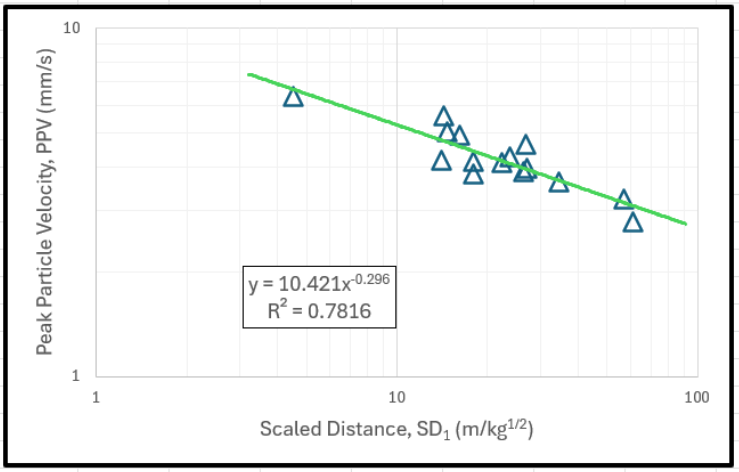

Annexure D

Ranking the performance of empirical models using regression model evaluation metrics.

Ranking Models – Conventional and Varistem® blast data

Ranking for Ambresys Model

Conventional blast			
Measured PPV (y_1)	Modelled PPV (y_0)	($y_1 - y_0$)	$(y_1 - y_0)^2$
14.57	9.01	5.56	30.9136
3.63	4.49	0.86	0.7396
4.36	4.13	0.23	0.0529
7.2	6.46	0.74	0.5476
7.24	7.83	0.59	0.3481
4.14	4.95	0.81	0.6561
11.07	9.07	2	4
14.66	17.11	2.45	6.0025
7.68	9.09	1.41	1.9881
12.96	13.94	0.98	0.9604
7.87	8.64	0.77	0.5929
6.32	5.56	0.76	0.5776
	Mean Absolute Error	**1.43**	
	Mean Square Error		**3.948283**
	Root Mean Square Error		**1.987029**

Ranking for BIS Model

Varistem blast			
Measured PPV (y_1)	Modelled PPV (y_0)	($y_1 - y_0$)	$(y_1 - y_0)^2$
2.82	2.85	0.03	0.0009
3.65	3.96	0.31	0.0961

3.8	4.11	0.31	0.0961
3.17	3.17	0	0
4.18	4.21	0.03	0.0009
3.73	3.41	0.32	0.1024
5.35	6.26	0.91	0.8281
2.45	2.92	0.47	0.2209
5.59	4.45	1.14	1.2996
4.27	4.03	0.24	0.0576
3.88	3.78	0.1	0.01
3.73	3.73	0	0
3.78	4.03	0.25	0.0625
4.66	4.45	0.21	0.0441
4.5	3.96	0.54	0.2916
	Mean Absolute Error	**0.324**	
	Mean Square Error		**0.20738667**
	Root Mean Square Error		**0.45539726**

Ranking for Langefors Model

Varistem blast			
Measured PPV (y_1)	Modelled PPV (y_0)	($y_1 - y_0$)	$(y_1 - y_0)^2$
2.82	2.69	0.13	0.0169
3.65	4	0.35	0.1225
3.8	4.19	0.39	0.1521
3.17	3.06	0.11	0.0121
4.18	4.32	0.14	0.0196
3.73	3.33	0.4	0.16
3.65	4.12	0.47	0.2209
2.45	2.75	0.3	0.09
5.59	4.75	0.84	0.7056
4.27	4.06	0.21	0.0441
3.88	3.8	0.08	0.0064

3.73	3.71	0.02	0.0004
3.78	4.12	0.34	0.1156
4.66	4.64	0.02	0.0004
4.5	4	0.5	0.25
	Mean Absolute Error	**0.287**	
	Mean Square Error		**0.12777333**
	Root Mean Square Error		**0.35745396**

Ranking for USBM Model

Standard blast			
Measured PPV (y_1)	Modelled PPV (y_0)	($y_1 - y_0$)	$(y_1 - y_0)^2$
14.57	9.98	4.59	21.0681
3.63	4.42	0.79	0.6241
4.36	4.1	0.26	0.0676
7.2	6.04	1.16	1.3456
7.24	8.74	1.5	2.25
4.14	4.83	0.69	0.4761
11.07	9.79	1.28	1.6384
14.66	16.82	2.16	4.6656
7.68	8.29	0.61	0.3721
12.96	14.17	1.21	1.4641
7.87	7.9	0.03	0.0009
6.32	5.63	0.69	0.4761
	Mean Absolute Error	**1.2475**	
	Mean Square Error		**2.870725**
	Root Mean Square Error		**1.694321**

Annexure E

The following attachments contain the student t-test calculations and the Comparison between Varistem® and Conventional PPV data.

Conventional vs Varistem blasts and t-Test calculations

Conventional vs Varistem blasts – Station A

Standard Blast			Varistem Blast	
SD	Measured PPV		SD	PPV
0.36	14.57		0.78	2.82
0.87	3.63		0.33	3.65
0.91	4.36		0.3	3.8
0.74	7.2		0.59	3.17
0.4	7.24		0.28	4.18
0.82	4.14		0.49	3.73
0.38	11.07		0.31	3.65
0.29	14.66		0.74	2.45
0.59	7.68		0.25	5.59
0.31	12.96		0.32	4.27
0.61	7.87		0.37	3.88
0.67	6.32		0.39	3.73
			0.31	3.78
			0.24	4.66
			0.33	4.5
Safety	Limit			
0.01	12.7			
0.02	12.7			
0.3	12.7			
0.4	12.7			
0.5	12.7			
0.6	12.7			
0.7	12.7			
0.8	12.7			
0.9	12.7			
1	12.7			

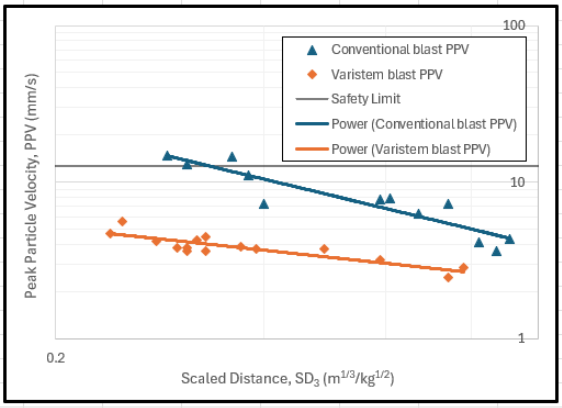

Conventional vs Varistem blasts – Station A

Standard Blast		Varistem Blast	
SD	Measured PPV	SD	PPV
0.37	8.24	0.73	3.62
0.82	7.14	0.31	5.05
0.99	3.98	0.38	4.12
0.97	3.89	0.91	2.77
0.38	7.34	0.33	3.81
0.9	4.62	0.81	3.23
0.43	5.92	0.38	4.65
0.34	8.1	0.63	3.95
0.87	3.83	0.31	4.18
0.37	6.63	0.36	4.27
0.87	3.54	0.47	3.88
0.76	5.43	0.35	4.93
		0.32	5.58
		0.2	6.36
		0.37	4.13

Safety	Limit
0.01	12.7
0.2	12.7
0.3	12.7
0.4	12.7
0.5	12.7
0.6	12.7
0.7	12.7
0.8	12.7
0.9	12.7
1	12.7

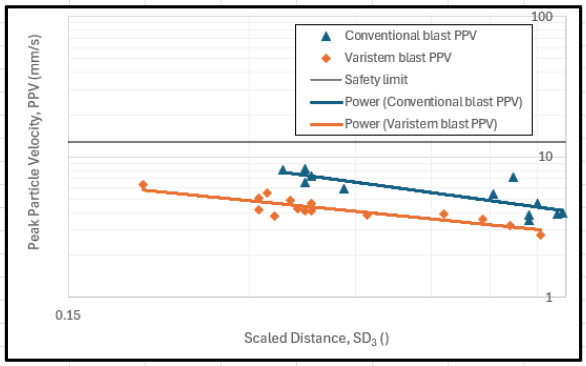

Student's T-test: Two Samples Assuming Unequal Variances

	Conventional PPV	Varistem PPV
	8.24	3.62
	7.14	5.05
	3.98	4.12
	3.89	2.77
	7.34	3.81
	4.62	3.23
	5.92	4.65
	8.1	3.95
	3.83	4.18
	6.63	4.27
	3.54	3.88
	5.43	4.93
		5.58
		6.36
		4.13
Mean PPV	**5.721666667**	**4.302**
Standard Dev.	**1.745611814**	**0.907415482**

t-Test: Two-Sample Assuming Unequal Variances

	Conventional PPV	*Varistem PPV*
Mean	5.721666667	4.302
Variance	3.047160606	0.823402857
Observations	12	15
Hypothesized Mean Difference	0	
df	16	
t Stat	2.554648557	
P(T<=t) one-tail	0.010601499	
t Critical one-tail	1.745883676	
P(T<=t) two-tail	0.021202998	
t Critical two-tail	2.119905299	

Annexure F

Bootstrapping calculations and data distribution calculations and plots.

NB: Please note that the Bootstrapping calculations keeps on changing as you click on the spreadsheet. This has affected the numbers used to calculate and sketch the data distribution. This also affected the PPV ranges calculated using the data produced by the Bootstrapping.

Bootstrapping calculations – Varistem® blast

Varistem® blast

	A	B	C	D	E	F	G	H	I	J	K	L	M	N	O	P	Q	R	S	T	U	V
1	2.82		3.73	3.65	3.73	2.82	3.8	3.88	4.27	3.73	4.66	4.5	3.78	3.65	4.27	3.65	3.88	3.73	4.5	2.45	3.65	2.45
2	3.65		3.8	3.17	2.82	3.73	4.18	3.78	3.8	3.88	3.17	3.17	2.82	2.82	3.17	2.45	3.17	3.73	3.65	3.65	4.66	2.82
3	3.8		4.27	4.18	5.59	3.8	4.27	3.65	3.65	2.45	3.88	3.65	4.5	3.73	3.65	3.8	4.5	3.65	3.8	4.27	3.78	4.27
4	3.17		3.8	4.27	3.65	5.59	3.65	2.82	4.5	3.73	2.82	4.5	2.45	5.59	3.17	3.65	4.66	4.27	3.17	2.82	3.88	4.66
5	4.18		3.65	4.5	3.65	3.65	3.65	3.73	3.65	4.66	3.17	3.73	3.73	4.5	3.65	3.8	3.88	4.18	5.59	4.66	3.73	4.66
6	3.73		3.65	3.65	2.45	4.5	5.59	3.17	3.73	3.78	3.65	4.66	3.88	3.65	3.65	3.65	3.17	5.59	5.59	4.18	3.65	2.82
7	3.65		4.5	3.88	3.17	3.88	4.18	2.45	3.78	2.82	2.82	5.59	4.18	3.17	5.59	3.78	4.27	3.65	4.5	3.8	3.73	3.88
8	2.45		3.78	5.59	3.73	3.8	4.27	4.18	4.27	3.88	2.45	5.59	5.59	4.5	4.27	3.78	4.27	3.73	2.82	4.18	3.65	2.82
9	5.59		3.73	3.73	4.27	4.66	3.65	4.18	2.45	4.27	3.73	4.18	2.45	3.73	3.17	3.78	3.65	3.65	3.88	2.45	3.65	3.78
10	4.27		2.45	4.5	3.65	3.8	2.45	3.8	4.5	2.82	3.73	2.45	3.8	4.27	2.45	3.73	3.65	3.73	5.59	5.59	4.18	3.65
11	3.88		4.66	2.45	3.78	3.88	3.73	3.65	3.65	4.27	5.59	3.88	4.5	4.66	3.65	4.18	3.17	3.73	3.65	2.45	4.27	4.18
12	3.73		2.45	3.78	3.73	2.45	3.65	3.78	3.8	3.65	3.73	2.45	3.17	4.27	3.17	3.17	2.45	3.88	2.45	4.5	4.27	4.27
13	3.78		3.65	3.78	3.8	3.65	3.73	3.73	4.5	3.73	4.18	3.65	3.78	5.59	4.5	3.73	3.65	3.8	3.78	4.18	3.73	5.59
14	4.66		3.8	3.65	2.82	3.88	3.65	4.27	3.65	3.65	3.88	3.65	3.73	3.65	3.73	3.73	2.82	3.73	3.65	3.88	4.5	2.82
15	4.5		4.27	4.27	3.73	3.73	3.65	3.65	4.66	4.18	2.45	3.73	3.88	2.82	2.82	3.88	3.65	3.73	2.82	3.88	4.5	3.65
16																						
17		MEAN	3.746	3.936667	3.638	3.854667	3.873333	3.648	3.924	3.7	3.594	3.958667	3.749333	4.04	3.660667	3.650667	3.656	3.918667	3.962667	3.796	3.988667	3.754667
18		Standard Dev	0.140111																			
19		Conf. Interval @95%	0.280223																			
20																						
21																						
22		Based on 20 runs																				
23		Mean of Means	3.802533																			
24		No. Blasts	20																			
25		Cut-off @ 2.5%	0.5																			
26		Lower Bound	3.594																			
27		Upper Bound	4.04																			

Data distribution

Varistem PPV				Bin	Frequency
3.51	Min	3.51		3.51	1
3.64	Max	4.16		3.618	2
3.98				3.727	3
3.74				3.835	6
3.8	BIN			3.943	4
3.81	3.51			4.052	2
3.74	3.618			4.16	2
3.61	3.727			More	0
3.96	3.835				
3.68	3.943				
3.84	4.052				
4.13	4.16				
3.6					
3.77					
3.91					
3.75					
3.93					
4.16					
3.67					
3.89					

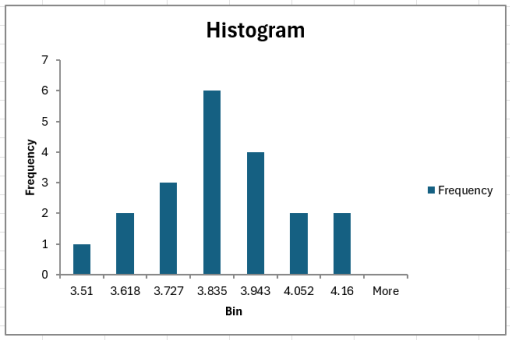

Bootstrapping calculations – Conventional blast

Standard Blast

14.57		4.14	7.24	11.07	7.24	7.87	12.96	12.96	7.2	14.57	14.66	3.63	3.63	4.36	7.24	12.96	11.07	4.36	12.96	6.32	11.07
3.63		3.63	14.66	11.07	7.68	6.32	7.68	6.32	7.87	12.96	6.32	11.07	4.14	14.66	11.07	7.2	7.68	11.07	3.63	4.14	7.68
4.36		4.36	14.66	3.63	3.63	4.14	6.32	14.66	11.07	4.36	4.14	3.63	7.68	6.32	6.32	12.96	7.2	3.63	4.14	14.66	12.96
7.2		11.07	4.36	3.63	4.14	11.07	11.07	7.87	7.2	12.96	7.2	4.36	4.14	3.63	12.96	7.2	7.87	14.66	14.57	14.66	3.63
7.24		7.24	7.24	14.57	7.24	3.63	12.96	7.24	7.2	7.2	4.14	7.24	6.32	3.63	3.63	14.57	11.07	4.14	4.36	14.57	7.68
4.14		14.66	7.24	7.68	7.87	4.14	7.68	3.63	7.68	7.24	12.96	14.66	4.14	4.36	7.87	4.14	4.14	14.57	4.14	7.68	14.57
11.07		4.14	14.57	12.96	4.14	7.87	7.87	6.32	11.07	14.66	3.63	14.66	14.57	4.36	11.07	7.68	7.24	4.14	6.32	6.32	3.63
14.66		6.32	3.63	7.68	7.87	4.14	6.32	4.36	4.36	4.36	11.07	4.36	11.07	14.66	6.32	7.87	4.36	7.2	7.24	7.87	14.66
7.68		4.14	3.63	7.2	7.2	11.07	4.36	4.14	14.57	7.24	6.32	14.57	14.57	3.63	7.2	7.2	11.07	14.66	14.57	4.14	6.32
12.96		6.32	7.87	3.63	7.2	4.36	4.36	7.87	14.66	3.63	4.36	12.96	7.24	14.57	7.2	7.87	6.32	12.96	14.57	7.87	4.36
7.87		11.07	3.63	14.57	7.87	12.96	11.07	7.24	11.07	6.32	7.68	7.68	6.32	4.14	7.87	7.87	14.66	14.57	14.57	12.96	4.36
6.32		6.32	3.63	7.2	6.32	14.66	4.14	14.57	7.24	7.87	3.63	7.24	3.63	11.07	4.14	3.63	7.2	7.24	7.24	7.2	14.66
	MEAN	6.950833	7.696667	8.740833	6.533333	7.685833	8.065833	8.098333	9.265833	8.614167	7.175833	8.838333	7.2875	7.449167	7.740833	8.429167	8.323333	9.433333	9.025833	9.0325	8.798333
	Standard Dev	0.821957																			
	Conf. Interval @ 95%	**1.643915**																			
	Based on 20 runs																				
	Mean of Means	8.159292																			
	No. Blasts	20																			
	Cut-off @ 2.5%	0.5																			
	Lower Bound	6.533333																			
	Upper Bound	9.433333																			
	Upper Limit	**8.981249**																			
	Lower Limit	**7.337334**																			
	Range	**7.337334**	**<PPV>**	**8.981249**																	

Data distribution

Conventional PPV						
8.5		Min	7.01			
7.19		Max	10.07			
8.55				*Bin*	*Frequency*	
8.17				7.01	1	
7.57		BIN		7.52	2	
8.86		7.01		8.03	2	
8.7		7.52		8.54	7	
8.1		8.03		9.05	4	
10.07		8.54		9.56	3	
9.41		9.05		10.07	1	
8.54		9.56		More	0	
7.55		10.07				
7.01						
8.21						
9.46						
9.05						
8.41						
8.48						
9.36						
7.22						

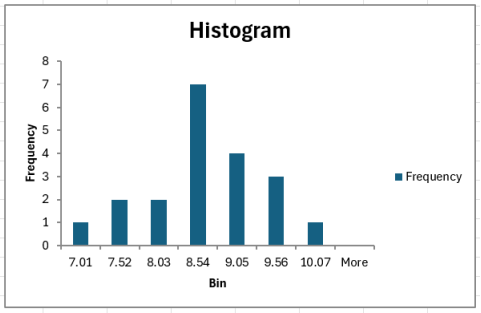

Annexure G

This is the data modelled from the BIS model.

	A	B	C	D	E	F	G	H
1		Conventional PPV	Varistem PPV			t-Test: Two-Sample Assuming Unequal Variances		
2		11.26	2.64					
3		4.65	3.85				*Conventional PPV*	*Varistem PPV*
4		4.4	4.2			Mean	8.355	3.837333333
5		5.5	3.05			Variance	14.03213636	0.39296381
6		10.57	4.49			Observations	12	15
7		4.92	3.43			Hypothesized Mean Difference	0	
8		10.57	4			df	11	
9		15.45	2.66			t Stat	4.131727903	
10		6.86	4.49			P(T<=t) one-tail	0.000833616	
11		13.43	4.2			t Critical one-tail	1.795884819	
12		6.65	3.85			P(T<=t) two-tail	0.001667231	
13		6	3.74			t Critical two-tail	2.20098516	
14			4.2					
15			4.49					
16			4.27					
17								
18	**Mean**	**8.355**	**3.837333333**					
19	**Standard Dev.**	**3.745949327**	**0.626868255**					
20								
21		**Standard Deviations are different, therefore we'll assume unequal variance.**						